



Terms and Conditions of Use of Digitised Theses from Trinity College Library Dublin

Copyright statement

All material supplied by Trinity College Library is protected by copyright (under the Copyright and Related Rights Act, 2000 as amended) and other relevant Intellectual Property Rights. By accessing and using a Digitised Thesis from Trinity College Library you acknowledge that all Intellectual Property Rights in any Works supplied are the sole and exclusive property of the copyright and/or other IPR holder. Specific copyright holders may not be explicitly identified. Use of materials from other sources within a thesis should not be construed as a claim over them.

A non-exclusive, non-transferable licence is hereby granted to those using or reproducing, in whole or in part, the material for valid purposes, providing the copyright owners are acknowledged using the normal conventions. Where specific permission to use material is required, this is identified and such permission must be sought from the copyright holder or agency cited.

Liability statement

By using a Digitised Thesis, I accept that Trinity College Dublin bears no legal responsibility for the accuracy, legality or comprehensiveness of materials contained within the thesis, and that Trinity College Dublin accepts no liability for indirect, consequential, or incidental, damages or losses arising from use of the thesis for whatever reason. Information located in a thesis may be subject to specific use constraints, details of which may not be explicitly described. It is the responsibility of potential and actual users to be aware of such constraints and to abide by them. By making use of material from a digitised thesis, you accept these copyright and disclaimer provisions. Where it is brought to the attention of Trinity College Library that there may be a breach of copyright or other restraint, it is the policy to withdraw or take down access to a thesis while the issue is being resolved.

Access Agreement

By using a Digitised Thesis from Trinity College Library you are bound by the following Terms & Conditions. Please read them carefully.

I have read and I understand the following statement: All material supplied via a Digitised Thesis from Trinity College Library is protected by copyright and other intellectual property rights, and duplication or sale of all or part of any of a thesis is not permitted, except that material may be duplicated by you for your research use or for educational purposes in electronic or print form providing the copyright owners are acknowledged using the normal conventions. You must obtain permission for any other use. Electronic or print copies may not be offered, whether for sale or otherwise to anyone. This copy has been supplied on the understanding that it is copyright material and that no quotation from the thesis may be published without proper acknowledgement.

**Characterisation of the Performance of
Single Point Diamond Dressers in
Abrasive Processes**

Stuart Murphy, B.Sc. (Ing.)

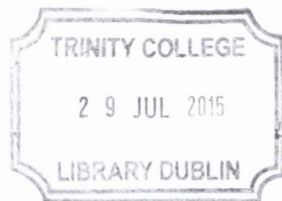
Department of Mechanical and Manufacturing Engineering
University of Dublin

A thesis submitted to the University of Dublin in partial fulfilment of
the requirements for the degree of Doctor in Philosophy

September 2014

Supervisor

Dr. Garret E. O'Donnell



Thesis 10673

Declaration

I declare that the work in this thesis is, unless otherwise stated, entirely my own work and has not been submitted as an exercise for a degree at this or any other University. I agree that Trinity College Library may lend or copy this thesis upon request.

A handwritten signature in blue ink, reading "Stuart Murphy", is written over a horizontal line.

Stuart Murphy

September 2014

Abstract

This thesis presents in-depth investigation and analysis of the dressing of conventional grinding wheels. Grinding is used in the manufacturing industry to achieve a high surface finish which is an important constituent of the overall productivity. Although the desired surface quality of a product is dependent on the functional requirements of the product, the surface finish itself is dependent on the process characteristics of the grinding process. One of the most important parameters that determine the workpiece surface finish is the dressing process as it has a direct impact on the topography of the wheel. A tool called a diamond dresser is used to condition the wheel. Like most machining tools, the diamond is subject to wear over time, which results in a change in the dressing parameters as the tool is in contact with the wheel for a great period of time. In this thesis work, wear of various types of diamond dressers are analysed under different machining environments in which they are exposed to. This knowledge of the wear of diamond dressers will lead to prolonged dressing tool life enabling more precise levels of machining to be maintained for a longer time without the need for a tool change.

Leading on from the work performed on the wear of diamond dressers, the dressing process will be characterised by considering the grinding specific energy and the workpiece surface following dressing. The effect of using different grinding wheel grit sizes under varying dressing conditions will be analysed to investigate whether a desired surface finishes can be achieved while consuming less specific energy during grinding. Using the vast array of experimental results obtained and the undeformed chip thickness model, values for parameters used in the equation which were previously estimated were given an exact value leading to accurate calculated undeformed chip thickness values.

Finishing passes are quite often used in the grinding process to achieve a smoother surface finish while also removing previous layers which may have experienced thermal damage due to high specific energies. The effect of performing a finishing pass during the dressing process was investigated to determine its outcome on the specific energy and workpiece surface roughness following grinding. The results of the specific energy and surface finish analysis indicate that overlap ratios with a finishing pass gave the same results as a dressing pass with twice the overlap ratio

value. This indicates that the outcome of the dressing pass is influenced by the amount of time the dresser spends in contact with the grits on the periphery of the wheel.

In order to maintain precise levels of surface finish while grinding, the dressing process was monitored using acoustic emission sensors. The surface finish and specific energy characteristics were analysed following dressing. It was revealed that a strong correlation existed between the acoustic emission response during dressing and the specific energy and surface roughness signals monitored and analysed during and following grinding. This shows that for a particular grinding process, monitoring the acoustic emission signal during dressing enables a prediction of the specific energy to be made based on the known correlation.

Acknowledgements

I would first like to offer my sincere thanks to my supervisor, Dr. Garret O'Donnell. He gave me the opportunity of pursuing a PhD, and since then has supervised my work with much enthusiasm, patience, guidance and constructive advice. I have learnt a lot from him over the years and his support is both gratefully acknowledged and appreciated.

Special thanks also to Dr. Jeffrey Badger, for all his advice, guidance and knowledge throughout the project. The support and feedback from an expert in the area has been invaluable throughout this research.

I would also like to thank those at Element Six, particularly Neil Perkins and Sean Kitson. Their support has been invaluable and it has been a very rewarding experience collaborating so closely with industry these past few years.

I would also like to acknowledge that this project has been funded by the Irish Research Council for Science, Engineering and Technology and Element Six under the Enterprise Partnership scheme.

Furthermore, I would like to thank all the staff of the Department of Mechanical and Manufacturing Engineering, Trinity College Dublin. Particularly; Michael Reilly, Sean Doonan, Gabriel Nicholson, JJ Ryan, Alex Kearns, Daniel Boardman, and Peter O'Reilly for their technical support.

To all the postgrads, past and present: Paul E, Paul H, Kev, Emma, Barry, Jeff, Aoife, Robin, Darren, Eoin, Rory, Peadar, Daniel and Gio. Thank you for all the friendship, encouragement and technical support over the years, and I wish you all the best for the future.

Thanks also to my parents, Ruby and David for their endless support and encouragement through the good times and the bad. I could not have reached this stage without you, so thank you for everything.

Table of Contents

Declaration	i
Abstract.....	iii
Acknowledgements	v
Table of Contents	vii
Nomenclature	xi
Chapter 1 Introduction.....	1
1.1 Research background and motivation	1
1.2 Research Objectives	5
2 Literature review	6
2.1 Dressing process characteristics	6
2.1.1 Introduction to dressing.....	6
2.1.2 Diamond dressers	7
2.1.3 Material removal mechanisms during dressing.....	10
2.1.4 Effect of dressing parameters on grinding wheel performance.....	11
2.1.5 Shape of dresser.....	15
2.1.6 Number of dressing passes	16
2.2 Grinding process characteristics.....	18
2.2.1 The grinding wheel.....	18
2.2.2 Grinding forces.....	21
2.2.3 Mechanics of grinding.....	22
2.2.4 Specific energy in grinding	26
2.3 Process monitoring in grinding	27
2.3.1 Acoustic emission sensors.....	27
2.4 Surface finish characterisation	35

2.4.1 Measurement of surface finish.....	36
2.4.2 Metallurgical damage to workpiece.....	38
2.4.3 Workpiece residual stress	38
2.5 Diamond dressing tools	40
2.5.1 Diamond manufacturing	40
2.5.2 Wear of Diamond Dressers.....	42
2.5.3 Anisotropy of diamond	45
Chapter 3 Wear characterisation of diamond dressers	47
3.1 Background and methodology for wear characterisation	47
3.2 Experimental set-up	48
3.2.1 AE sensor.....	49
3.2.2 Microscope and camera	51
3.2.3 Scanning Electron Microscope	51
3.3 Tooling and Materials.....	52
3.3.1 Diamond dressers.....	53
3.3.3 Grinding wheels.....	53
3.5 Dressing Strategy Investigations	54
3.5.1 Experimental methodology.....	55
3.5.2 Experimental results	56
3.5.3 Discussion of results	58
3.6 Directionality Tests.....	62
3.6.1 Experimental methodology.....	62
3.6.2 Experimental results	64
3.6.3 Discussion of results	67
3.7 Change in geometry of the diamond.....	69
3.8 Abrasive material.....	71

3.8.1 Methodology	72
3.8.2 Experimental results	72
3.9.3 Discussion of results.....	74
Chapter 4 Dressing process characterisation methodology.....	77
4.2 Equipment	81
4.2.1 Grinding machine	81
4.2.2 Dynamometer	82
4.2.3 Acoustic emission sensor	84
4.2.4 Stylus profilometer	84
4.3.1 Diamond dressers	85
4.3.2 Grinding wheels	86
4.3.3 Workpiece Material	86
4.4 Experimental procedure	86
4.5 Wheel wear measurement.....	88
4.6 Feature extraction	88
4.6.1 Acoustic Emission	88
4.6.3 Grinding forces.....	89
4.6.4 Surface finish of workpiece.....	92
Chapter 5	95
Experimental Results: Dressing Characterisation Investigations.....	95
5.1 Background	95
5.1.1 Effect of overlap ratio on specific energy	96
5.1.2 Effect of overlap ratio on grinding force ratio.....	98
5.1.3 Effect of overlap ratio on surface finish	100
5.1.4 Ra vs. specific energy.....	106

5.2 Effect of finishing pass	113
5.2.1 Effect of finishing pass on AE signal	113
5.2.2 Effect of finishing pass on specific energy	115
5.2.3 Effect of finishing pass on surface finish.....	117
5.3 Acoustic emission signal and specific energies during grinding	118
5.3.1 Effect of overlap ratio on acoustic emission.....	118
5.3.2 Application of AE to grinding specific energy	122
5.3.3 Acoustic emission and diamond wear.....	123
Chapter 6 Conclusion	127
6.1 Wear characterisation of the diamond dresser	127
6.2 Dressing characterisation results	130
6.3 Acoustic emission	132
6.4 Future Work.....	134
References.....	135

Nomenclature

Symbol	Definition
a	depth of cut (mm)
a_d	dressing depth of cut (μm)
AE	Acoustic Emission
b	grinding wheel width (mm)
b_d	Effective width of the diamond dresser (mm)
C	active cutting points per unit area
CBN	Cubic Boron Nitride
CVD	Chemical Vapour Deposition
d_e	equivalent diameter (mm)
d	wheel diameter (mm)
e_{ae}	specific AE dressing energy ($\text{V}/\text{mm}^3/\text{s}$)
e_c	grinding specific energy (J/mm^3)
e_d	specific dressing energy (J/mm^3)
f_d	diamond dresser feed rate (mm/rev)
F_n	normal force (newtons)
F_{nc}	normal chip formation force (newtons)
F_{nf}	normal friction force (newtons)
F_t	tangential force (newtons)
F_{tc}	tangential chip formation force (newtons)
F_{td}	tangential dressing force (newtons)
F_{tf}	tangential friction force (newtons)
GUI	Graphical User Interface
h_m	maximum chip thickness value
HPHT	High Pressure High Temperature
i_{ae}	AE signal intensity (Volts)
Mhz	Mega Hertz
MRR	Material Removal Rate (mm^3/s)
n_c	number of active grits per unit surface area (grits/mm)
P	grinding power (Watt)
P_d	dressing power (Watt)
PF_{ae}	acoustic emission power factor (millivolts/Watt)
$P_{air\ cut}$	recorded active spindle power for air cut or spindle idling (Watt)
Q_d	dressing grit removal rate (mm^3/s)
Q_w	workpiece material removal rate (mm^3/sec)
r	shape factor of grit
R_c	Rockwell Hardness
R_a	average surface roughness (μm)
RMS	Root Mean Square
R_p	maximum profile peak height (μm)
RPM	Revolutions Per Minute
R_{pv}	peak to valley height of profile (μm)
R_t	maximum height of profile (μm)

R_v	maximum profile valley depth (μm)
R_w	local workpiece radius (mm)
S_d	dressing lead
t'	undeformed chip thickness
U_d	overlap ratio
U	specific energy (J/mm^3)
V_b	percentage volume of bond material
V_g	percentage volume of grains
V_p	grinding wheel porosity percentage
V_{tr}	traverse speed of diamond dresser (mm/min)
V_w	workpiece speed (mm/min)
V_s	grinding wheel speed (mm/s)
v_s	wheel speed (m/s)
v_w	workpiece speed (mm/s)
ω_s	rotational wheel speed (rev/min)

Chapter 1 Introduction

Grinding is traditionally a finishing process employed to achieve a high quality surface, in the production of components requiring smooth surfaces and tight tolerances. This is possible due to the increased number of cutting edges that are present in grinding, compared to traditional cutting processes such as turning or milling [1]. Despite its industrial importance, the productivity of grinding is comparatively less and operating costs are considerably higher compared to other machining processes. Furthermore, of all the machining processes in common use, grinding is said to be one of the most complex and least understood due to the random nature of the large number of cutting points [2]. Therefore, there is a need to improve the productivity and reduce the cost of the grinding process as well as increase knowledge on the behaviour of the process under varying conditions.

1.1 Research background and motivation

When manufacturing parts, the surface integrity is important as it affects various properties of the manufactured parts like fracture toughness, corrosion rate, stress corrosion, cracking, wear, magnetic properties and dimensional stability [3]. The surface integrity of a product also includes metallurgical changes and residual stresses which can be difficult to control as the outcome of the surface finish is determined by a high number of factors as listed below in Figure 1.1.

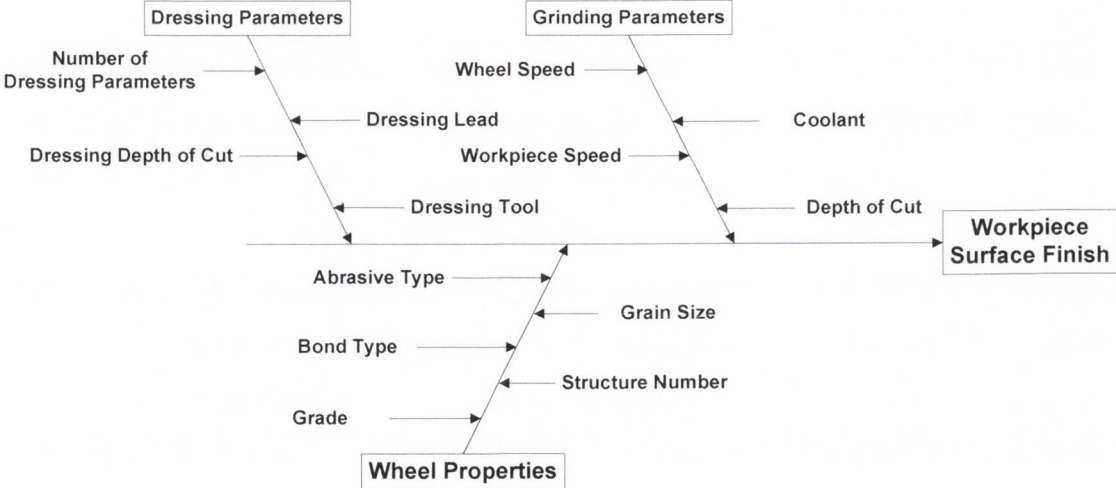


Figure 1.1: Grinding variables affecting the workpiece surface finish, adapted from [4]

One of the main processes that determine the topography of the wheel is the dressing process [5]. The dressing operation achieves two purposes. The first is to true the wheel surface to obtain profile accuracy and concentricity, while the second is to re-sharpen the grains on the periphery of the wheel to restore their cutting capabilities. Grinding wheels are usually dressed when the wheel no longer achieves the desired cutting actions and a poor surface texture is present [6]. The poor surface finish can come in the form of chatter marks through wheel loss of form leading to grinding vibration or it can present itself in grinding burn when blunt grits plough the workpiece resulting in high specific grinding energies. Conventional grinding wheels made from aluminum oxide or silicon carbide which are used for finish grinding are most commonly dressed with diamond tools. This is because diamond is one of the only materials hard enough to dress the aluminium oxide abrasive without experiencing excessive wear itself. However, over time wear of the diamond is seen and the area of contact between the diamond dresser and the grits on the wheel increases. This causes a change in the contact time between the dresser and the grinding wheel which can influence the shape of the grits on the wheel and the material removal mechanism during machining.

Traditionally natural diamond dressers have been used to dress wheels. However, recently due to the demand of high quality diamond from the jewellery trade and a shortage in supply, the cost to supply diamond for dressers has increased. As a result, companies are starting to use synthetic diamonds to dress grinding wheels which has only been employed in the last 15 years. The use of synthetic diamond dressers is quite a new approach in grinding industry when you consider that the machining process dates back to 28,000 years ago, where ground stones have been found in the far east [7]. As a result, the depth of knowledge of the use of synthetic diamonds as dressers is still quite limited. One area which needs more attention is the wear mechanisms and the wear rates of the diamonds under various conditions. Considering that natural polycrystalline diamonds begin as a near pyramid shape with a sharp point that can result in an effective width of 0.1mm, the wear of the diamond is an important factor as a wear flat can quickly develop with use, which will increase the contact time with the grinding wheel, and alter the grinding performance in terms of the forces, specific energies, temperatures, wheel wear and surface finish [8].

Natural diamond is highly anisotropic and it has been suggested that aligning the diamond in a certain direction can have a significant impact on the life of the diamond with wear rates varying by up to two orders of magnitude [9, 10]. It has been stated that below a critical load, the anisotropy of the diamond virtually disappears. However, it has not been investigated whether the effect of dressing conventional grinding wheels meet the criteria for anisotropy of diamond dressers to occur creating different wear properties depending on the direction in which the diamond is presented to the wheel. Synthetic diamonds are reported to be isotropic as the grains are uniform in size due to the controlled conditions in which the diamond is grown. However, there is little research performed on synthetic diamond dressers which confirm this and analyse the geometry of the diamond as it wears which could have a significant impact on the dressing performance.

Grinding of metals is similar to other machining processes in that material is removed through the action of a shearing process to create chip formation. In most metal cutting operations, a tool with a known geometry and orientation is used, but with grinding, numerous cutting edges of varied geometry and size are used to create the surface finish. Up to 540'000 of these grits can interact with the workpiece per second [4], this creates a smooth surface finish but due to the small depths of cut used and the nature of the geometry of the grits, there are often accompanying high grinding specific energies associated with the grinding process which can lead to workpiece surface damage [11]. The trade off between specific energy and surface finish under various dressing parameters has been well documented. However, the effect of using a different grinding wheel grit size on the specific energy and surface finish under a range of dressing conditions has not been established.

The undeformed chip thickness model is one of the main equations used in grinding calculations to predict surface roughness and specific energy values [12, 13]. The equation uses known machining parameters, wheel speed, workpiece velocity, equivalent diameter and depth of cut. However, the values used for parameters C , the cutting point density and r , the shape factor of the grit are unknown and are often estimated which can result in inaccurate theoretical values depending on the value chosen. The value of r can change considerably as different dressing conditions and

grit sizes are used. Therefore, there is a need for more accurate values r to be available for various grit sizes and dressing conditions in order to obtain more precise values.

The grinding process is a high value process where precision and high efficiency are needed to produce parts of such high quality. In order to maintain these standards, the process must be as efficient and as accurate as possible. Process monitoring can enable this high efficiency production through the avoidance of and compensation for process disturbances as well as prevention of workpiece damage [14]. Process monitoring can be used to detect tool condition, process condition, workpiece surface integrity and chatter detection [15]. Examples of sensors currently used for process monitoring include force dynamometers, accelerometers, power meters, acoustic emission sensors, thermocouples and strain sensors.

As previously mentioned, the wear experienced for natural diamond dressers can be quite severe due to their pyramid shape, which in turn, can have quite a significant impact on the grinding wheel performance. It is therefore important to monitor this wear and any subsequent change in the overlap ratio which is defined as the number of times the diamond dresser comes in contact with a point on the wheel. Changes in the dressing process can then be detected at an early stage in the preparation of the part which will avoid parts being scrapped, saving time and costs.

When monitoring the dressing process, acoustic emission sensors have been used over force sensors due to their temperature stability, high sensitivity, high dynamics, size and cost [16]. For this reason, AE sensors were used in this research to identify any diamond wear and a corresponding change in the overlap ratio. The grinding process is often monitored during cutting to assess the forces experienced on the workpiece and power consumed during the process which gives an indication of the grinding specific energy. However, it is the dressing process which precedes this process that determines the specific energy during the initial stages of cutting. Very little research has been performed which links signals monitored during the dressing process with the outcome of the grinding process. From the work that has been carried out, the authors have only looked at the dressing forces [17, 18], even though acoustic emission sensors have previously been used in the dressing process for the detection of contact between dresser and the grinding wheel, achieving wheel concentricity and determining the grinding wheel profile [15, 19-22].

1.2 Research Objectives

The aim of this research focuses on the characterisation and monitoring of dressing vitrified bonded grinding wheels with stationary diamond dressing tools. The investigations will examine diamond tool wear and its effect on the specific energy and workpiece surface finish of the grinding process. This will be achieved through the analysis of the wear of the diamond tools, monitoring of the dressing and grinding process and evaluation of the workpiece surface finish.

The objectives of the project are to:

- Study the influence of the diamond dresser orientation, grinding wheel abrasive type and tool path on the wear of both natural and synthetic diamond dressers and investigate their anisotropic or isotropic wear properties.
- Study the effect of wheel grit size and dressing a grinding wheel with a finishing pass on the surface finish of workpiece and specific energy during grinding with a range of overlap ratio values.
- Establish knowledge of more accurate values of C and r which may be used in future undeformed chip thickness model calculations.
- Investigate the use of an acoustic emission sensor to monitor the dressing process which could then be utilized to predict grinding specific energies and workpiece surface roughness values.

The wear characteristics were investigated using microscopic techniques to study the progression of the wear throughout the diamond tool life. Wear tests of each diamond dresser were performed by dressing 6000 passes of a grinding wheel using a rig which was developed from a CNC lathe. This allowed precise depths of cuts and dressing feed rates to be achieved. The grinding specific energy was investigated by monitoring the force signal using a dynamometer, which enabled tangential and normal forces to be recorded. Assessment of the surface finish was carried out using a stylus profilometer with further analysis performed using white light interferometry. An acoustic emission sensor was implemented into the dressing process to determine the dressing intensity which could then be analysed against the recorded grinding specific energy and surface finish which directly preceded the dressing process.

2 Literature review

2.1 Dressing process characteristics

2.1.1 Introduction to dressing

Grinding is used in manufacturing as a final finishing process to achieve high dimensional accuracy of the workpiece. The performance of the grinding wheel has a great influence on the quality of the part and the efficiency of the process [13]. Accurate and repeatable results are sometimes difficult to achieve, as the grinding process is influenced by so many factors as previously illustrated. One of the most important inputs to the grinding is the dressing process which prepares the wheel for grinding [23]. The purpose of dressing the wheel is to produce the correct geometrical and run-out accuracy as well as produce a micro-topography that is suitable to the specific grinding process. The wheel may also lose its form during grinding when the grits and bond on the periphery of the wheel are subject to wear over time. Depending on the severity of the grinding process, this wear can develop into macro-wear, where the shape of the tool is altered and no longer matches the profile of the workpiece. Alternatively, the wear experienced is micro-wear, whereby changes in the topography result in the wheel being either too smooth or too rough for the grinding task.

Preparation of the wheel also encompasses balancing which aims to compensate for any imbalances in the wheel, that could have been created during the manufacturing process, from previous grinding processes or a positioning fault when mounting the wheel onto the spindle of the grinding wheel [24]. The other processes involved in preparing the wheel are termed conditioning. Conditioning of the wheel involves three steps, profiling, sharpening and cleaning, where profiling and sharpening come under the general term of dressing as illustrated in Figure 2.2. Due to the porous nature of conventional vitrified bonded wheels, the term dressing is used to describe the preparation process of these wheels and encompasses both the profiling and sharpening of the wheel at the same time.

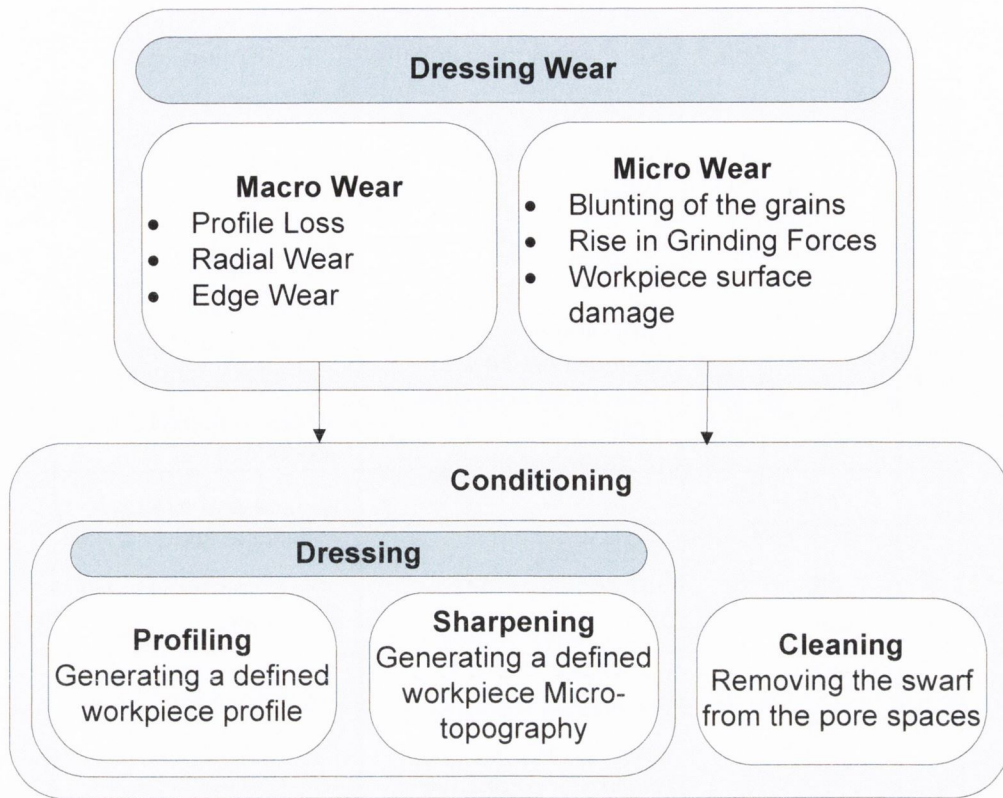


Figure 2.2: Grinding wheel wear which is preceded by wheel conditioning, adapted from [25]

2.1.2 Diamond dressers

The dressing process is carried out with the use of a tool known as a dresser. These come in the form of either a stationary or rotary tool. Stationary dressing tools have no movement in the circumferential direction and travel by an axial movement along the outer edge of the grinding wheel. They are most suited to dress straight or cylindrical wheels, or wheels containing a single profile. The main use of stationary dressers would be dressing conventional aluminium oxide and silicon carbide wheels. As only a small amount of diamond is present in each stationary tool, using them to dress CBN or diamond wheels may not be suitable due to the wear that would occur.





	dressing tool	grinding wheel profile	application
single-layered	single-point diamond 	rectilinear (cylindrical, taper) single-profile (convex and concave radii)	surface, cylindrical and centreless grinding single and small batch production
	profile diamond 	multi-profile (complex profile with steep sides and close radii)	surface, external cylindrical and centreless grinding single and small batch production
multilayered	multi-point diamond 	rectilinear (cylindrical, Taper)	surface and external cylindrical grinding single and small batch production
	dressing blade 	rectilinear (cylindrical, taper) single-profile (convex and concave radii)	surface, external cylindrical and centreless grinding single to mass production

Figure 2.3: Different stationary dressing tools

Rotary dressing tools have an additional movement of rotation as they traverse across the edge of the wheel. As rotary dressers have a layer of diamonds on the periphery of the wheel, they encounter much less wear than stationary diamond dressers. This enables the diamond roller to maintain its shape for longer, which results in the grinding wheel keeping its desired geometrical and dimensional accuracy for a greater period of time after dressing. Common rotary diamond dressers are diamond profile rollers, diamond form rollers and diamond cup wheels as illustrated in Figure 2.4.

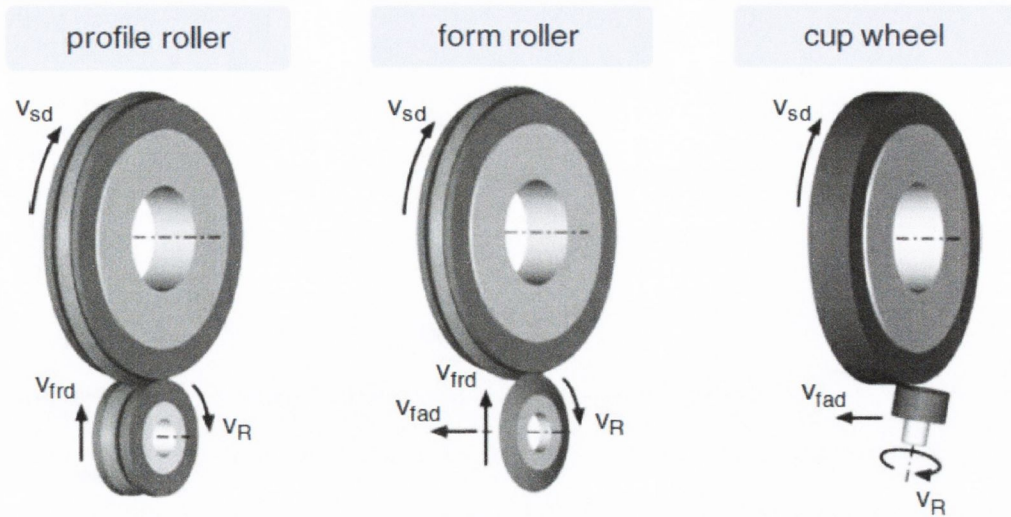


Figure 2.4: Different types of rotary dressers [26]

It is the relative motion of the diamond with the wheel, the characteristics of the wheel and the shape of the diamond that determine the wheel topography. In earlier research, the dressing process was described as a wheel cutting process whereby the dressing tool moves across the wheel surface with a dressing overlap ratio, U_d and a dressing depth of cut a_d as described in Figure 2.5 [27, 28].

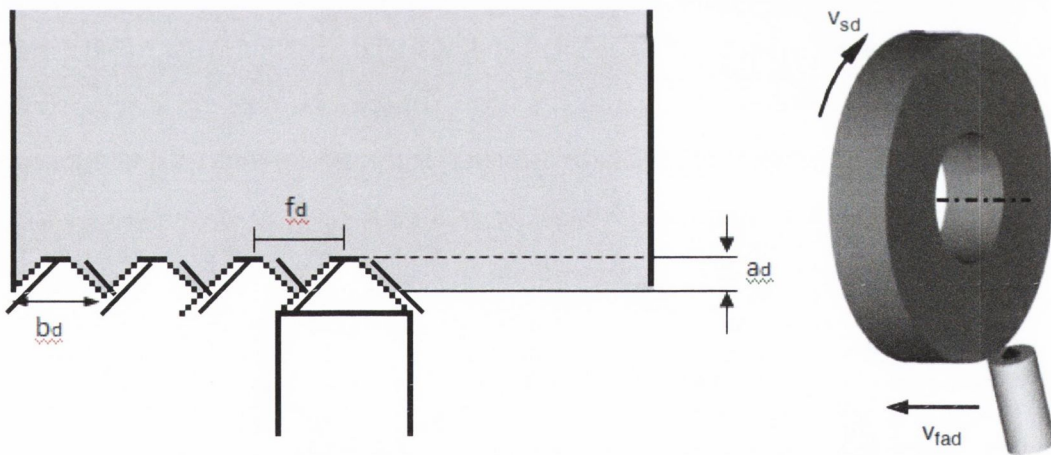


Figure 2.5: Dressing overlap ratio and process kinematics

The overlap ratio is the most important parameter in determining the outcome of the wheel topography [29]. It is defined as the width of contact over the truing lead or the distance the dressing tool moves per wheel revolution. It gives an indication as to how many times a point on the grinding wheel is engaged with the dressing tool. The lower

limit of the overlap ratio is one whereby each point on the wheel is engaged with the diamond dresser once. The overlap ratio value is given by Equation 2.1:

$$U_d = \frac{b_d}{f_d} \quad (2.1)$$

Where: b_d = width of diamond in mm

f_d = axial feed of diamond cutting point per rotation of grinding wheel

The overlap ratio is a comprehensive parameter which connects diamond shape to the dressing kinematics. However, as reported by Linke, the diamond shape is not a completely controllable and stable output, due to wear that occurs throughout its tool life [30]. The grinding process is also influenced by the dressing depth of cut, however to a much lesser extent than the overlap ratio with only a slight increase in the cutting point density seen with an increase in the depth of dressing [31]. However, it is important that a sufficient depth of cut is used in order to remove any wheel loading caused by previous grinding operations [32].

2.1.3 Material removal mechanisms during dressing

In theory, the mechanisms involved in the dressing process include grit breakage, grit pull-out and attritious wear of the grits as illustrated in Figure 2.6 [33]. These mechanisms will vary depending on the dressing parameters. Fine dressing operation refers to the combination of a small dressing lead and a small dressing depth. Conversely, a dressing operation with a large dressing depth and a large lead is described as a course dressing operation [34].

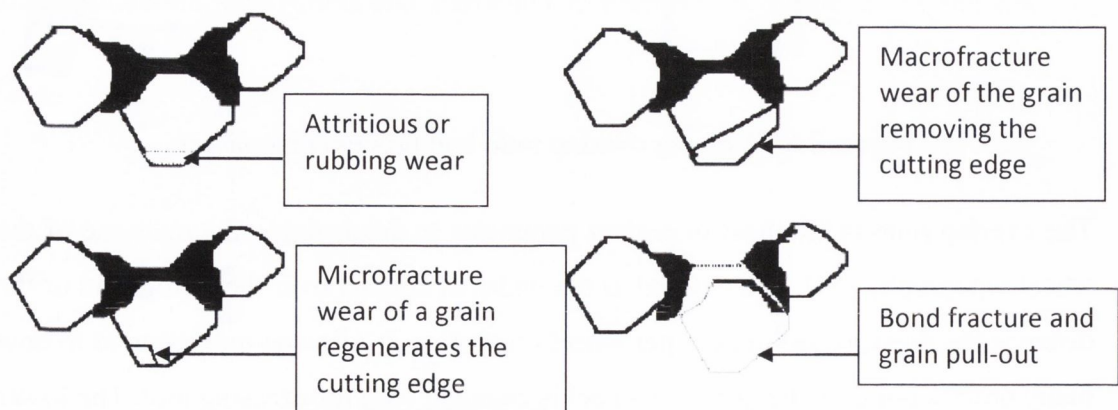


Figure 2.6: Dressing mechanisms

After a wheel has been dressed, a pattern based on the grain cutting theory is created on the wheel topography. This pattern is then transferred onto the workpiece surface during grinding. The maximum peak to valley height of the profile is based on the diamond tip angle, θ and also the diamond dresser feed rate, f_d as illustrated in Equation 2.2 [28].

$$R_{pv} = \frac{f_d}{2 \tan(\frac{\theta}{2})} \quad (2.2)$$

According to this equation, the overlap ratio and the shape of the single point diamond are particularly important in the generation of the desired wheel topography and workpiece surface finish. Bhateja [35] recorded wheel and workpiece profiles by stylus measurement. Dressing features clearly appeared on the workpiece surface but could not be detected on the surface of the wheel. The suggested reason for this was due to the roughness of the wheel being greater than the grooves on the wheel created by the dressing process.

Malkin [17] studied the size distribution of particles from the wheel after the dressing process. It was reported that the particles removed were finer than the original grain, but much bigger than the dressing depth of cut and that a harder wheel also gives finer dressing particles. Therefore, it would imply that the mechanism for removal would be grain fracture, followed by bond fracture, with a harder wheel retaining the grains better, resulting in a greater degree of grain fracture (fragmentation), prior to dislodgement of the grit. Abundant cracks could be found on the grain bond of the dressed wheel surface, which supports the conclusion that dressing is a fracture process of abrasive grains and bond. Bhateja suggested that the dressing process consisted of a macro and micro action, whereby the macro cleaves the grains or breaks the bond between them, owing to the gross characteristic of the wheel surface [35].

2.1.4 Effect of dressing parameters on grinding wheel performance

It has been reported by a number of authors that dressing the wheel with small dressing lead and a small depth of cut produces a wheel with a high density of blunt cutting points [6, 8, 36-40]. This type of grinding wheel topography results in high cutting forces, increased workpiece temperature, good surface finish and low wheel wear rate.

Ishikawa [36] looked at the effect of truing depth on the grinding power consumption, surface finish and radial wheel wear. It was noted that as the truing depth increased, the power consumption decreased and the surface roughness increased. This is due to the greater depth of cut causing macro fracture of the grits, creating a sharper wheel topography. While wheel wear increased slightly, as the exposed sharp grits are more likely to fracture at a lower force compared to worn or dull grits. The effect of truing lead on power consumption, surface finish and wheel wear was also studied. It was noted that as the truing lead increases, the power consumption decreases and the surface finish decreased. This occurs because, with a slower truing lead, the grits on the wheel will become dull as the diamond dresser comes into contact with the grit more often, causing abrasive wear on the wheel.

Davis [41] reported the same phenomena while dressing diamond resin bonded wheels, with a small depth of cut which the author defined as “fine dressing”. Unlike conventional aluminium or silicon grinding wheels, the grits did not pull out due to the strength of the bond structure in the diamond abrasive. This created a glazed surface on the wheel whereby the bond material and diamond grits were on the same plane (Figure 2.7)

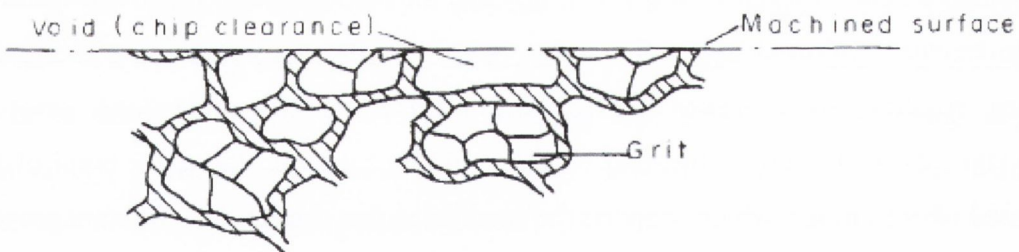


Figure 2.7: Diagram showing bond and grit materials on the same plane due to strength of bond structure

The wheel would now have a high dimensional accuracy, however it would not be possible to achieve high removal rates, as a large material removal rate would cause the wheel to become loaded as the wheel would have no exposed grits.

Davis also observed that increasing the dressing depth of cut made the wheel more open, which allowed for clearance of the grits with a higher removal rate. However

this resulted in greater damage to the bond and grit during the initial stages of grinding, which caused high wheel wear leading to dimensional inaccuracy of the wheel.

Brinksmeier [42] looked at the number of collisions between the diamond dresser and the grits on the wheel, by building a mathematical model based on the dressing parameters and wheel characteristics. They found that high collision numbers caused blunting of the wheel, which lead to increased forces during grinding.

Patterson and Chisolm [43] performed tests whereby the feed and depth of cut was changed. They observed that the coarser the dressing feed, the greater the initial wheel wear as can be seen in Figure 2.8.

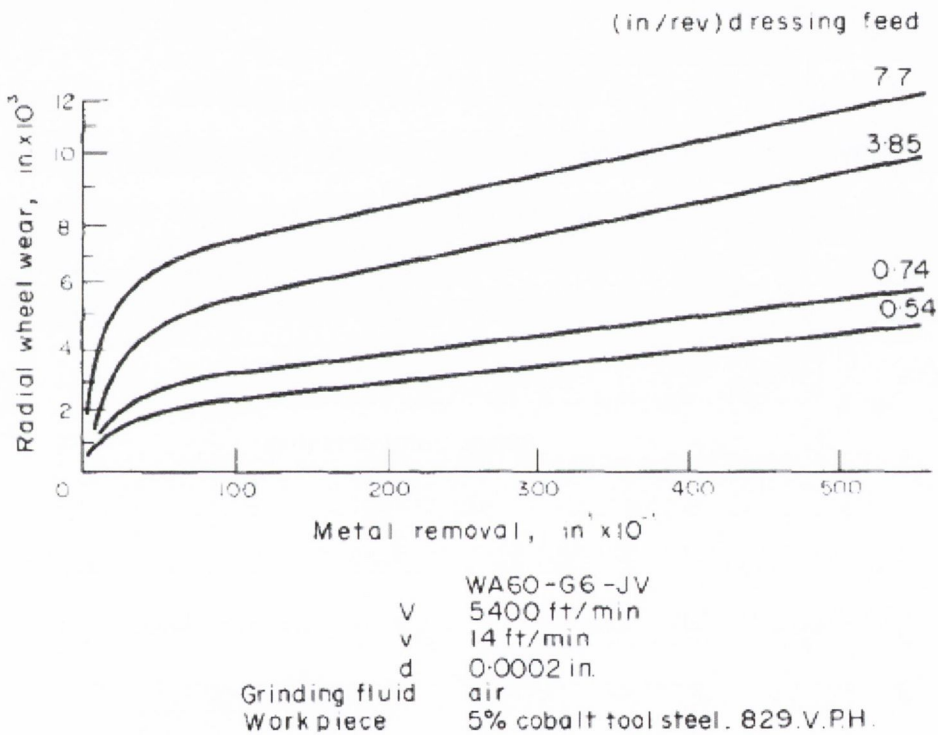


Figure 2.8: Graph of initial wheel wear versus dressing feed

Marinescu *et al.* [33] reported that dressing the wheel with a single point dresser usually resulted in the particles being small, compared with the original abrasive grain size. To protect the wheel structure, maintain its integrity and obtain the maximum life of the grinding wheel, it was reported that the optimum dressing depth of cut should be smaller than the abrasive grit size.

Puerto *et al.* [44] looked at the radial wear when grinding after dressing for various dressing leads and depths for “soft” and “aggressive” grinding conditions. It was found

that the radial wear of the wheel only increased by 5 microns from 24.6 to 29.2 at “soft” grinding conditions with a decrease in the dressing feed from 400mm/min to 100mm/min at 10 microns. Whereas the radial wear increased to 202 and 269 microns when aggressive grinding conditions were used after dressing the wheel with a feed of between 100mm/min and 400mm/min. Therefore, it is seen that the radial wear of the grinding wheel is influenced mainly by the grinding conditions used and not the preceding dressing conditions.

Malkin studied the effect of the dressing parameters on the grinding performance and also the related Ra workpiece surface finish value. It was found that a trade off relationship could be established between the grinding energy and surface finish whereby larger specific energies resulted in smoother surface finishes for higher overlap ratio values (Figure 2.9). Whereas low overlap ratios produced rougher surface finishes created with lower grinding specific energies [45]. However, despite this relationship being well established, the effect of different grinding wheel grit size on the trade off between specific energy and surface finish has yet to be considered.

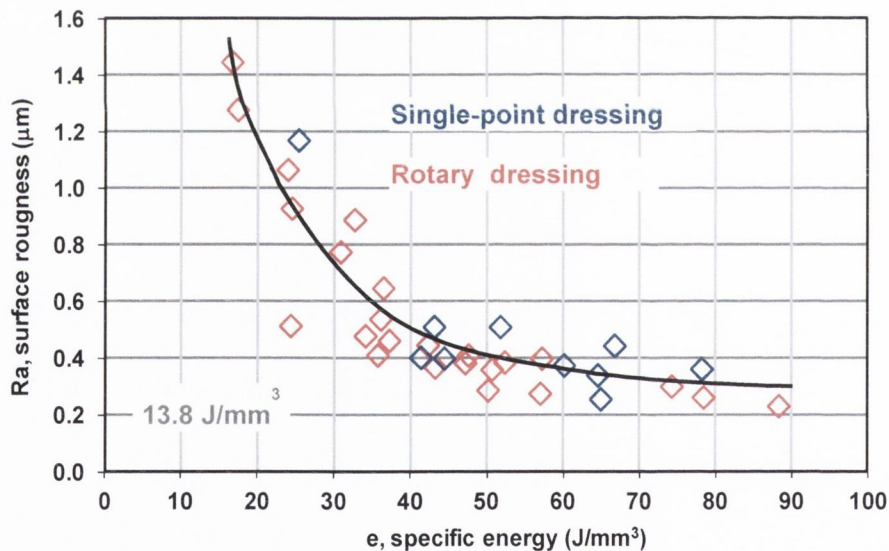


Figure 2.9: Trade off in the relationship between specific energy and surface roughness at different overlap ratio values for single point and rotary dressing, adapted from [45]

On average, only 10% of the active volume of the wheel is worn away by grinding, the remaining 90% is removed by the wheel conditioning operation [33]. Therefore it is

important that the dressing parameters, depth of cut, feed rate and number of dressing passes are fully understood, in order to achieve the desired grinding wheel conditions without consuming too much of the wheel.

Sharper wheels usually have a higher material removal rate, lower grinding forces and power consumption [46]. Higher material removal rate will allow the part to be made in a shorter time frame. Low grinding forces will result in less wear of the wheel as threshold forces for grits breakage and pull are not achieved but, conversely microfracture and dulling of the wheel occurs. Lower forces also result in less specific energy and reduce the risk of thermal damage to the workpiece [47, 48].

2.1.5 Shape of dresser

A number of other factors affect the dressing performance of the wheel. One of the most influential is the diamond shape as reported by many researchers [49-51] which has a significant effect on the stability of the dressing process. As a single point diamond is used over time, wear begins to develop on the tip of the diamond, resulting in a larger dressing effective width, b_d . As Malkin stated, this reduces the localized stresses as it cuts into the abrasive grain. In theory, this should increase the dressing force and the occurrence of bond fracture, instead of grit fracture, which would result in less active grains. However, it was found that the wheel dulled as the grits on the surface plastically deformed, instead of fracturing at the grain tips. This can lead to varying wheel sharpness levels, depending on whether the prevailing dressing mechanism is macrofracture or attritious wear of the grits. Fracture of the grits would make the wheel sharp while plastic deformation would cause the wheel to become dull. Therefore there is, an uncontrolled variation in the wheel topography depending on the grit removal mechanism used during dressing [17].

Matsui *et al.* looked at the effect of dresser type on the surface topography and performance of the grinding wheel. Their attention focused on single point and impregnated diamond dressers, no tests were performed on synthetic diamond. The wheel topography was measured by taking a replica of the wheel and measuring the surface finish using a stylus, grinding forces were also measured after dressing with both a worn and sharp diamond dresser. It was found that dressing the wheel with a sharp dresser produced a rough surface finish on the wheel and lower grinding forces

[52]. Koziarski looked at the effect of the worn dresser which was characterized by the diamond nib abrasion width. Tests were performed with two diamond dressers, one having a width of 0.1mm and the other 0.5mm. The cutting surface of the grinding wheel was then assessed by measuring the number and height of static edges on the surface using a profilometer. It was found that dressing the wheel with a small diamond width resulted in more static edges with a greater height, indicating a sharper wheel, while a wheel dressed with a larger diamond width resulted in more static edges with a lower height [53].

Scott and Baul investigated the effects of dressing tool shape on the wheel surface topography. Three dressing tools were used, two single point diamond dressers with a wear flat area of 0.14mm² and 1mm² and one multi point diamond dresser. The surface of the wheel was measured after dressing using a stylus profilometer. They found that the main dressing mechanism occurring was bond post fracture with the small single point dresser, predominately grain fracture with multi point dresser and grain fracture and grain smoothing with the larger single point diamond. They investigated the grain cutting theory and found that the predominant frequency cut into wheel did not exist on the workpiece surface. Only when one dressing pass was used, could the dressing tool path be detected on the surface [54].

2.1.6 Number of dressing passes

The number of dressing passes depends on the level of loading present in the wheel, the size of grit and the depth of wear pattern to be removed [55]. Usually the effects of previous dressing passes and grinding conditions can be eliminated in three or four dressing passes. A final spark out pass can also be taken where the depth of cut is not incrementally increased into the grinding wheel. Each spark out pass, results in less material being removed which results in a finer wheel topography. However, unnecessary dressing passes, beyond the desired wheel topography results in a reduction in the wheel diameter and wheel loss, leading to frequent wheel changes and increased manufacturing costs, as well as unnecessary wear of the diamond dresser.

The dressing process requires a break in the grinding production, in order to sharpen the wheel. This comes at an added cost, as the machine requires downtime leading to longer production times. The dressing interval depends on the wheel chosen, the

material being ground and the grinding parameters. To reduce non machining time, the method of continuous dressing was introduced [37]. By using this method, the wheel remains sharp and a high material removal rate is achievable for hard to grind materials. Diamond dressing rolls are generally used compared to single point diamonds. However, continuous dressing can come at a cost, as a high rate of wear can occur on the diamond dresser with continued use [32].

In an ideal grinding operation, a grinding wheel would retain its true form and re-sharpen itself fully as it breaks down due to the friable grains on the wheel surface. With conventional vitrified bonded wheels, self-dressing may be performed by increasing the removal rate, which increases the normal forces on the grinding wheel resulting in bond fracture. However, the increase in removal rate may result in larger specific energies, leading to thermal damage of the workpiece. Alternatively, the wheel can dress itself as the grains become dull and fracture which exposes a new cutting grain. Both of these methods require the normal grinding force to reach a certain level. This normal grinding force (F_n) is dependent on the ratio of the peripheral surface speed of the wheel (v_s) and the workpiece material removal rate (Q_w) given by Equation 2.3.

$$F_n = K \cdot \frac{v_s}{Q_w} \quad (2.3)$$

Where K is a constant which depends on the workpiece material and the sharpness of the grains.

However, what is most often seen is dulling of the grits as the wheel fails to achieve this self-dressing process. Manual dressing of the wheel would then have to be performed. This can be caused by performing an operation with a low removal rate to achieve a low roughness value on the workpiece material. Alternatively, it can occur when the wheel in use is one or two grades too hard for the workpiece material being ground or the removal rate. With dulling of the grits and continuous grinding, the wheel can become glazed and wheel loading occurs. This happens when some of the material being cut becomes compressed and embedded into the spaces around the active grits. As a result, a reduction in the chip space is seen, which can decrease the cutting ability of the wheel. Subsequently, this can increase grinding forces and may reduce the surface roughness of the material [56]. These high forces can lead to problems such as

wheel loading and vibrations. It has also been found that the wear of the dressing diamond is higher during dressing of a loaded grinding wheel.

The loading of a wheel is highly influenced by the choice of material to be ground and the grinding parameters. Ductile materials such as aluminium or titanium alloys would cause a high degree of wheel loading under certain grinding conditions. The use of a water based coolant over a grinding oil coolant can also result in greater wheel loading.

The decision to dress a wheel is either based on a certain time period and is performed periodically, based on previous understanding of the grinding process or the wheel can be decided to be dressed by monitoring the workpiece surface, forces and power consumption of the machine and dressing will commence once one of these features exceeds or reaches a certain threshold [33].

2.2 Grinding process characteristics

2.2.1 The grinding wheel

The behaviour of the grinding wheel depends not only on the dressing conditions but also on the composition and structure of the grinding wheel. The structure of the grinding wheel comprises of grains, bond material and pores as shown in Figure 2.10. The grains are the abrasive material on the surface that cut the workpiece, with each grit in a grinding wheel being equivalent to the cutting tool in a lathe. The grains are held together by a bond material and the spaces in between the grain and bond structure is known as the porosity. These spaces are important in order to deliver coolant to the workpiece and to provide space for chip formation [57].

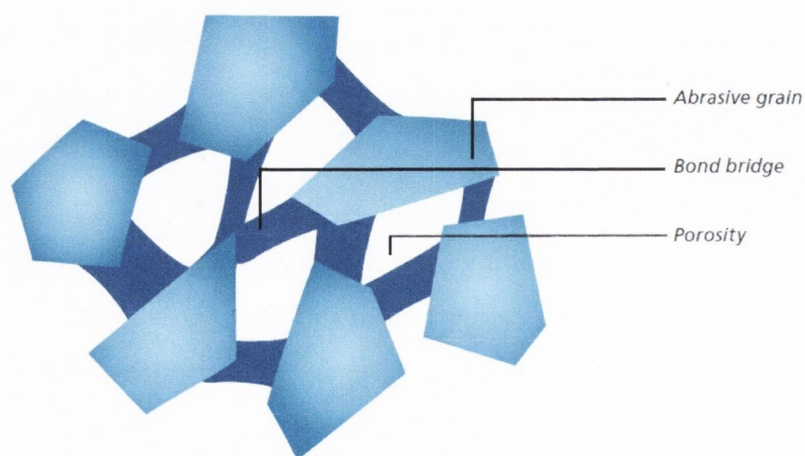


Figure 2.10: Diagram showing the structure of a grinding wheel [57]

The structure of the wheel comprises of the following equation:

$$V_g + V_b + V_p = 100\% \quad (2.4)$$

Where V_g represents the volume of grains present, V_b represents the volume of bond material and V_p represents the porosity. When a smaller volume of abrasive grains or bond material is used, the result is increased porosity which weakens the structure. On the other hand, increasing the volume of grains or bond material in the grinding wheel would strengthen the structure. Therefore, the composition of the material has a direct relationship on the wear behaviour of the wheel during grinding. In order to specify the characteristics of a grinding wheel, a notation is used to identify the following characteristics [58]:

- i) Abrasive type
- ii) Abrasive grain size
- iii) Hardness grade of the wheel
- iv) Structure of the wheel
- v) Bond material

An example is given below in Figure 2.11.

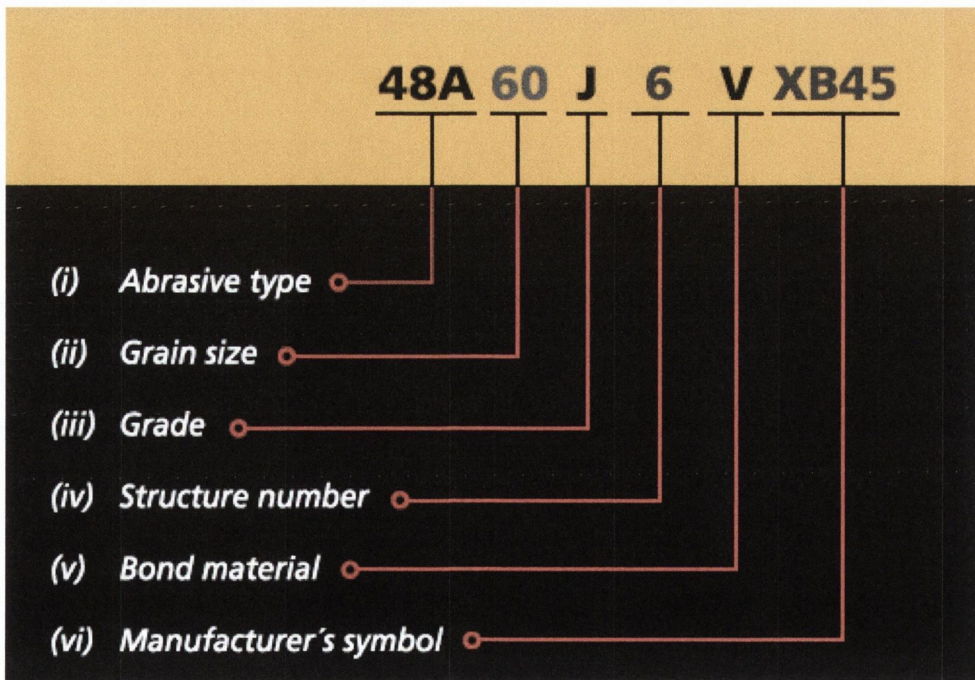


Figure 2.11: Grinding wheel notation [57]

There are four main types of grits: CBN, diamond, aluminium oxide and silicon carbide. CBN wheels are used to grind high speed steel and high alloy steels. It is impact resistant and chemically less active compared to diamond. CBN would be used to grind ferrous materials over diamond due to the reaction of ferrous materials with Carbon at elevated temperatures, which can be experienced during grinding. Diamond is generally used to grind hard materials such as tungsten carbide, stone and glass [59]. Aluminium oxide and Silicon Carbide are referred to as conventional abrasives. Aluminium oxide wheels would be used to grind high tensile strength materials such as steels and ferrous metals. While Silicon Carbide abrasives are more friable and are used for grinding cast iron, non ferrous and non-metallic materials. Grits come in various sizes ranging from 10-600 with coarse grits used for aggressive stock removal having a low number [60]. While grits with a higher number have a very fine grit with which very little metal would be removed and a lower Ra surface roughness value could be achieved. Investigations performed by Demir *et al.* show that surface roughness and grinding forces increased with an increase in the grit size [61].

The grade of a wheel can be defined as the amount of bond material, relative to the amount of abrasive which indicates the strength of the bond structure. It is rated on a scale of A – Z with A being the weakest bond and Z being the strongest. In terms of vitrified bonded wheels, the grade refers to the relative fraction of bond material and porosity in the wheel. A weak bond is preferred for grinding harder materials in order for new chips to be exposed once they become blunt. While a stronger bond is preferred when grinding softer materials. It is important to choose the correct grade, as a bond which is too strong for a material may lead to dull grits, which in turn could cause burning of the workpiece. Tests performed by Kaiszer and Singhal indicate that a wheel with a higher grade would produce a better surface finish of the workpiece. Sailini carried out tests along with Kaliszer who found that a higher grade wheel produced greater forces. This was attributed to the wear flats that were created over time as the grits remained in the wheel due to the strength of the bond material.

The structure of a wheel can be described as the spacing between the abrasive grains. The higher the structure number, the more open the wheel, which would imply that less grits are involved to do the work. An open structure would be 12 or higher while a closer structure would be 6 or lower. An open structure would consist of less grits,

while a closer structure would have a higher density of grits. Open structure wheels allow for greater chip formation and a flow of coolant to the part being ground. They should be used when high volumes of material are required to be removed.

2.2.2 Grinding forces

Measuring grinding forces is one of the most valuable ways to evaluate the grinding forces. Forces in grinding are created from the interaction of the grinding wheel and the workpiece. Grinding forces are dependent on the grinding parameters chosen and the condition of grinding wheel [62]. The forces can be broken down into three components, the tangential F_t , the normal force F_n and a component force acting along the direction of longitudinal feed, this force is usually ignored due to its insignificance when analysing the grinding process [17]. The normal and tangential forces are made up of chip formation forces, F_{tc} and F_{nc} and friction forces F_{tf} and F_{nf} as shown in Figure 2.12 [63]. The tangential forces generally influence the specific energy, the power consumption of the machine and the life of the wheel, while the normal force acts to engage the wheel with the workpiece and affect the surface deformation and the roughness of the wheel. Whereas normal forces affect the surface deformation and roughness of the workpiece. As a result, high normal forces may cause part problems, such as chatter while high tangential forces can cause heat generation and thermal damage [25]. Measuring grinding forces gives a great insight into the condition of the grinding wheel and this method is used in this research work for assessing the condition of the wheel after the dressing process [64].

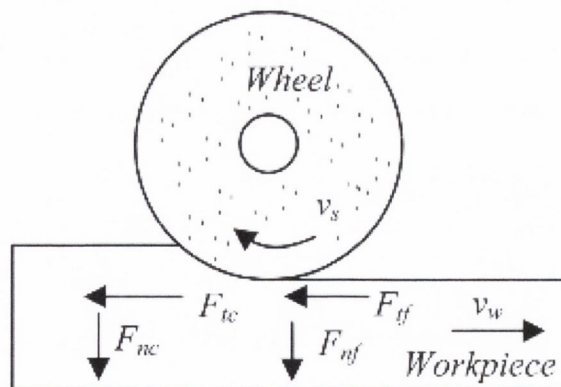


Figure 2.12: Diagram of the principle grinding forces [63]

Grisbrook *et al.* studied the grinding forces for the whole tool life of the grinding wheel between each dressing process. The change in forces observed can be divided into four stages [65]. The first stage involved a rise in the forces and a steady state was reached once the tool is fully engaged with the workpiece, which has previously been observed [43, 66]. In the second stage, forces are seen to remain constant. Depending on the bond strength of the wheel, self dressing may occur when the grits become dull and forces rise above the bond strength. If the bond strength is too strong for the particular grinding conditions, stage three occurs, where there is a progressive build up of forces and grinding power. During this stage, the attritious wear on the grit cause the grits to adopt geometries and shapes which are difficult to fracture, and as a result, the number of fractures decrease and the grits become dull. The resultant effect is an inefficient grinding process, where rubbing and ploughing dominate the grit removal mechanism and the forces rise. The final stage occurs when the forces rise significantly and vibrations become evident in the machining process. At this stage, continuation of grinding would be detrimental to the part as the forces experienced would result in the onset of grinding burn.

2.2.3 Mechanics of grinding

Grinding is typically characterised by the multiple random cutting edges with large negative rake angles removing small chips at a high removal rate. In order to understand the forces and surface finish created by the process, it is important to understand the mechanisms of the formation of these chips. The engagement of each active cutting edge with the workpiece can be divided into three successive stages friction, ploughing and cutting as shown in Figure 2.13. In phase 1, the grain comes in contact with the grit and causes elastic deformation of the material. As the grain continues to travel, plastic deformation occurs and the normal forces increase. In phase two, when the normal force between the cutting edge and the material exceeds the yield stress of the material, the cutting edge penetrates the materials causing plastic deformation. While in phase three, the actual chip removal takes place when the grit reaches a critical depth of penetration and the workpiece material piles up to the front and to the sides of the grain to form a groove. A chip is formed when the workpiece material can no longer withstand the tearing stress. The critical depth for chip formation depends on the grain geometry, material properties, type of coolant and

grinding conditions [12]. The chip formation process is called cutting. Cutting is considered to be the most desirable process in terms of producing an efficient material removal process. Whereas rubbing and ploughing are considered inefficient as energy is wasted in deformation and friction as material flows to the sides of the engagement zone, without contributing to material removal.

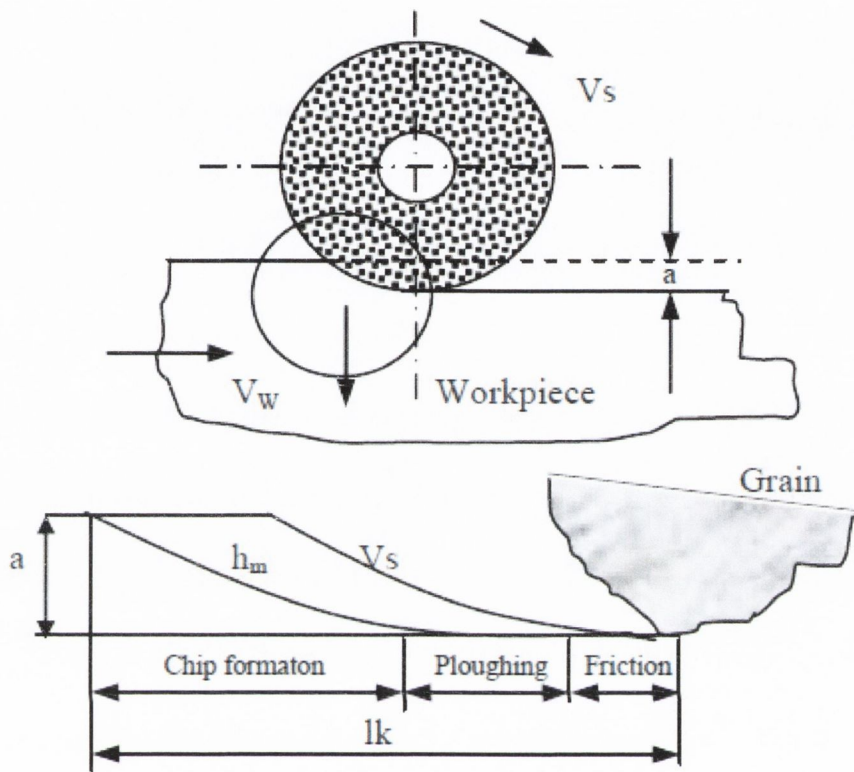


Figure 2.13: Chip formation in grinding [28]

The chip formation and material removal process depend primarily on the microstructure of the grinding wheel, the workpiece material and the grinding kinematics. Figure 2.14 shows a flowchart of the parameters controlling the chip formation. It can be seen that the grinding kinematics, workpiece and grinding topography all have an impact on the chip formation, which affect the surface roughness, grinding force and wheel wear [67].

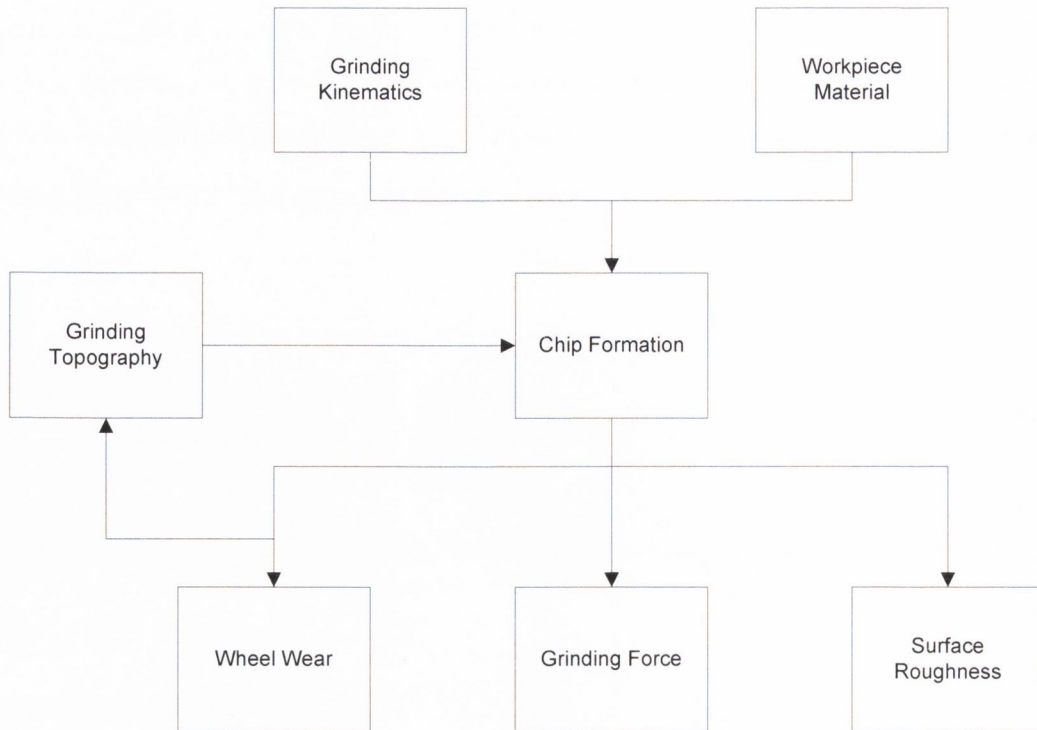


Figure 2.14: Factors affecting chip formation in grinding

One of the main equations used in grinding is the chip thickness model. The model takes into account the microstructure of the grinding wheel given by the grain geometry and the static grain density in terms of the radial depth into the wheel [12]. It gives an indication of the single grit interaction and has a direct influence on the modelling of process variables such as power consumption and surface roughness. As described by Malkin [17], the model is based on an idealised grinding wheel with cutting points uniformly distributed over the wheel surface. Therefore, the value calculated corresponds to an average undeformed chip thickness. The chip thickness value is reported to have a direct relationship with the specific energies experienced in grinding, where thicker values correspond to chip formation, and a lower specific energy, while shallower values result in ploughing of the material and create higher specific energies as illustrated in Figure 2.15.

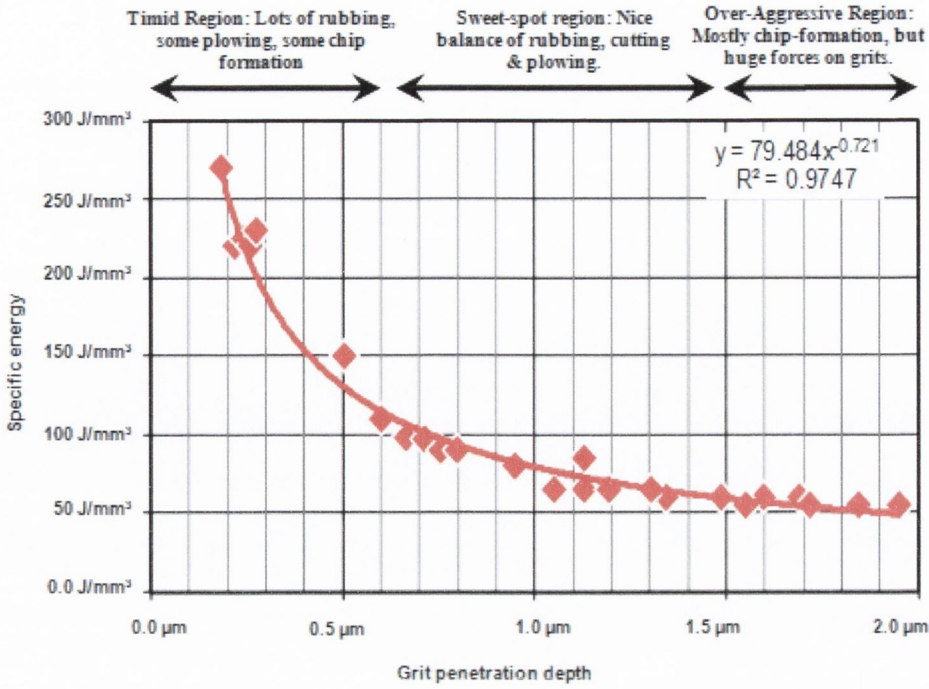


Figure 2.15: Graph of the specific energy vs. the grit penetration depth [68]

A large amount of friction occurs between the individual grains and the workpiece which is converted to heat. Figure 2.16 shows the distribution of the heat for a single grit. As is evident, most of the heat flows into the workpiece, while a small portion flows into the chips and the surroundings such as the coolant, lubricant and atmosphere. This temperature increase can cause thermal damage in the workpiece such as thermally induced residual stresses, structure changes or cracks.

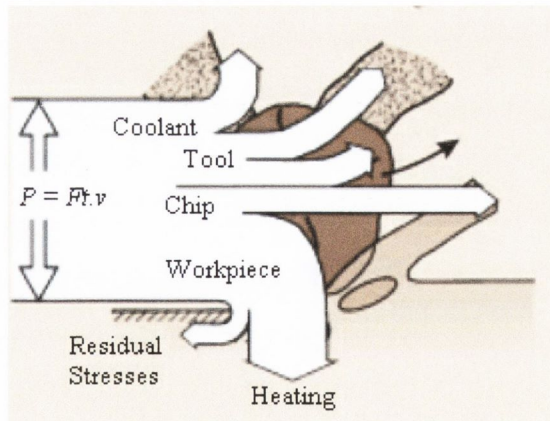


Figure 2.16: Distribution of heat from a single grit, adapted from [69]

2.2.4 Specific energy in grinding

As mentioned, the specific energy which is defined as the energy expended per unit volume of material removed is a fundamental parameter for characterising the efficiency of the grinding process. It is the calculation of the grinding power (in watts)/Material Removal Rate (in mm³/s) as shown in Equation 2.5:

$$e_c = \frac{F_t v_s}{v_w ab} = \frac{P}{Q_w} \quad (2.5)$$

Where the numerator, P is the power and the denominator, Q_w is the volumetric removal rate which is calculated based on the grinding parameters.

The specific energy in grinding is much higher than conventional cutting processes such as turning and milling. Shaw reports that typical specific energies for turning of steel lie in the range of 3 – 9 J/mm³, whereas specific energy values of 14 - 69 J/mm³ were experienced when grinding steel [70]. While Posinasetti claims that the specific energy in grinding is higher than single point dressing processes by a factor of 10 [71].

In conventional cutting processes, the cutting tool has a defined geometry and a positive rake angle which results in shearing of the workpiece material and reduced friction between the tool and the workpiece [72]. Whereas in grinding, the cutting tool is made up of random cutting edges with highly negative rake angles [17, 73]. Graham and Baul state that the average effective rake angle of the grain could be expected to lie within the range -45° to -75° [74]. This would result in high shear strains, friction and plastic deformation of the workpiece material.

Another important phenomenon contributing to high specific energies in grinding is the size effect. This was first discussed by Backer, Marshall and Shaw [75] who found that the specific energy became much larger when the undeformed chip thickness was decreased with a reduction in the material removal rate of the grinding process. The size effect is the energy dissipation between a combination of ploughing, sliding and chip formation mechanisms as a result of the interaction between the abrasive grain and the work surface. Malkin summarised the mechanisms into specific chip formation energy, specific sliding energy and specific ploughing energy as illustrated in Equation 2.5. Specific chip formation energy is the minimum grinding energy required to removed a chip. Specific sliding energy is expended due to sliding action of dulled flattened grits against the workpiece surface. Specific ploughing energy is the energy

expended when the cutting edge of the grain first makes contact with the workpiece, and before the chip formation process, plastic flow or ploughing of the material occurs whereby material is displaced to the sides and beneath the cutting edge. The energy that is expended due to the ploughing contributes to the overall ‘size effect’ of the specific energy [76, 77].

$$U = U_{chip} + U_{plough} + U_{rub} \quad (2.5)$$

2.3 Process monitoring in grinding

Process monitoring in grinding can be divided into two main signal types, process signals and output signals. Process signals when monitoring an operation may include forces, power, temperature, acoustic emission and vibration [78, 79]. These can all provide valuable information on the state of the grinding operation in terms of wheel condition, process parameters such as grinding vibration, burn and chatter. Output signals in grinding include information on the parts integrity and surface finish and also the condition of the wheel.

Research and development of process monitoring is constantly seeking to optimise process parameters that allow increased productivity, quality and economics in manufacturing [22]. Process monitoring in grinding is helping engineers to produce higher quality surfaces and a repeatable grinding process [79]. This is especially true for dressing of the grinding wheel to ensure that effective conditioning is taking place [23].

2.3.1 Acoustic emission sensors

Acoustic emission sensors are the preferred choice of sensor to monitor dressing over other sensors such as force and power monitors due to their temperature stability, high sensitivity and high dynamics. A diagram of aforementioned sensors and the level of precision to be achieved through process monitoring is shown below. As can be seen in Figure 2.17, AE sensors are highly desirable for precision manufacturing due to their sensitivity and signal to noise ratio, with levels of AE being detected at extremely low depths of cut. In grinding, this is particularly useful as even though chip formation may diminish due to wheel-workpiece interaction, rubbing and ploughing of the grits on the surface can still be detected [80]. Another advantage of AE is that it tends to propagate

at frequencies well above the characteristic frequencies attributed to machining, such as spindle RPM which minimizes the inclusion of noise into the signal. However, it is important to note that the boundaries for each sensor type may change as continuous improvement of sensor technology will allow sensors to cover a wider range of parameters with increasing sensitivity.

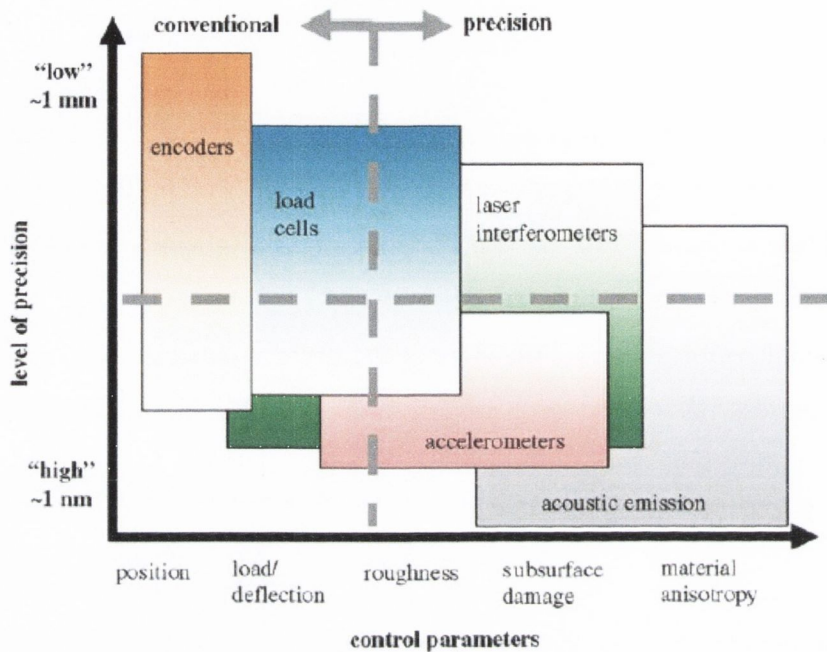


Figure 2.17: Sensor application vs. level of precision and control parameters [80]

Furthermore, AE sensors are easy to mount due to their size and are inexpensive compared to other monitoring devices [81]. Hence, a number of researchers have used AE sensors to monitor dressing, which include detecting dresser-wheel contact, monitoring dressing depth and dressing lead, diagnosing dressing faults and determining when to complete the dressing process [19, 21, 22, 82]. There are limiting factors to the use of AE sensors, which include damping of the AE signal, frequency dependent speed and reflection of the waves as they propagate through the material [83]. Therefore placement of the sensor is of great importance and changing the location of the sensor during experiments may lead to varying results.

Hundt *et al.* identified the sources of AE in grinding (Figure 2.18) and stated that every single grain contact generates a stress pulse in the workpiece. The aim of their work was to develop a monitoring strategy to analyse every grain contact and identify its condition in terms of wear.

Further investigations also looked at identifying the grit removal mechanism and to distinguish whether it was bond fracture, grit fracture or pullout. Individual contacts could be identified in the AE signal when using a modified tooth shaped grinding wheel with each tooth representing one large grain. However, due to the high frequency of contacts between the grains and the workpiece and the large amount of data processing, the process at the time was said to be not suitable for workshop conditions [83].

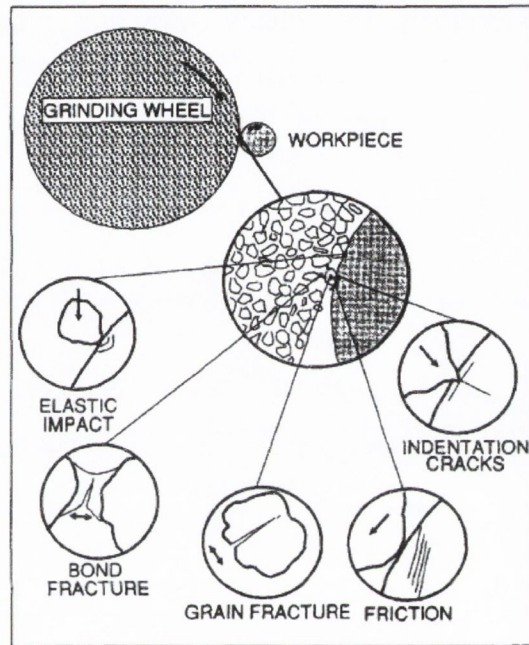


Figure 2.18: Sources of AE in grinding [83]

Lee *et al.* discussed different signals of AE from three sources at the tool-chip interface. The author states that in conventional machining, AE is typically generated in the primary shear region ahead of the tool, secondary shear zone which is the contact region between tool and chip and finally the tertiary shear zone which is the contact of the machined surface and the tool flank. It is believed that when machining on a precision scale of less than $1\mu\text{m}$ that the sources of AE come from the interaction of the tool with micro structural features such as voids, inclusions, grain boundaries and bulk dislocation interactions in the shear zone [80].

Webster identified that many previous studies only focused on analysing the AE_{RMS} signal while monitoring the grinding process. The work that was performed investigated the frequency characteristics of the AE_{raw} signal. Again because of the

frequency of the collisions, identification of single grit collisions was not possible as a number of grits would be in contact with the workpiece at any one time. He labelled this process as wheel contact which caused a continuous type AE signal to occur [84].

In a CIRP keynote paper on Tool Condition Monitoring by Byrne *et al.*, the authors recognized that several features could be extracted from the AE signal. One area was evaluation of the dressing process, this was performed by gathering acoustic emission data from the diamond tool and grinding wheel interaction and converting it into an RMS value. The data was recorded in columns, each one representing a full rotation of the grinding wheel which was then given a colorscale based on the level of AE_{RMS} data received (Figure 2.19).

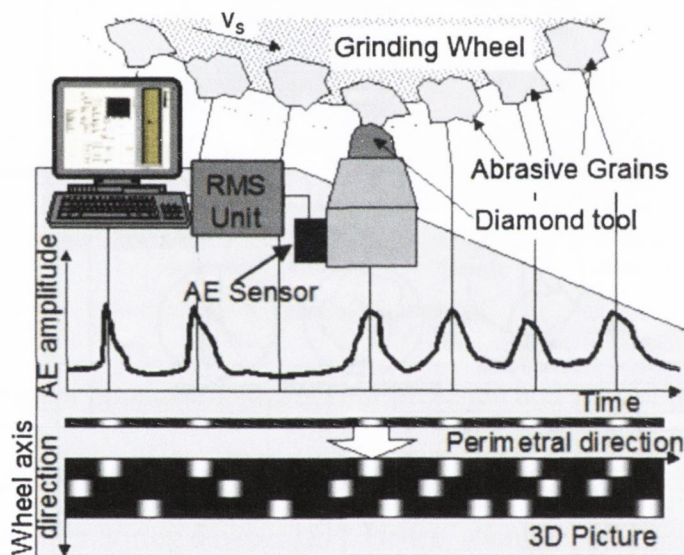


Figure 2.19: Image construction process for RMS analysis of the dressing process

[15]

During the dressing operation, the columns are mapped together to give an illustration of the dressing operation, darker regions representing areas of less RMS value indicating no dresser contact or a shallower depth of cut and lighter regions representing area with a greater RMS value. This can be seen in Figure 2.20 where an L shape has been removed from the grinding wheel and the corresponding L shape shows up in the map based on the AE data received [20].

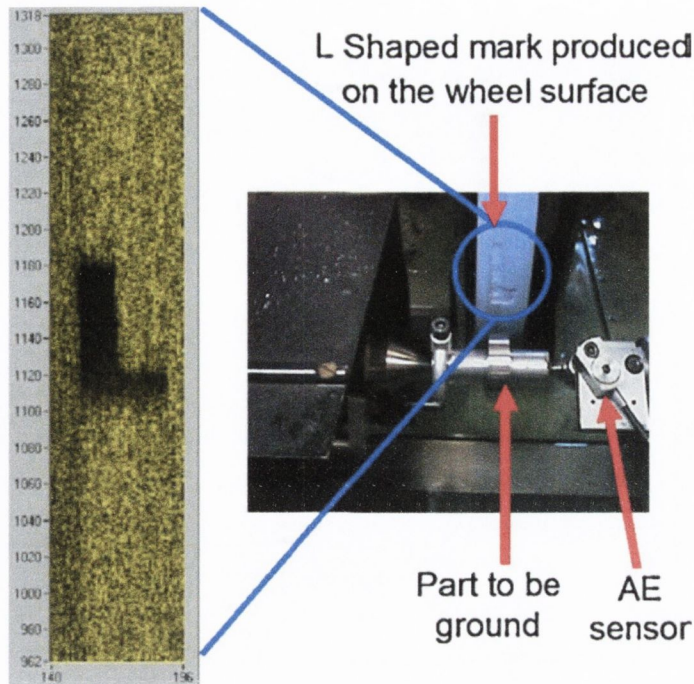


Figure 2.20: An output of the acoustic emission mapping system

While several studies have focused on the effect of various machining parameters on the resultant AE signal, Liu investigated the depth of cut vs. AE signal for diamond turning. The author found that a strong relationship existed between chip thickness, cutting speed and AE_{RMS} [31]. Similar work was performed by Chen who established an exponential decrease in specific AE_{RMS} vs. chip thickness [85]. AE signals could be detected for a chip thickness value of $0.01\mu\text{m}$ indicating the sensitivity of the sensor. It was also noted that a sharp change in the AE_{RMS} signal was observed between a worn and sharp tool. The increase in the AE signal for a worn tool was believed to be due to the ratio of tool edge to uncut chip thickness. As the uncut chip thickness decreases below the edge radius of the tool, a transition in the cutting mechanism takes place where in effect a negative rake angle is seen on the tool which results in rubbing and ploughing of the material (Figure 2.21).

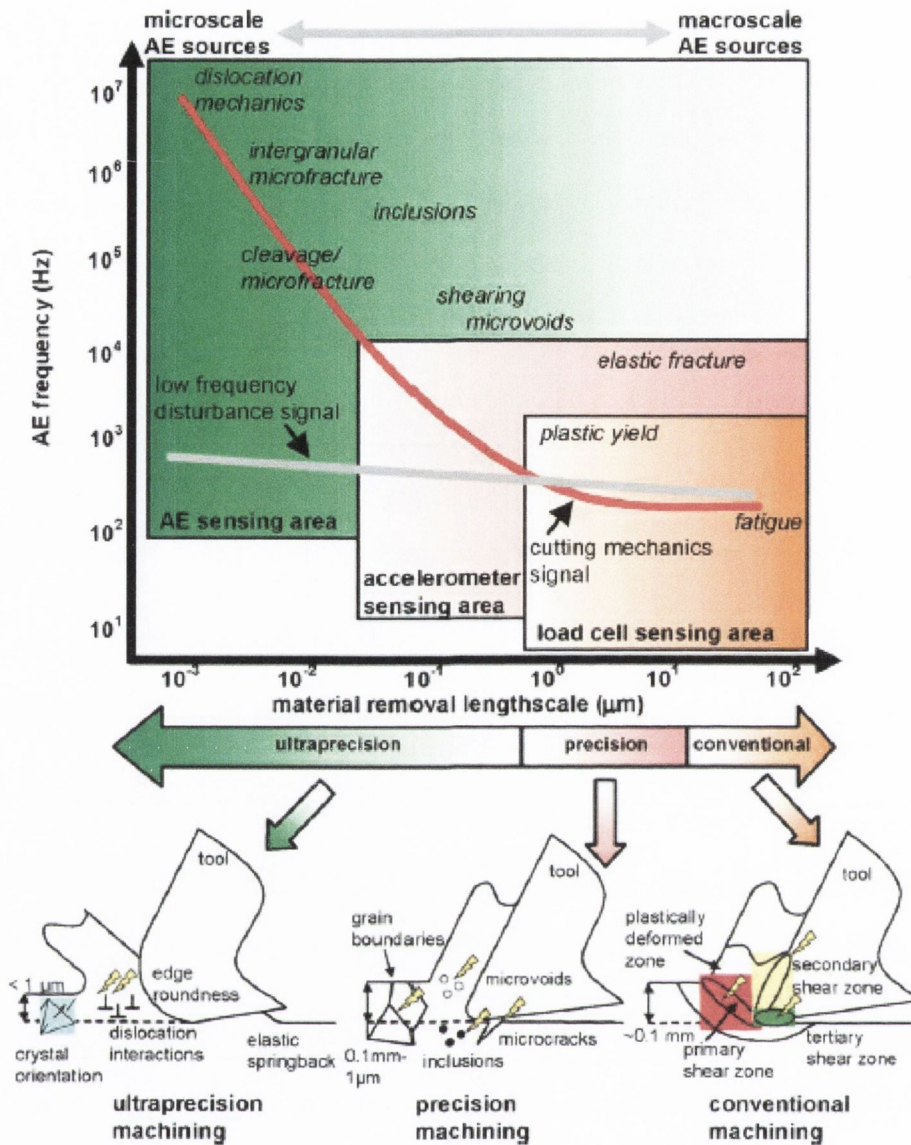


Figure 2.21: Sources of AE for different material removal mechanisms [80]

Oliveira *et al.* used AE to measure the grinding wheel profile. This was done by using the dressing tool as a touch probe with an AE sensor mounted to the tool. The dressing tool is fed into the grinding wheel until contact is picked up by the AE sensor. This produces an AE_{RMS} signal due to the elastic contact between dresser and grinding wheel. Once the AE signal reaches a certain threshold, the dressing tool retracts and the process is repeated along the wheel surface to obtain the grinding wheel profile [86].

Karpuschewski *et al.* used an AE sensor to detect contact between the dresser and grinding wheel. This reduces the idling and cycle time in the grinding process. Detection of dresser and grinding wheel contact is made possible by using the last

stored CNC position during the grinding process and adding a safety factor. Once touch detection is made, a defined number of passes may be performed and the dressing process can be terminated. This cuts down on unnecessary dressing passes which results in reduced wheel wear [21].

Inasaki performed similar work in the 1980's whereby he analysed the AE signal to determine whether a true dressing depth of cut occurred across the grinding wheel width. His concern was that when a grinding wheel wears, it does not wear uniformly and in fact a cross section of the wheel may appear to be convex in shape. If dressing was to be performed on such a wheel, the dressing depth of cut would vary across the wheel. This is illustrated in Figure 2.22 where a convex wheel produces an AE signal with varying amplitude. A recorded signal with a steady amplitude or one which has a standard deviation below a prescribed value would result in a uniform grinding wheel profile [22].

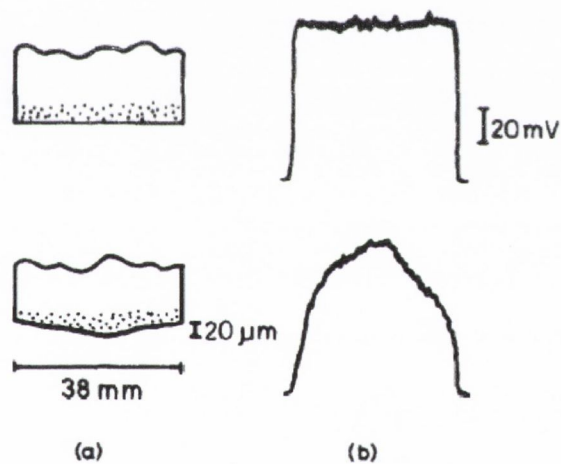


Figure 2.22: Cross sectional profile of a) grinding wheels and b) corresponding AE signal

Determining when to exactly terminate the dressing process is a major concern for manufacturing companies. Figure 2.23 shows the AE signal recorded throughout the dressing process and a graph of the difference in amplitude between each dressing pass.

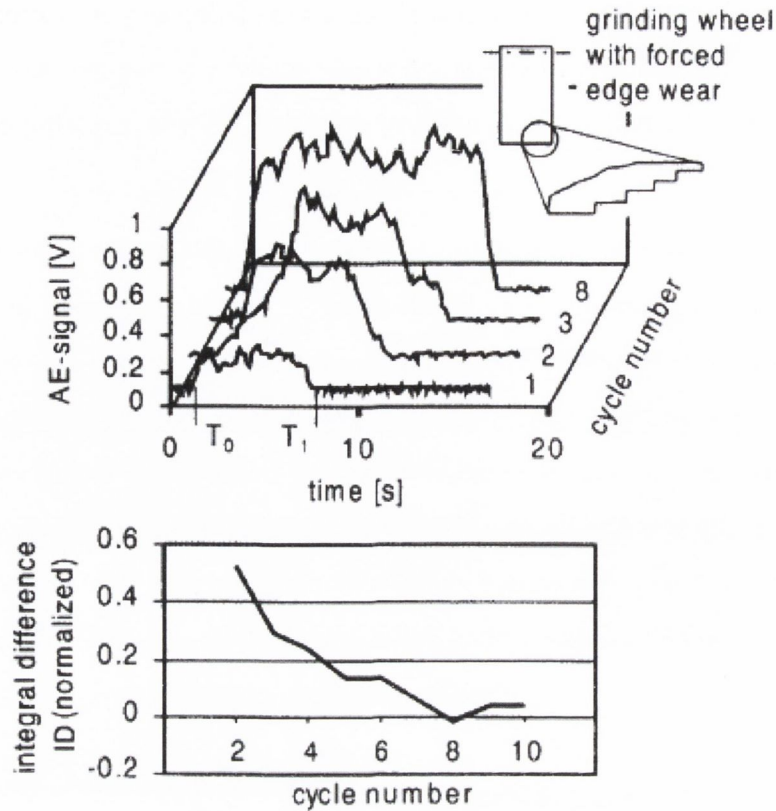


Figure 2.23: Monitoring of the dressing process using an AE sensor [21]

The difference between two AE-signals is calculated by integrating and normalising it to a current value. Based on experimental results, a value of ± 1 must be achieved twice in consecutive order. Once this is achieved, a certain number of finishing strokes can be performed and the process can then be terminated [21].

Takagi and Meng used the dressing force as a measure of quantifying the dressing process [18]. Haung followed on from this work and established the average resultant force acting on each grain and called this the dressing intensity. It was calculated by finding the resultant force from the normal and tangential forces and dividing this force by the number of grits involved in the dressing process, which is the product of the grit number per unit area and the dressing contact area [6]. After measuring the dressing intensity, the authors then studied the grinding forces and surface roughness of the material. It was found that as the dressing intensity increased, the grinding forces decreased, as the greater depth of cut lead to a sharper topography of the wheel surface. This indicated that measuring the dressing intensity could give a measure of the grinding wheel performance. It was also found that as the dressing intensity decreased,

a greater quality in surface finish was achieved as the lower dressing intensity resulted in micro chipping of the grains leading to a dull wheel.

Byrne *et al.* studied the use of power monitoring to identify conditions whereby thermal damage may occur to the workpiece. In the case of severe wheel wear, leading to a dull wheel, the power may rise. A user defined threshold is set to prevent grinding from continuing and causing surface damage to the workpiece once this limit is reached [15].

Pande *et al.* studied the grinding forces, amplitude of vibration and onset of burning and determined the wheel life based on whichever detection method reached its threshold limit first. [87]. The authors also evaluated the effect of the dressing process by studying the size distribution of dressing particles collected during the final pass to determine the type of fracture occurring. When the wheel was dressed with a high depth of cut and low cross-feed rate (0.5m/min), they found that most of the particles collected (approx 70%) were the same size as the grains on the wheel indicating a high percentage of bond fracture resulting in a sharp wheel. While at a low dressing depth of cut and high cross-feed rate (1.5 m/min), they found that the wheel experienced more grain fracture compared to bond fracture which was less than 30% [87].

2.4 Surface finish characterisation

The surface integrity that results from the grinding process plays a significant part in the components performance over its lifetime. High precision parts that have been achieved through grinding have a wide range of applications in the optical, automotive and communication industry as well as in medical and life sciences [88]. The generation of a ground surface is made up from the geometrical relationship of the grinding wheel, the workpiece material and the mechanics of the grinding process [89]. The mechanics of the grinding process depend on the density of the grits, their geometry and distribution of the protrusive cutting points on the wheel surface, both of which are affected by the dressing process. The wheel properties also play an important role, namely the elasticity and fracture strength of the bond and grit. It is seen that when a grain passes through the workpiece surface, its profile is transferred onto the workpiece surface as it removes material. As the cutting edges on a grinding wheel surface are randomly distributed, the cutting path of each grain is different and

only the outermost active grits on the wheel surface cut through the workpiece. This creates an irregular rough surface on the workpiece. Shaw and Brinksmeier describe the surface integrity of the part under three headings which are the surface finish, metallurgical damage and residual stress [55, 90]. Surface finish of a workpiece relates to macro-topography features such as the roundness, straightness, flatness of a part and micro-topography features that include the surface texture. Metallurgical damage and residual stresses relate to structural changes of the material usually as a result of increased work temperatures.

2.4.1 Measurement of surface finish

The surface geometry of a workpiece is made up of three components which are the form, waviness and roughness. The (latter) waviness and roughness of the profile make up the surface texture as shown in Figure 2.24. The surface roughness of a piece is the most common feature measured. This measurement can then be used to assess the performance of the machine parameters and the required surface roughness tolerances of the part. The most common metric to measure surface roughness is the Ra value which is a centre line average of the peaks and troughs on the surface. Some companies use Rt which is the maximum peak to valley roughness value of the profile.

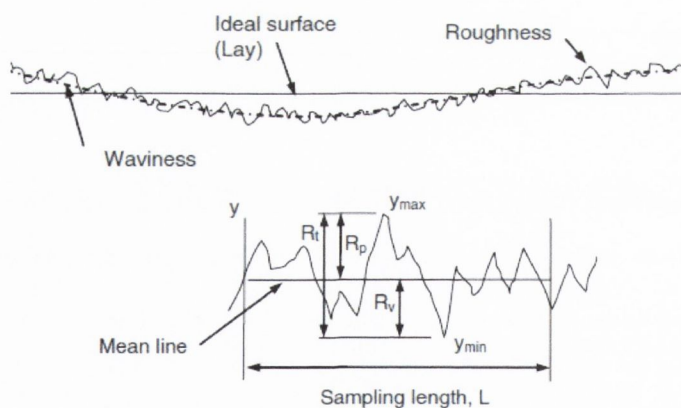


Figure 2.24: Schematic representation of a machined surface profile [91]

There are various methods used to measure the surface roughness of a part, these include contact and non-contact instruments [92]. Contact measurements include the use of profilometers which are equipped with a fine stylus. These take a trace of the surface perpendicular to the direction of grinding and produce a 2D profile. Recent developments have enabled the use of 3d profiles to be produced by taking multiple

traces and mapping them together. Radii of styluses range from $2\mu\text{m}$ to $50\mu\text{m}$ with smaller radii being used for surfaces with a finer finish. Non-contact measurement devices generally employ optical methods such as digital phase interferometry. These methods can produce a 3D surface map in one measurement and can measure surfaces with an Ra value of $1\text{-}2\text{nm}$ due to its sub-nanometre resolution.

The surface finish of the workpiece can be predicted by two main methods. These include theoretical modelling, whereby all the different wheel conditions created under various parameters are analysed. The other is empirical modelling, whereby models are built based on the known empirical constants from previous work. Yossifon and Rubenstein attempted to link grinding parameters with workpiece roughness to produce the relationship for Ra as shown in Equation 2.7 [93].

$$R_a = \left(\frac{v}{V} \cdot \frac{x}{W} \cdot \frac{1}{r \cdot n_c} \cdot \frac{d}{D_e} \right)^{\frac{n}{2}} \quad (2.7)$$

Where:

W – wheel width

d – depth of cut

v – workpiece speed

V – wheel speed

x – transverse rate

D – wheel diameter

n_c – no of active grits per unit surface area

r – average width-depth ratio of groove produced on the surface

This equation relies on the constants n_c and r which are the active grits per unit area and the grit radius. Both of these parameters are difficult to determine even for electroplated bonded materials where the wheel surface is not being constantly eroded. These values are often estimated and given a broad value of 10-40 based on previous work performed [94].

2.4.2 Metallurgical damage to workpiece

Grinding is considered to be quite an aggressive process with high specific energies due to the rubbing, cutting and ploughing that takes place to remove material. As a result, the majority of the energy produced during these material mechanisms is converted to heat. It has been reported by a number of authors that this heat can result in metallurgical damage to the workpiece material [95-97]. Methods commonly used to detect grinding burn include visual identification of a bluish temper colour on the ground surface which is as a result of an oxide layer formation. This can be done by mounting the part in epoxy, polishing the surface of interest while preserving the part. The polished surface is then etched to reveal the microstructure which can then be identified and categorised according to the degree of discolouration [98]. However this method is quite subjective, as some coolant types may leave a bluish discolouration on the surface of the workpiece. Another factor to consider is that subsequent spark out grinding passes may remove the discolouration on the surface without the removal of the associated damage below. A microhardness test is another method used to test for thermal damage. Extreme temperatures may cause re-austenisation of the material and hence re-hardening of the surface layer, the latter is commonly referred to as white layer [17]. As testing for thermal damage is quite subjective, it is therefore desirable to try and avoid the metallurgical damage and reduce specific energies during grinding.

2.4.3 Workpiece residual stress

The grinding process can induce residual stresses into the surface of the workpiece which can have a significant effect on the mechanical properties of the part [99]. Torrence *et al.* showed that fatigue life decreased with increasing specific energy during grinding [100]. Field and Koster investigated the fatigue life of parts and found that an increase in the residual tensile stress drastically reduced the fatigue life [101]. These tensile stresses are formed when the surface is strained beyond its plastic limit, the induced stresses remain as residual stresses which can penetrate into the material to various depths. The severity of the residual stresses is dependent on the temperature experienced and the grinding forces [102]. They can come in the form of both tensile and compressive residual stresses. Usually mechanical plastic deformation leads to compressive residual stresses, however, thermal plastic deformation can lead to both compressive and tensile stresses, depending on the volume increase or decrease of

material that results from the phase transformation of the material [103]. Compressive residual stresses are desirable for some engineering components, however, high thermal loading as a result of aggressive grinding can induce tensile residual stresses which can lead to fatigue failure as the surface is prone to micro cracking [104]. Residual stresses experienced in manufacturing of components are illustrated below in Figure 2.25.

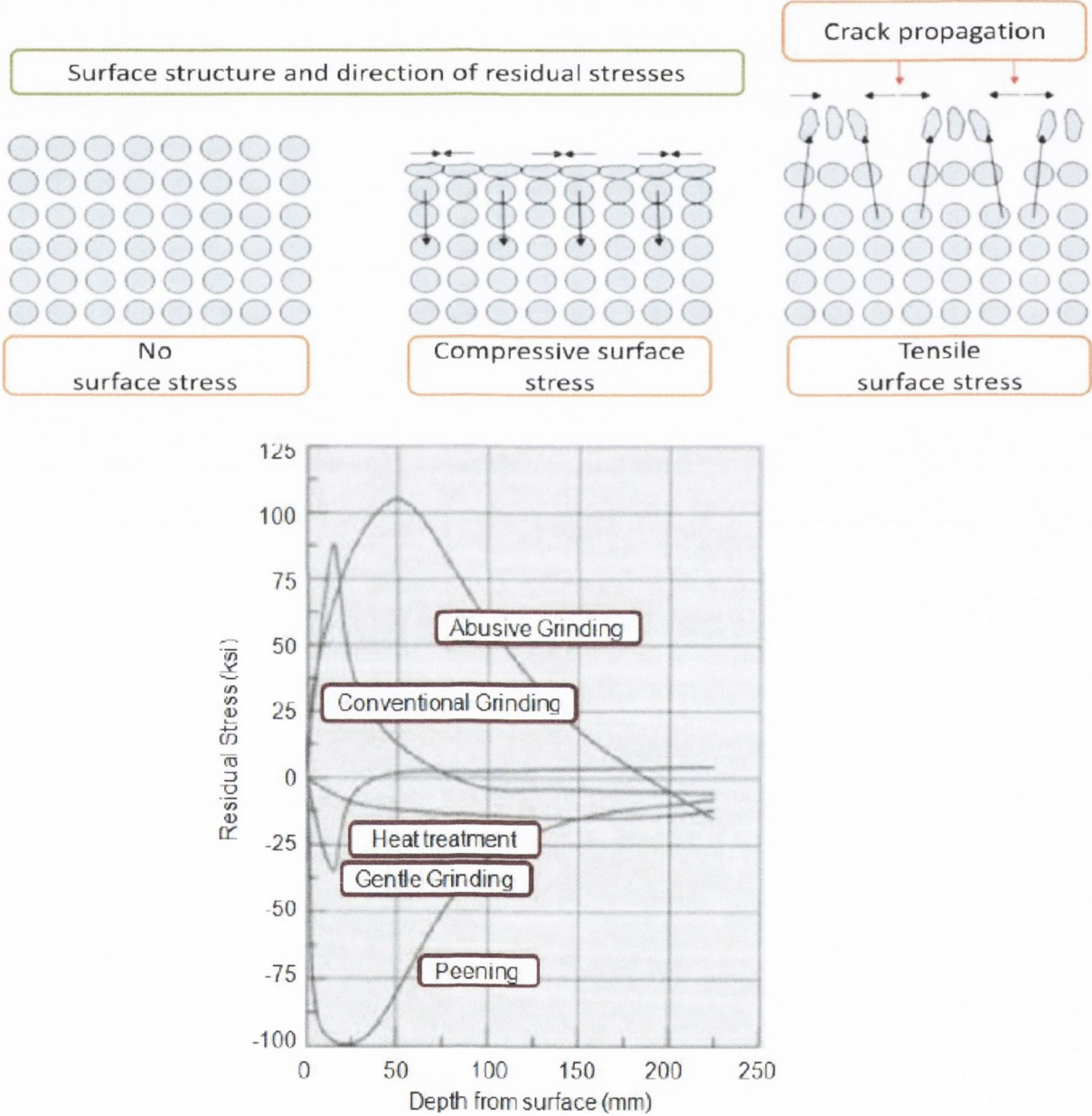


Figure 2.25: a) Types of residual stresses experienced during machining and the associated lattice structure b) residual stresses and the depth of penetration for various machining processes [105]

2.5 Diamond dressing tools

Diamond is the hardest material known in nature and as a result, it is primarily used to dress grinding wheels which also exhibit high hardness of materials. It is a crystalline structure made up of strong carbon covalent bonds which are packed together tightly in a tetrahedral arrangement and formed at high temperatures and high pressures. Diamond hardness depends on properties like purity, crystalline perfection and crystal direction [106, 107]. As the distances between the carbon atoms differ depending on the crystal plane, the diamond hardness varies with different crystal direction and therefore it has highly anisotropic wear properties. Diamond is hardest for a flawless pure crystal orientated in the $\langle 110 \rangle$ direction on the $\{111\}$ plane which is the longest diagonal of the cubic diamond lattice [9, 108, 109].

As well as hardness Diamond also exhibits exceptional physical characteristics in its thermal conductivity with values reaching $2,320 \text{ W}\cdot\text{m}^{-1}\cdot\text{K}^{-1}$ [110]. However, this can be a problem in dressing as a build up of heat can generate in the dressing tool holder, during the dressing process which could result in damage to the diamond and its casing. For this reason, temperatures above 900°C should be avoided to prevent graphitisation of the diamond [111]. In order to prevent this, sufficient coolant should be present when performing harsh dressing processes. As stated previously, the physical properties of the diamond have quite a large range, which is strongly influenced by its manufacturing process.

2.5.1 Diamond manufacturing

Diamond dressers are manufactured using natural and synthetic diamonds. Synthetic diamonds are manufactured using both Chemical Vapour Deposition (CVD) and High Pressure High Temperature (HPHT) methods. Both methods can produce monocrystalline and microcrystalline diamonds with different material properties to suit the application in which the diamond is being used. Natural diamonds are also used in diamond dressers, Type Ia is the most common as it makes up 98% of the diamonds mined. As these diamonds vary in shape, size, crystal purities (Nitrogen impurities) and dislocations (up to 0.3%), abrasion resistance and wear rate can vary greatly. These diamonds vary in grade depending on the Nitrogen purities and dislocations present within the carbon lattice which can be up to 0.3%. Type IIa natural diamonds make up 1-2% of all natural diamonds. These diamonds are almost devoid

of any impurities, are almost colourless and have the highest thermal conductivity. A summary of the diamond types used in diamond dressers can be seen below in Figure 2.26.

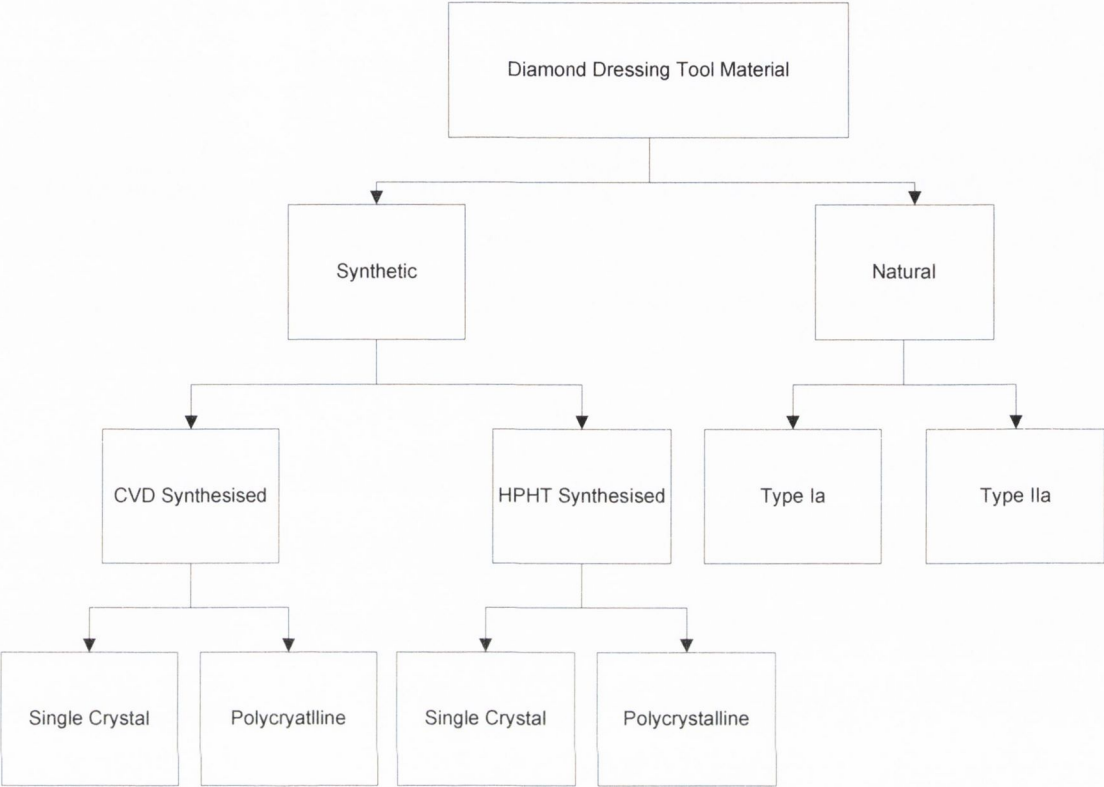


Figure 2.26: Types of diamond that can be used in diamond dressing tools

Single crystal (MCD) diamonds are produced using a process whereby graphite is synthesised under extremely high pressures and high temperatures using a metal catalyst [112]. The diamond dresser logs are then laser cut from monocrystalline diamond blanks. The homogeneous crystal orientation of MCD leads to a constant abrasion resistance or wear rate along their length, however, due to the anisotropy nature of MCD logs, the wear resistance is orientation dependent. Synthetic diamonds are said to have reproducible characteristics as they are manufactured under such controlled conditions. Due to the high manufacturing costs involved in producing MCD, they are generally only used when there is a high risk of wear occurring on the tool, as would be the case with stationary diamond dressers.

Polycrystalline diamonds (PCD) are made up of synthetic diamond particles which are bound together in a sintering process using a binder matrix that is primarily cobalt or

tungsten. The properties of PCD are determined by the grain size of the diamond particles which lie in the range of between 2 and 25 μ m. Due to the diamond crystal structure, PCD with a binder phase, does not have a hard or soft direction in terms of its wear resistance and is therefore said to be isotropic. However, due to phase element present in PCD diamond, it is said to be one of the softest diamonds available on the market. PCD diamonds are frequently used in the diamond crushing rollers and form rollers.

Chemical Vapour Deposition (CVD) produces diamonds without the binder phase as mentioned above. The advantage of the CVD diamond lies in its great fracture strength, due to the homogeneous nature of the diamond and the close packing density of its structure. As CVD diamonds can be produced in extremely thin structures, its application is suited to coating form rollers.

The behaviour of a diamond dresser is strongly influenced by the grit size of the diamond where it is seen that smaller diamonds are stronger than larger diamonds. The main reason for this is because smaller diamonds would have fewer and smaller defects. Another factor contributing to the wear of the diamond is the concentration of diamond present on the surface of the diamond roller with an increase in the diamond leading to prolonged tool life. However, a reduction is seen of the surface roughness of the dressed wheel with an increase in the grit density.

For CVD diamond dressers, the diamond is enclosed within a soft metal casing, as dressing is performed, the matrix is soon cut back to expose the diamond for dressing. On the other hand, if a hard material is chosen to enclose the diamond, the bond matrix may not wear to allow the diamond to protrude and dress the wheel. As a result, the wheel ends up being dressed by both the diamond and the bond matrix which results in a greater effective width and smoothening of the wheel during dressing.

2.5.2 Wear of Diamond Dressers

Many authors have investigated the wear of diamond tools in recent years [106, 113-115]. Different wear mechanisms outlined before include mechanical, thermal and chemical effects which all contribute to diamond tool wear [30, 116-118]. However, the predominant wear mechanism present and wear rate of the diamond will depend on the machining parameters used in the tests.

Linke studied the effects of dressing temperatures on the diamond dressing tool wear. As wear of the diamond is dependent on cooling type, supply and amount [119, 120], thermal wear mechanisms have to be the main reason for dressing tool wear. Linke measured the dressing temperatures using a two-color pyrometer. Results from tests performed show that decreasing the dressing feed resulted in decreased temperature. This was due to the lower collision rate of grits with the diamond, which resulted in less friction, thereby reducing the rise in temperature. The affect of grinding wheel speed on temperature rise was also studied by Linke. It was noted that as the grinding wheel speed increased there was also an increase in temperature. The reason for this was again due to the greater number of grit collisions with the dresser which results in more friction. The final dressing parameter Linke studied with relation to dressing temperatures was the depth of cut and surprisingly in these tests, it was found that as the depth of cut increased the dressing temperature decreased. One possible explanation for this was that dressing with an increased depth of cut resulted in bond fracture whereas dressing with a lower depth of cut resulted in more friction causing greater heat generation [23].

Tian *et al.* studied the wear mechanisms of impregnated single diamond bits in hard rock drilling and found that the wear characteristics of diamond depended not only on their structure and material properties but also on the machining parameters. The relationship between forces and the type of wear mechanism occurring were also investigated. It was noted that under low thrust force, predominately large abrasive wear flats were produced. While under higher forces, micro fracture was found to be the main wear mechanism [121]. Tolkowsky also found that the rate of wear was proportional to the load on the diamond, further work performed by Wilks and Wilks confirmed this conclusion [122].

The effect of wheel speed was studied by Wilks and Wilks who found that the diamond material removal rate was proportional to the wheel speed [123]. This is due to the high temperatures that are experienced in the contact zone when two surfaces come in contact with each other at high speeds. Therefore it can be assumed that the higher cutting speeds would produce higher excess temperatures resulting in greater wear rates.

This statement is supported by investigations performed by Thorton and Wilks where a diamond tool was used to turn mild steel. The authors found that as the cutting speed increased, the wear rate also increased with cutting speeds of 30ms^{-1} resulting in wear that was 50 times greater than when a typical cutting speed of 11ms^{-1} was used [124].

Erosion tests performed by Telling on CVD diamond on different planes showed that an increase in the diamond grain size resulted in a decrease in the erosion rate of the diamond [116]. The results from the tests performed by Telling can be seen below in Table 2.1.

Surface Orientation	Grain Size (d) (μm)	Mean erosion rate (mg kg^{-1})
<111>	30 ± 8	4.0 ± 0.1
<111>	190 ± 50	1.89 ± 0.2
Mixed <311>/<111>	38 ± 4	2.63 ± 0.05
Mixed <311>/<111>	280 ± 80	1.47 ± 0.05

Table 2.1: Table of diamond grain size and the corresponding mean erosion rate

The roughness of the diamond is critical as it controls the amount of friction and abrasive damage on the surface of the diamond. Reducing the surface roughness of the diamond by polishing or controlling the diamond growth process can lead to reductions in both friction and wear of the surface [125]. Uhlmann studied the adhesion wear of the diamond and found the main cause of this type of wear was due to the roughness of the diamond. Tests performed on a diamond with very low roughness resulted in almost no material being deposited on the cutting surface. Whereas a thicker diamond film with higher roughness resulted in large areas of material being deposited on the materials cutting surface. This was due to workpiece material particles being embedded and then smeared on the surface of the diamond once the frictional process between tool and workpiece took place [126]. The frictional properties of diamond can vary depending on the crystal face and direction of sliding that occurs on the diamond face [127, 128]. It has also been reported by Grillo that the presence of a lubricant does not reduce the coefficient of friction from its ambient value. They reported that two traditional mechanisms, adhesion and surface roughness are responsible for the friction of the diamond [129]. Hayward looked at the effect of roughness on the friction properties of CVD diamond and found that roughness and friction was severe at the beginning. These properties then reduced as the diamond wore and smoothed [128].

2.5.3 Anisotropy of diamond

As previously mentioned, the hardness is strongly dependent on the crystal direction. Grains on the {111} plane are the most resistant to polishing wear. This is due to the {111} plane having a higher atomic density of 7.83×10^{14} atoms/cm². It is the grains orientated on the {100} plane which are the least wear resistant with a density of 6.78×10^{14} atoms/cm² that results in longer distance between the carbon atoms on that plane. [9, 108, 109, 130, 131] [132]. The exact material removal mechanisms which create this anisotropy is not fully understood. Yuan suggests that the difference in wear rates between different planes may be due to the difference in friction. The author also noted that there was not only a difference in the friction between planes but also a difference in the friction between directions in the same crystal planes [9]. Pastewka *et al.* suggest the anisotropy is due to the order in which individual the sp³ and sp² atomic bonds are mechanically removed from the surface. This results in the creation of an amorphous layer in which the depth of the layer depends strongly on surface orientation and sliding direction. The final removal mechanism of the amorphous layer is caused by either mechanical removal of the material through friction or by etching with the ambient oxygen [133].

Chapter 3 Wear characterisation of diamond dressers

3.1 Background and methodology for wear characterisation

The aims of the investigations in this chapter were to examine the wear characteristics of new grades of CVD diamond dressers, by considering direct comparison with the well established literature, and investigations undertaken using natural diamond stationary dressers. The methodology and analysis approach is illustrated in Figure 3.1. Experimental investigations were developed to examine fundamental aspects such as:

- The influence of dressing strategy with consideration of tool path.
- The influence of directionality whereby the diamond was presented to the abrasive wheel at various orientations.
- The influence of abrasive materials, where two grades of abrasive materials were examined, namely; mono-crystalline aluminium oxide and microcrystalline ceramic abrasives.

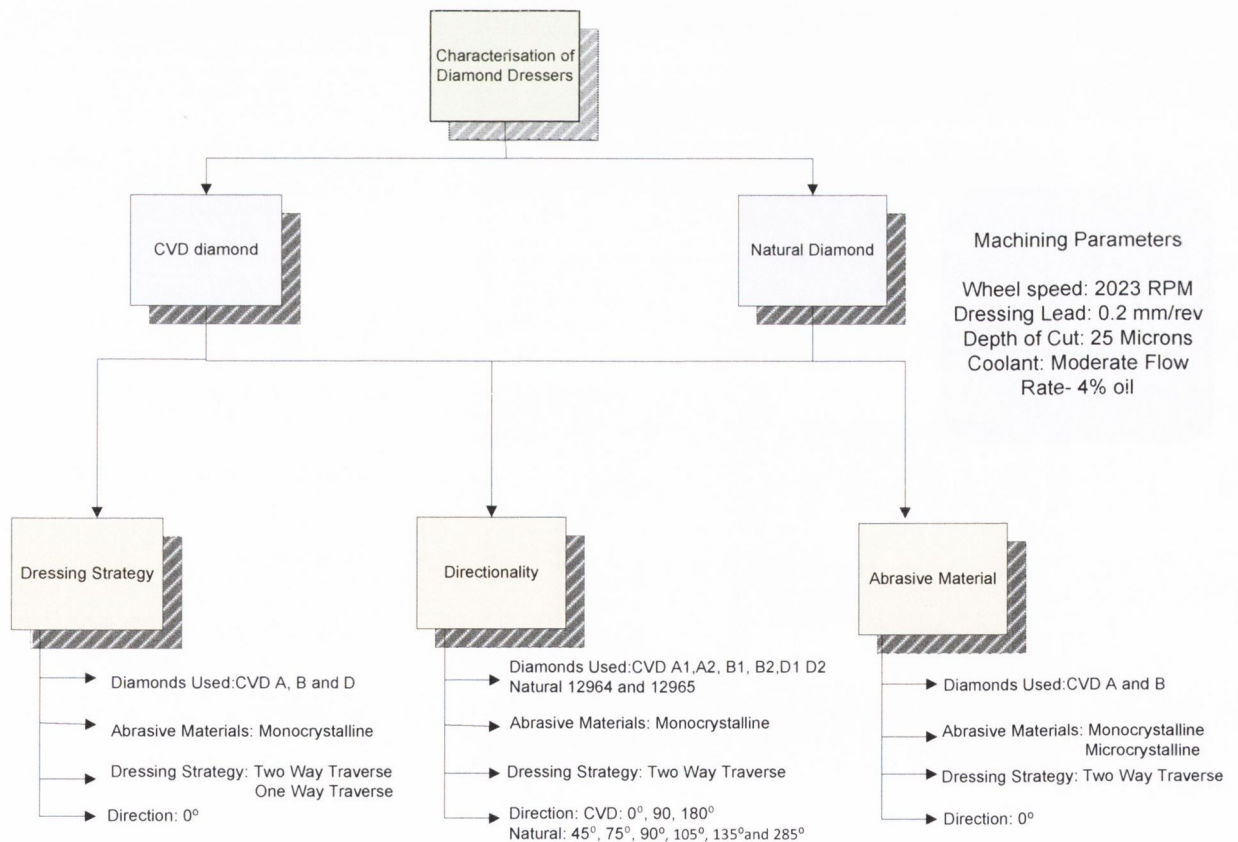
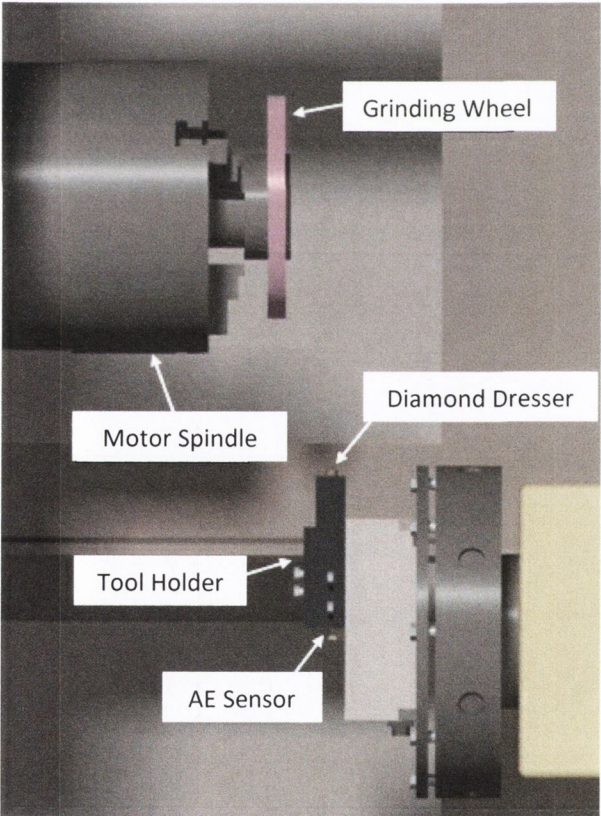


Figure 3.1: Flow chart of the experimental campaign

The wear mechanisms of the diamond were examined using Scanning Electron Microscopy (SEM). Micro and macro analysis of profile and shape evolution were also examined using microscopes with developed image acquisition and analysis approaches. Acoustic emission was recorded during the dressing wear investigations and the signals were examined for correlation between wear on the diamond and signal intensity.

3.2 Experimental set-up

A dedicated test stand was developed in order to carry out the dressing investigations, which involved adapting a CNC lathe. Fixtures were manufactured to enable the machine to facilitate the grinding wheel and dressing tool, and G-codes were written to replicate the dressing parameters that are seen in industry, where dressing speeds of 400mm/min and dressing depths of 25 microns could be achieved. The experimental set-up is illustrated in Figure 3.2.



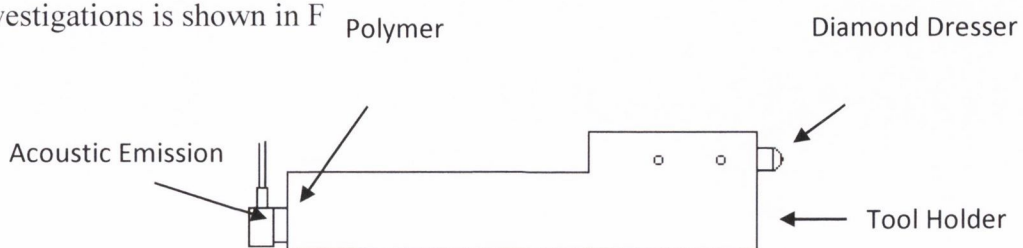
Harrison VS450 CNC Lathe	
Machine Type	Horizontal
Control	Fanuc
Number of Axes	2
Cutting Diameter	450mm
Tool Stations	1
Spindle Speed	20-2000 RPM

Figure 3.2: Experimental Testing Rig

The machine has a built in coolant system which was used throughout the dressing wear investigations. The coolant is delivered to the dressing tool via two loc-line coolant hoses using a low pressure, flood cooling strategy, with the nozzles directed at the tip of the dressing tool at a flow rate of 20 litres/min. The fixtures and adaptations to the CNC lathe included the manufacturing of a mandrel to hold the grinding wheel and enable rapid wheel change. One side of the mandrel adaptor consisted of an arbour 80mm in length and 60mm in diameter which was clamped into the chuck of the spindle while the other side consisted of an arbour 30mm in length with a diameter of 31.75mm for 11mm of the length so as the bore of the grinding wheel would fit onto the shaft. An interface plate was manufactured and was secured onto the turret of the machine, which allowed the dressing tool holder to be fixed to the plate. The tool holder also enabled the mounting of the acoustic emission sensor.

3.2.1 AE sensor

The Acoustic Emission (AE) sensor used for the dressing wear investigations was a Kistler type 8152B1 piezotron AE sensor. The AE sensor was mounted on the diamond dresser tool holder with an M6 bolt. A piece of polymer was placed in between the AE sensor and tool holder to attenuate the output of the AE signal as can be seen in Figure 3.3a. The mounting of the AE sensor is an important factor as the further the sensor is mounted away from the source of acoustic emission, the greater the attenuation of the signal. Previous authors have been able to mount the AE sensor on a CBN wheel [21], however, this method is not a suitable option for vitrified bonded grinding wheel used in these tests as the porous material is a poor medium for wave propagation [83]. Both raw and filtered acoustic emission signals were recorded for subsequent analysis. The raw acoustic emission signals require sampling rates of 1 MHz, a powerful custom built workstation was used with the appropriate hardware to acquire the data. The schematic for the data acquisition system during the dressing investigations is shown in F



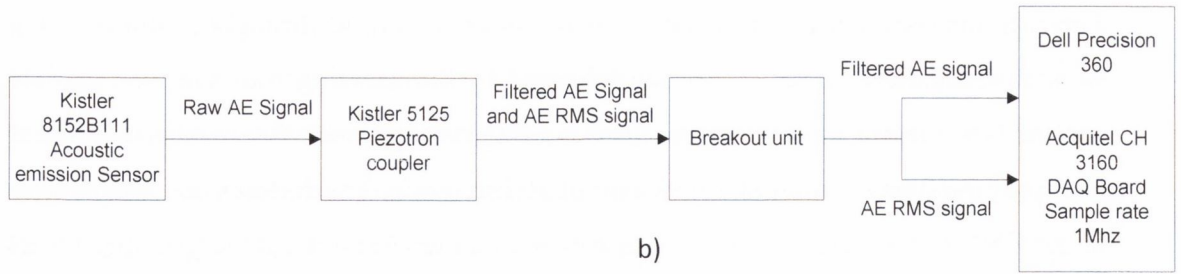


Figure 3.3: a) Acoustic emission set-up and b) Acoustic Emission measurement chain

A MATLAB graphical user interface (GUI) was used to process the data. The application takes in the parameters, acquisition time in seconds, sample rate and the filename for the test through the GUI. Data could be recorded by either setting a trigger level and choosing to ‘enable trigger’ or by simply pressing the ‘start acquisition’ button to record the data immediately. After a signal has been recorded, the data was plotted and the user could then choose to name and save the .mat file. The saved file contained a one-dimensional vector of the experimental data and the sample rate for further analysis. The process of the MATLAB interface is described in a flow chart in Figure 3.4.

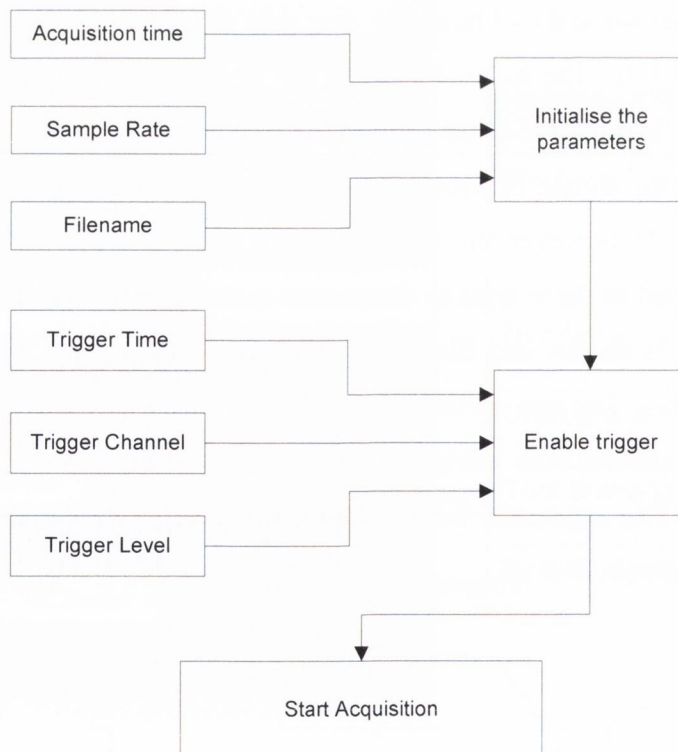


Figure 3.4: Flow chart of the MATLAB data acquisition GUI

3.2.2 Microscope and camera

In order to calculate the wear of the diamond dressers, a microscope was used to examine the diamond wear flat area after each test. An image of the diamond was taken using a digital camera. Image analysis was used to extract quantifiable metrics from the sample including the wear flat area of the diamond and the diamond height as can be seen below in Figure 3.5. An image of the calibration slide was taken at the same focal length and lighting so as an accurate scale bar could be used while analysing the images.

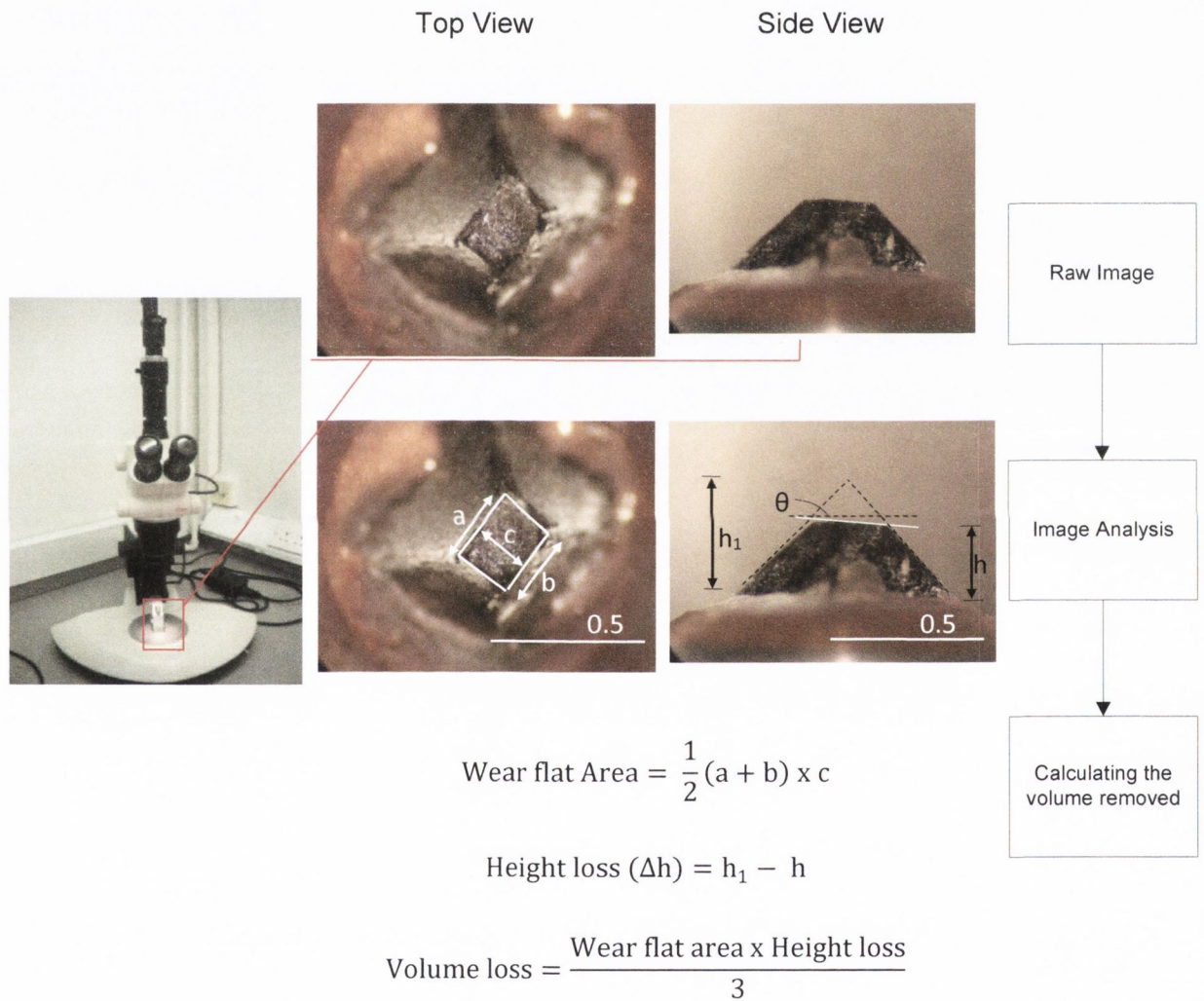


Figure 3.5: Image capture of diamond dresser and calculation of volume loss

3.2.3 Scanning Electron Microscope

In this study, detailed analysis was performed using a Tescan Mira XMU Scanning Electron Microscope. The use of electrons rather than light to form an image enables

the user to produce a high resolution image to perform detailed analysis of the topography of the surface of the diamond. Preparation of the samples is outlined in Figure 3.6c. As diamond is an insulating material, the samples were first cleaned with rubbing alcohol and sputter coated in a 10nm thick layer of gold to make them conductive and to prepare them for analysing. The samples were then held in place in the vacuum chamber using specially made clamps.

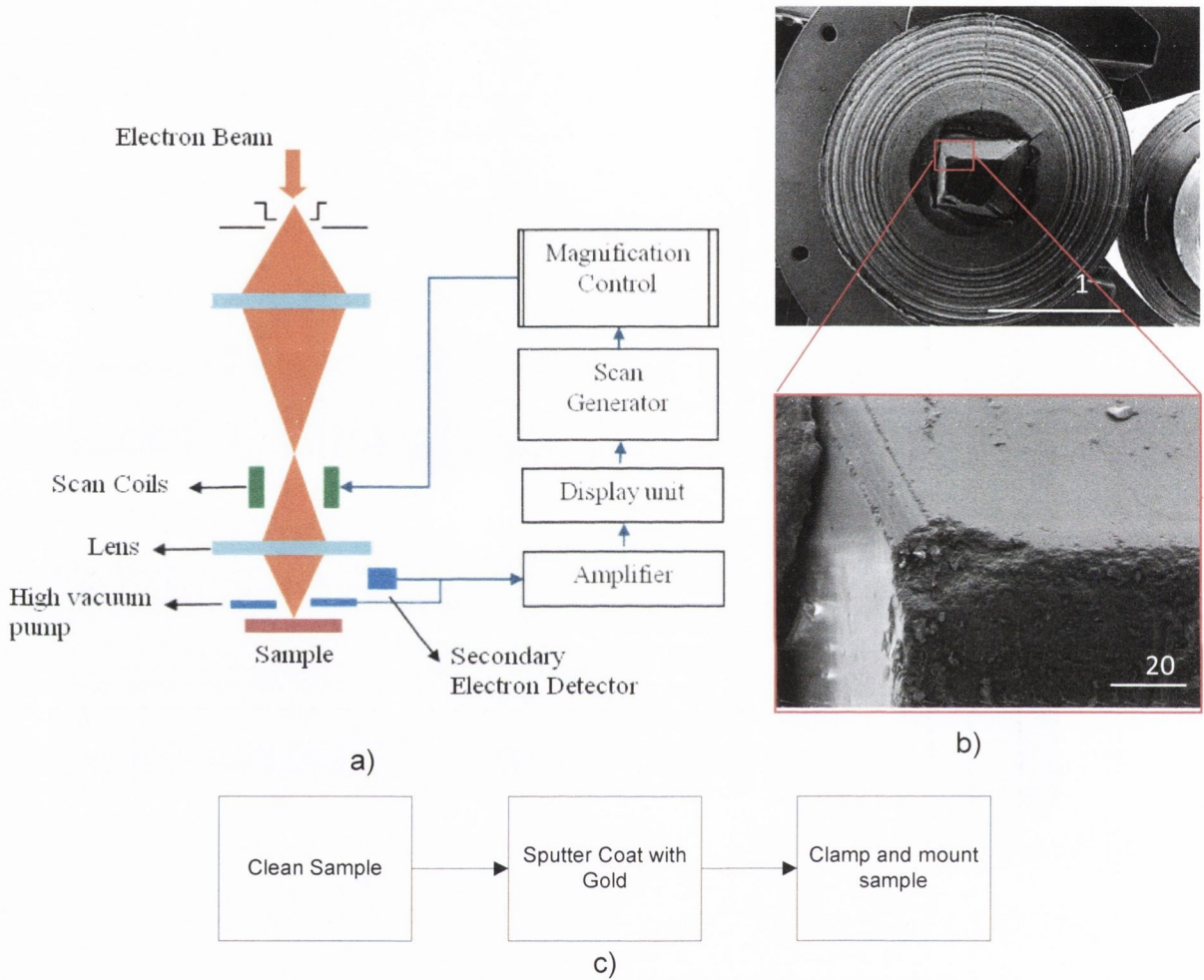


Figure 3.6: a) Schematic diagram of a Scanning Electron Microscope, b) Image capture and feature extraction, c) Preparation of sample

3.3 Tooling and Materials

The diamond dressers were sourced through the projects industrial sponsor; three specimens of each diamond were supplied for repeatable testing. The grinding wheels were bought in one order ensuring that all the wheels came from the same batch. No modifications were made to the diamond dressers or grinding wheels prior to testing.

3.3.1 Diamond dressers

The diamonds used in these tests consisted of two CVD polycrystalline diamonds A and B with grades of 5 and 3 respectively and a HPHT polycrystalline diamond, labelled D with a grade of 5. A Type Ia natural diamond with a grade of 2 was also used as a comparison with the synthetic diamonds. The diamond length and the geometry of the diamond were all measured and recorded prior to testing. In order to understand the wear characteristics of the diamond dressers, knowledge of the physical and mechanical properties of the CVD and natural diamonds is important. The properties of diamonds A, B and D are shown in Table 3.1.

Properties	A	B	D
Density (g/cc)	3.52	3.52	3.52
Hardness(GPa)	85-100	50	85-100
Fracture Toughness (MPa.m ^{1/2})	8.5	8.81	8.5
Young's Modulus (GPa)	1000-1100	1000-	1000-1100
Poisson's Ratio	0.07	0.07	0.07
Tensile Strength (MPa)	560-1100	1260	560-1100
Compressive Strength (GPa)	9	7.6	9
Thermal Conductivity @ 20°C (W/m.K)	1800-2200	400-500	800-1200
Thermal Conductivity @ 200°C (W/m.K)	1700-2100	300-400	700-1100

Table 3.1: Material properties of synthetic diamonds A, B and D

3.3.3 Grinding wheels

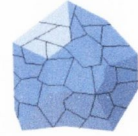
The wheels used for directionality and dressing strategy tests were conventional aluminium oxide wheels with a mono-crystalline (32A) grit size of 60, hardness grade of J and a vitrified bond. The wheels were 203mm in diameter and 12mm in width. Ceramic grit wheels were also used in wear tests with a Microcrystalline (5SG) grit size of 60, hardness grade of J and a vitrified bond. Conventional wheels are made up of 100% mono-crystalline aluminium oxide grit while ceramic wheels consist of 50% sol-gel microcrystalline grit and 50% conventional aluminium oxide grit. It can be seen that the difference between conventional and ceramic wheels is the structure of the grits. Conventional wheels are made up of monocrystalline grits while ceramic wheels consist of microcrystalline structure, a schematic of both grits can be seen in Figure 3.7b.

	Conventional	Ceramic
Wheel	32A60JVBE	5SG60JVS
Grit	Monocrystalline	Microcrystalline
Grit Size	60	60
Grade	J	J
Bond	Vitrified	Vitrified

Monocrystalline Grit



Microcrystalline Grit

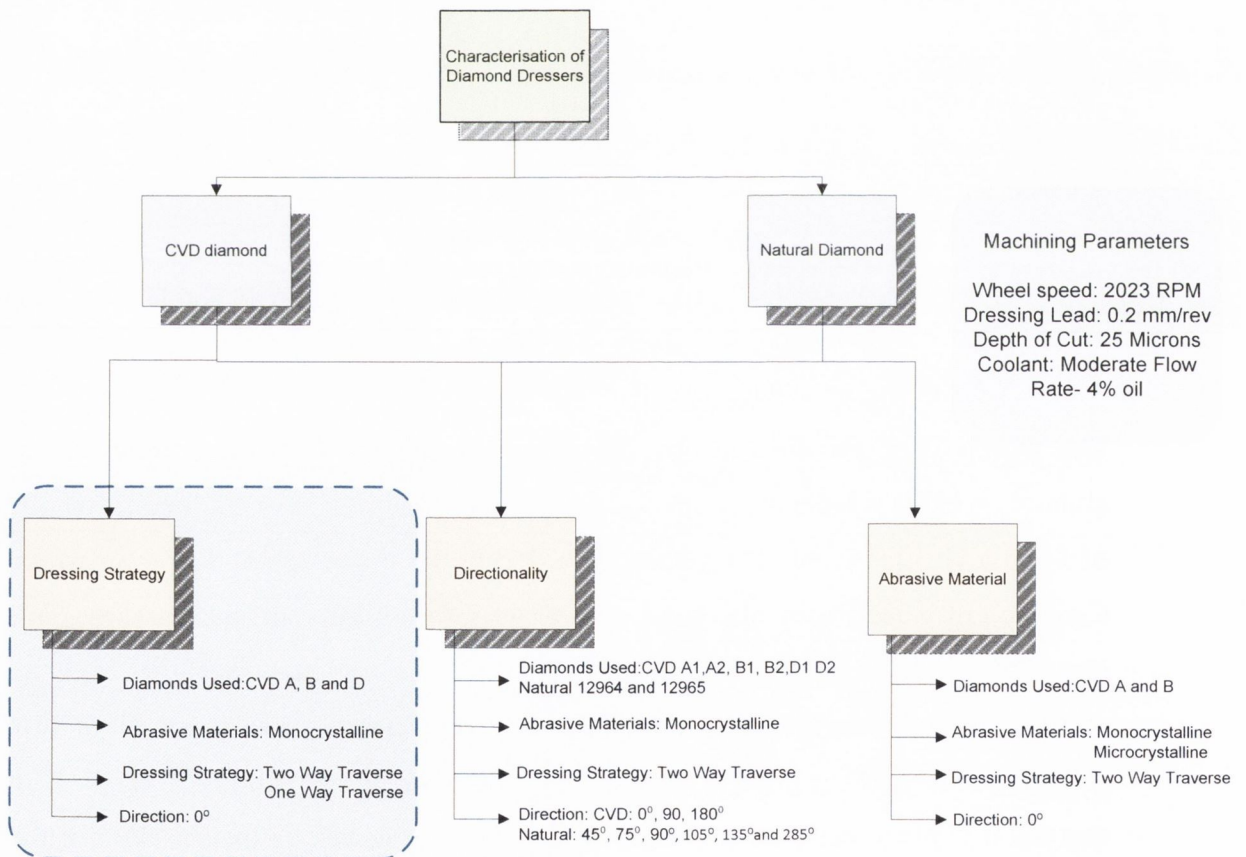


a)

b)

Figure 3.7: a) Grinding Wheel Specifications. b) Schematic diagram of Monocrystalline Grit and Microcrystalline Grit

3.5 Dressing Strategy Investigations



3.5.1 Experimental methodology

Tests were performed on three synthetic diamond dressers to assess the effect of the tool path on the wear of the diamond dresser. Two tool paths were chosen, one-directional and two-directional traverse tool paths. In the case of the one-directional traverse tool path, the diamond dresser engages the wheel from one side only whereby the dresser feeds down 25 microns, traverses across the face of the wheel, retracts and returns to the home position. In the case of the two-directional traverse tool path, the diamond feeds in 25 microns, traverses across the wheel from the left, feeds in another 25 microns and traverses back across the wheel from the right. The tool paths for both methods can be seen in Figure 3.8.

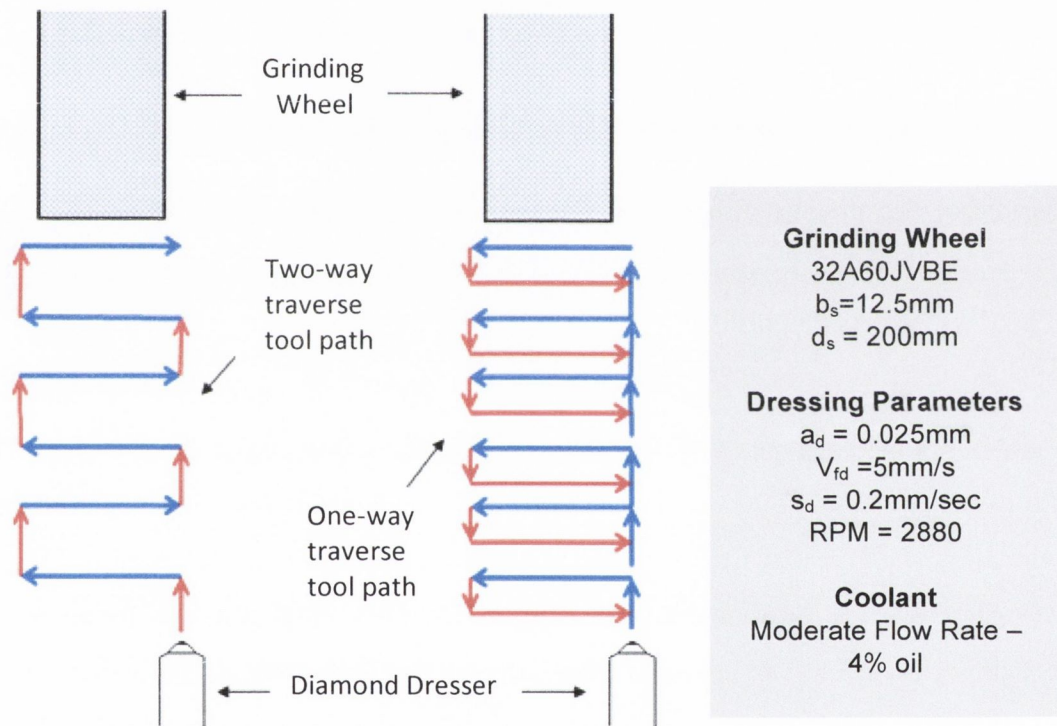


Figure 3.8: Illustration of one-way and two-way traverse tool path strategies

The dressing strategy tests were performed on the adapted Harrison CNC lathe set-up. The grinding wheels used were conventional aluminium oxide wheels, 32A60JVBE. Three diamond dressers were tested, two CVD polycrystalline diamonds, labelled A and B respectively and a polycrystalline HPHT diamond labelled D. The dimensions of the diamond face were typically 0.8mm square and 5mm in length. The diamond dresser length was measured prior to testing using a micrometer with a resolution of 1 micron. The diamond was then inserted into the tool holder in the machine and the

offsets were set by lining the diamond dressing tool up with the edge of the grinding wheel. Using the G-code implemented in the machine, 250 passes were performed with a dressing lead of 0.2mm/rev and a 25 μ m depth of cut. Coolant was supplied to the dressing zone via two loc-line nozzles at a flow rate of 20 litres/min and a pressure of 1MPa. Measurements of the diamond dresser length were taken at 0, 250, 500, 750 and 1000 passes for the break in period and every 1000 passes for the remaining 5000 passes.

3.5.2 Experimental results

A parameter known as the G-ratio is used in grinding to define the ratio of the volume of workpiece material ground to the volume of wheel lost [17]. Similarly, the diamond lost when dressing grinding wheels can be termed as the D-ratio which is defined as:

$$\text{D-ratio} = \left(\left(\left(\frac{\pi \cdot d_i^2}{4} \right) - \left(\frac{\pi \cdot d_f^2}{4} \right) \right) \cdot b \right) / (A_d \cdot \Delta h) \quad (3.1)$$

Where d_i is the initial grinding wheel diameter, d_f is the final grinding wheel diameter, b is the grinding wheel width, A_d is the area of the flat on the diamond and Δh is the change in diamond height.

The volume of diamond lost was calculated based on the measurements of the diamond length and plotted against the volume of grinding wheel that was dressed to give a D-ratio value. An initial high rate of wear was experienced during the break in period due to the wear slant created from a previous one directional test as illustrated in Figure 3.10. The wear of the diamond following a two directional test was more linear throughout the test as the profile of the diamond was consistent for both sides. This will be discussed in further detail in section 3.5.3. After the break in period, a linear relationship of the wear of the diamond dresser against volume of grinding wheel removed can be seen as the diamonds wear profile stays consistent for the remainder of the test. The wear of the diamond follows the pattern of a typical tool life curve whereby an initial break in period is seen followed by a steady state wear region (Figure 3.10)[134]. The D-ratio value is calculated from the linear region by adding a regression line to the steady state region and taking an inverse of the slope.

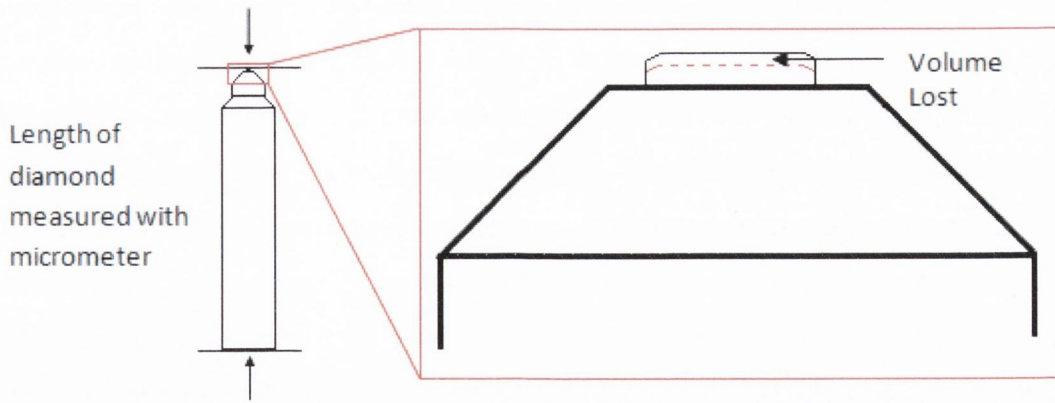


Figure 3.9: Measurement of the diamond wear

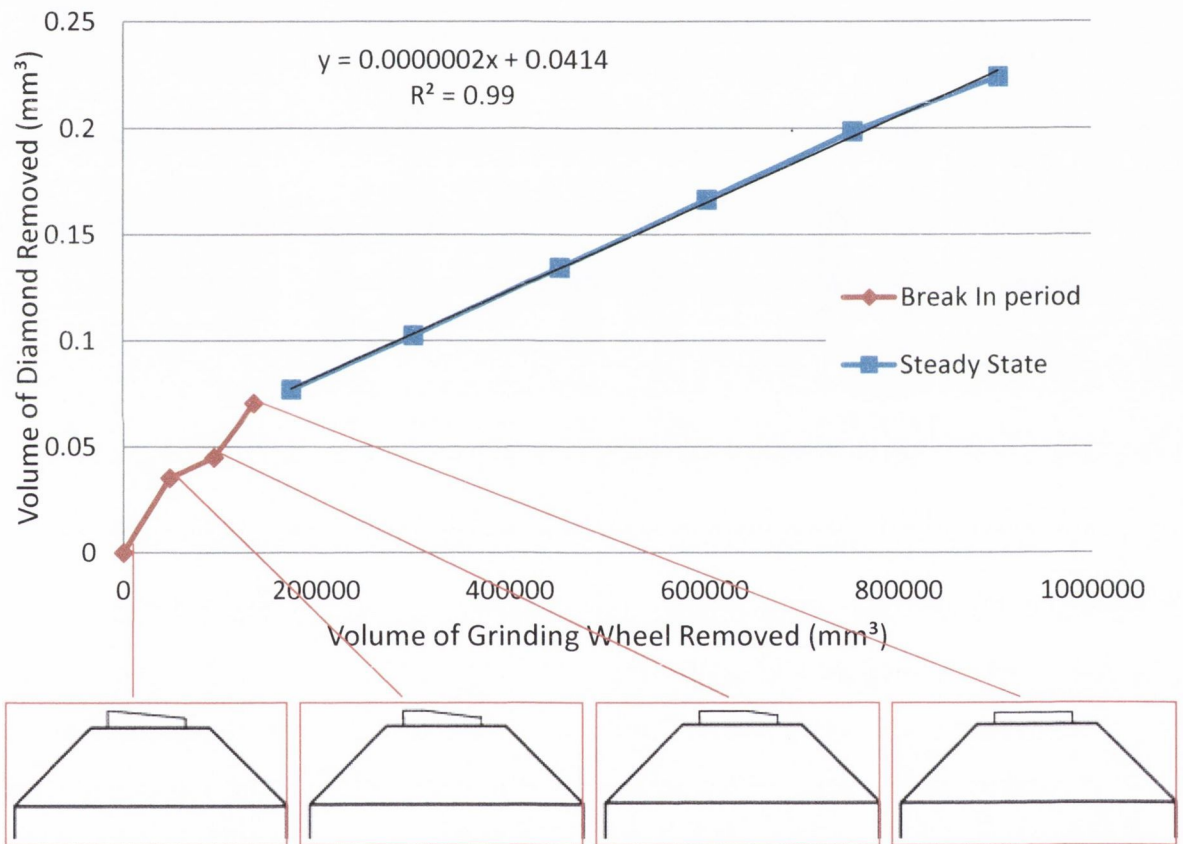


Figure 3.10: Wear graph of diamond dresser showing the break in period of the diamond dresser

D-ratio values of the dressing strategy tests can be seen below in Figure 3.11. Standard error bars were applied based on the deviation of the mean of 5 tests. A difference in D-ratio value of 25 million for one directional wear tests compared to 12.3 million for two-directional tests can be seen for diamond A. The two-directional D-ratio value is

almost half the value of the one directional test indicating that dressing the wheel from both sides results in twice the amount of diamond dresser wear compared to dressing the wheel from one side only. This trend is repeated for diamonds B and D also whereby a difference in D-ratio value of 11.2 compared to 6.3 can be seen for diamond B while D-ratio values of 20.6 and 10.7 were recorded for diamond D. There is also a difference between the individual diamond dresser with a grade 5 CVD diamond A giving similar results to the grade 5 HPHT diamond D. CVD diamond B with a grade of 3 results in a smaller D-ratio values of 11.2 compared to 20-25 million for diamonds D and A respectively.

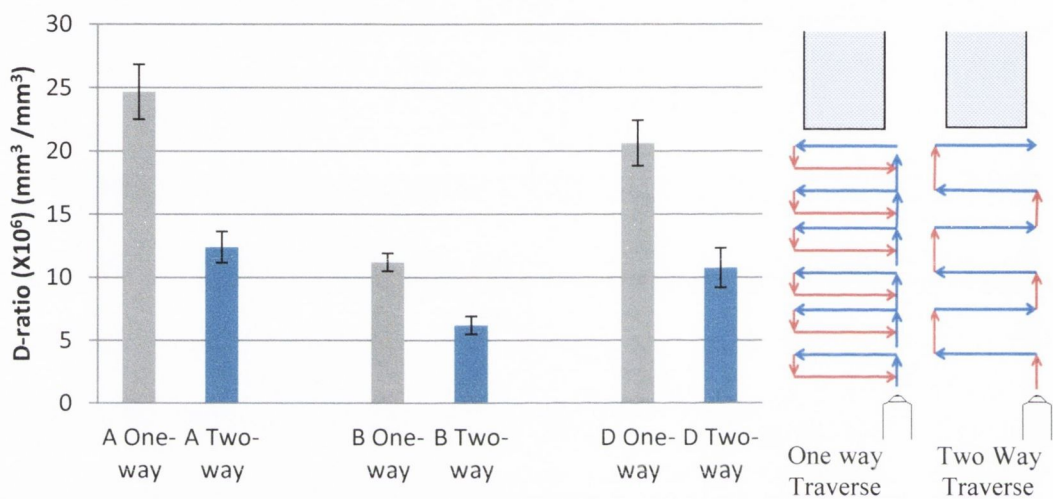


Figure 3.11: D-ratio values of diamonds A, B and D for one way and two way traverse tests

3.5.3 Discussion of results

It is hypothesised that the engagement of the diamond dresser with the grinding wheel is a factor contributing to the increased wear while dressing the wheel with two directions compared to one direction. During dressing, a taper would develop on the diamond dresser in the direction of the dressers traverse (Figure 3.12). For the one way traverse test, a slant would develop from one side only in the direction that the diamond engages with the wheel as can be seen in Figure 3.13 where an angle of 6° was measured. In this case, the overlap ratio of the diamond would be 4 as the full effective width of the diamond of 0.8mm is used to dress the wheel and the effective depth of dress would range from 0 to $0.025/4 = 0.006\text{mm}$. In the two directional tool path, a roof top effect would develop and a slant of 12° occurs on both sides of the diamond

as it comes in contact with the wheel from both sides. In this case, the overlap ratio would be 2 as the effective width would be 0.4mm due to the roof top effect and the effective depth of dress would be 0.0125mm indicating that an increase in the effective depth of cut would result in an increase in the wear of the diamond. However, Linke found that the depth of cut did not affect the grit collision frequency and had little effect on the diamond dresser temperature [30]. Linke did find that smaller overlap ratios gave larger dressing temperatures as would have been seen in the two directional tests. This increase in temperature due to the reduction in overlap ratio would cause the diamond to experience thermal fatigue which has been said to be one of the main reasons of diamond wear [135].

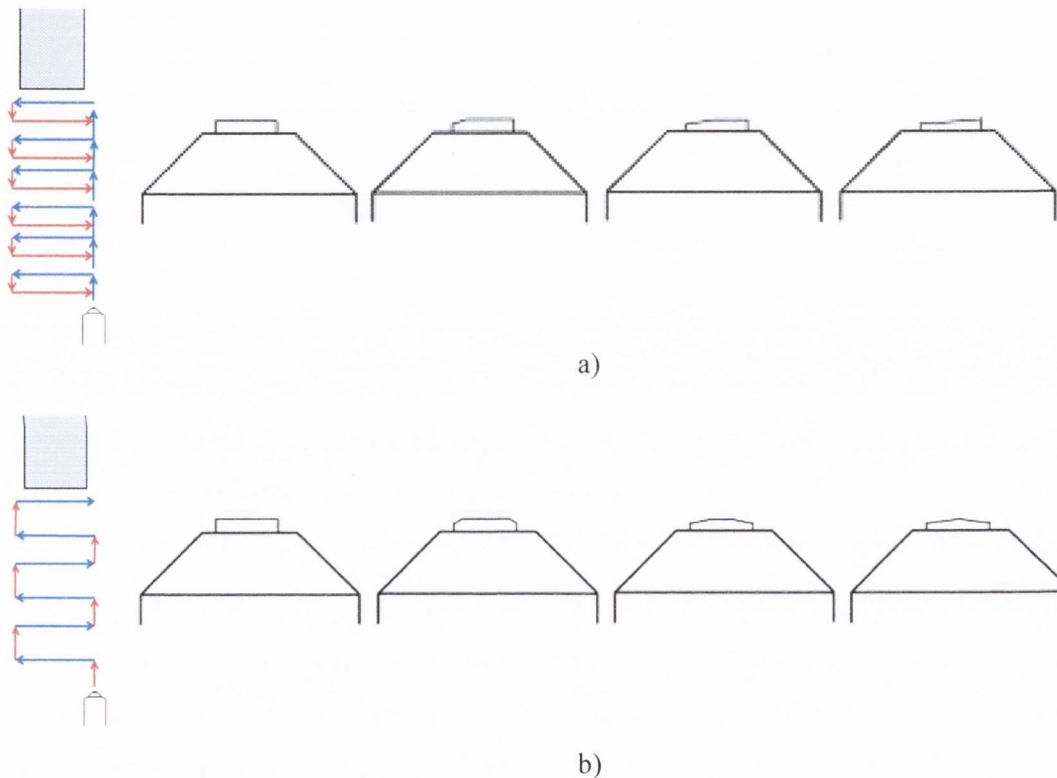


Figure 3.12: Wear profile change of the diamond dresser after a) One way traverse b) Two way traverse dressing paths

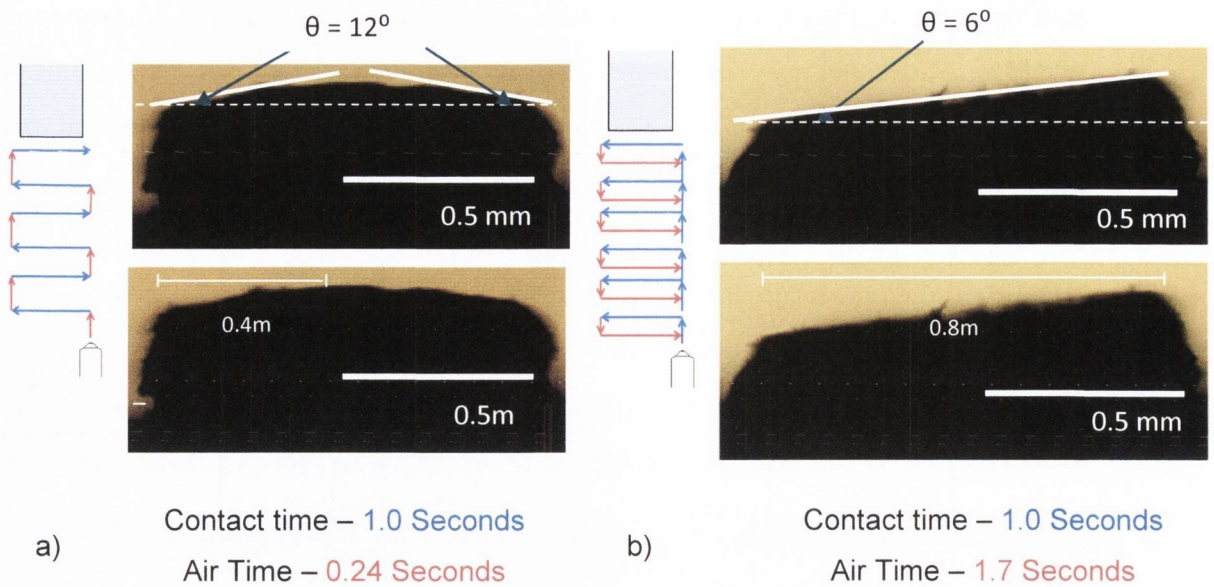


Figure 3.13: Diagram showing a) Tool path and diamond profile for two way traverse tests. b) Tool path and profile for one way traverse test

The second hypothesis is that during the dressing process, a large amount of friction occurs as the diamond dresser traverses across the face of the wheel which results in a temperature rise of the diamond dresser. It has been reported that temperature effects are one of the main factors contributing to the wear of the diamond [136]. The two-directional tests resulted in twice as much wear as the one directional tests. During the two-directional tests, the diamond is almost always in contact with the wheel as it traverses back and forth across the wheel. It has a contact time of one second where the diamond dresser engages the wheel creating friction and heat. This is followed by 0.24 seconds of cool down time as the dresser feeds in 25 microns, after which it is in contact with the wheel again resulting in more friction and an increase in the heat occurring. This process is repeated for 250 passes whereby the heat builds up after each pass which would lead to a significant rise in temperature causing the diamond to graphitize and wear.

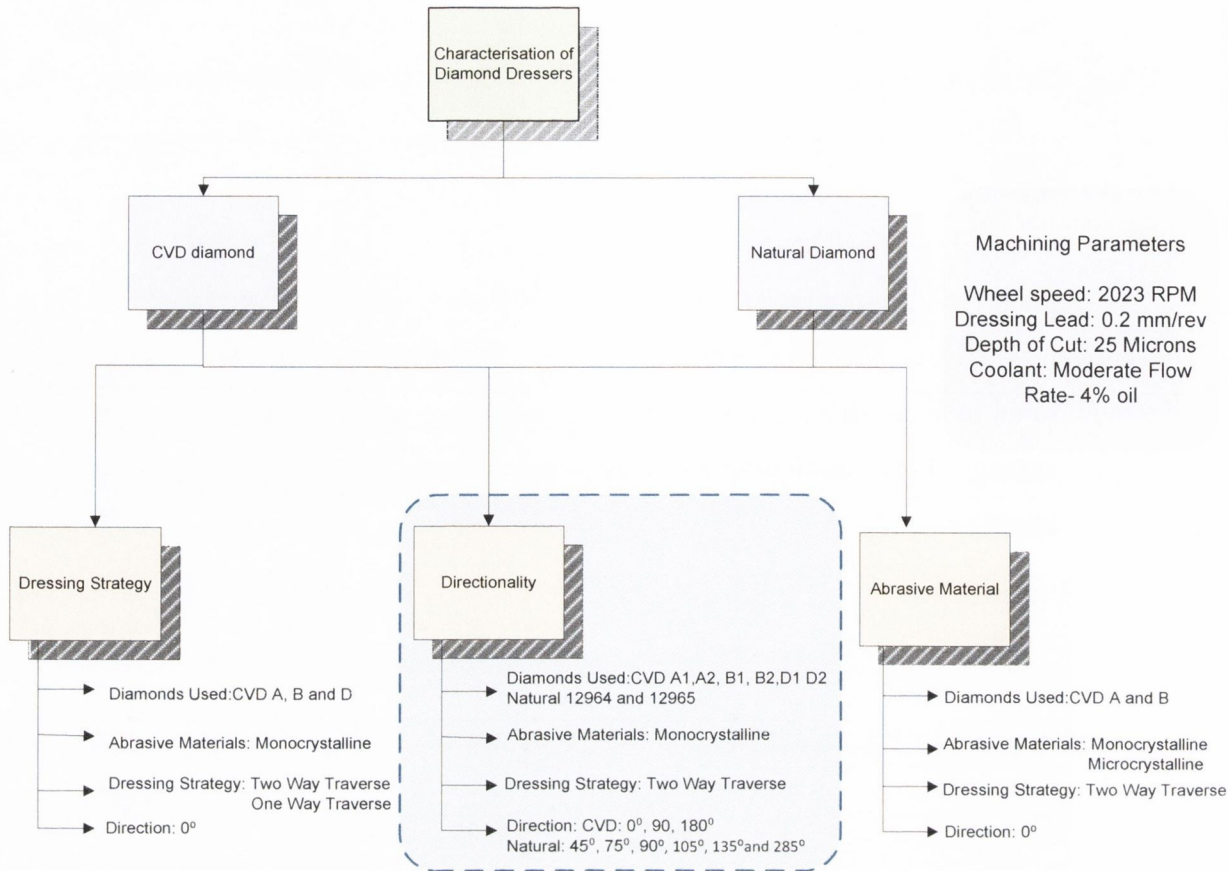
Whereas with one-directional tests, the diamond is in contact with the wheel for one second as it traverses across which is followed by a cool down time of 1.7 seconds as the diamond returns to the homing position as can be seen in Figure 3.14. This would result in less of a temperature rise as the diamond losses heat during this cool down phase.

Table 3.2 shows the material properties of diamond types A, B and D. It can be seen that the density, hardness, fracture toughness, Young's modulus and Poisson's ratio are all inherent properties of polycrystalline diamond and are independent of grade and manufacturing process for fully dense materials. However, the thermal conductivity of the three synthetic diamonds is different with grade 5 CVD polycrystalline diamond A, grade 3 CVD polycrystalline diamond B and grade 5 HPHT polycrystalline diamond having thermal conductivities of between 1800-220, 400-500 and 560-1100 respectively. Therefore it would seem that the main wear mechanism occurring is due to an increase in temperature of the diamond dresser based on the dressing tool path strategy chosen as all other material properties apart from the thermal conductivity are identical.

Properties	A	B	D
Density (g/cc)	3.52	3.52	3.52
Hardness(GPa)	85-100	85-100	85-100
Fracture Toughness (MPa.m ^{1/2})	8.5	8.5	8.5
Young's Modulus (GPa)	1000-1100	1000-1100	1000-1100
Poisson's Ratio	0.07	0.07	0.07
Tensile Strength (MPa)	560-1100	560-1100	560-1100
Compressive Strength (GPa)	9	9	9
Thermal Conductivity @ 20°C (W/m.K)	1800-2200	400-500	800-1200

Table 3.2: Material properties of polycrystalline diamonds A, B and D

3.6 Directionality Tests

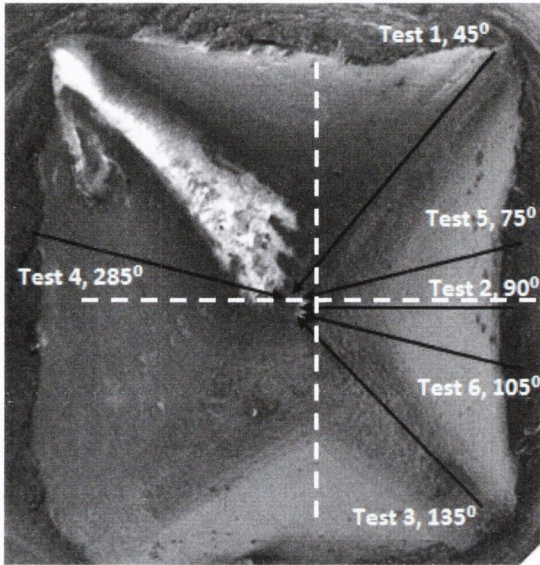


3.6.1 Experimental methodology

Directionality tests were performed on natural diamond dresser 12965 and synthetic diamond dressers A, B and D to investigate the wear properties of the diamonds in different directions. The crystal structure and manufacturing method for each diamond can be seen in Table 3.3. Three conventional aluminium oxide wheels (32A60JVBE) were dressed in each direction with a depth of cut of 25 microns and a dressing lead of 0.2mm/rev. The two directional tool path as described in section 3.5 was used to dress the wheels from an initial diameter of 203mm to a final diameter of 103mm. Tests were performed on the natural diamond single point dressing tool in the directions 45°, 75°, 90°, 105°, 135° and 285° as can be seen in Figure 3.14.

Diamond	Manufacturing	Crystal	Grade
A	CVD	Polycrystalline	5
B	CVD	Polycrystalline	3.5
D	HPHT	Polycrystalline	3-4
12965	Natural	Monocrystalline	6

Table 3.3: Diamonds used in the directionality tests



a)

Natural Diamond Directionality Tests	
Diamond	Natural 1a
Depth of Cut	25 Microns
Dressing Lead	0.2mm/rev
Dressing Strategy	Two-Directional
Coolant	Moderate Flow-4% oil
Grinding Wheel	32A60JVBE

b)

Figure 3.14: a) Test directions used for Natural Diamond Directionality tests b) Table of the testing parameters

The synthetic diamond dressers were dressed in the directions of 0° , 90° and 180° . Figure 3.15 shows a schematic diagram of the microstructure of these polycrystalline diamonds. As can be seen the grain size changes from its nucleation side where the grains are smaller to larger grains on the growth side. Therefore, tests were performed whereby the grinding wheel first came in contact with the nucleation side (0°), growth side (180°) or the intermediate side (90°) to investigate any effect of the grain sizes on the wear rate.

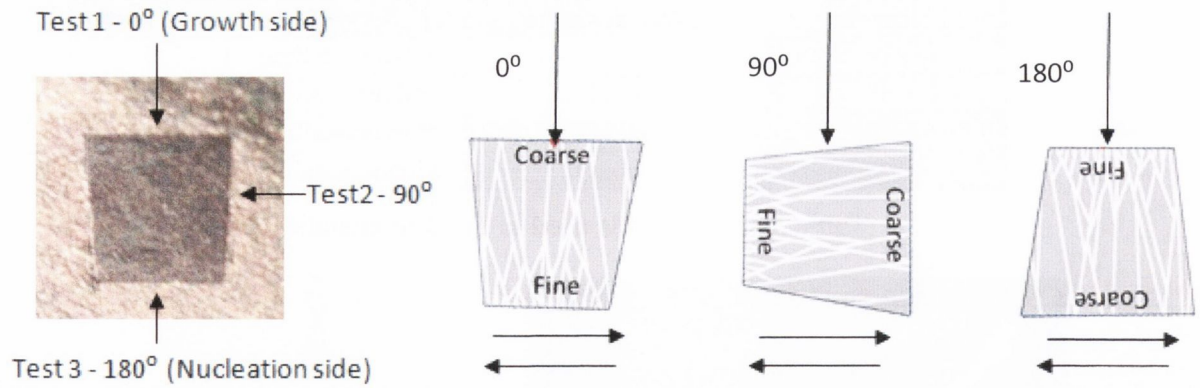


Figure.3.15: Diagram showing the test directions used and the microstructure of the diamonds

Measurements of the diamond length and wear area were made at 0, 250, 500, 750 and 1000 passes during the break in period and for every 1000 passes for the remaining 5000 passes. In order to ensure correct alignment, the directions were scribed on the housing of the diamond using a vernier height gauge. These marks were then lined up with a datum line on the tool holder.

3.6.2 Experimental results

Natural diamond

As has been reported by a number of authors, natural diamond is reported to be highly anisotropic with the diamond having different wear removal rates for various crystal planes and various directions on the crystal planes [9, 108, 109, 122, 130, 131]. Tests were performed on a natural diamond on the 100 plane (Figure 3.16) in the directions 45°, 75°, 90°, 105°, 135° and 285° as previously shown in Figure 3.14 by aligning a datum line on the diamond dresser with a line on the diamond dresser tool holder.

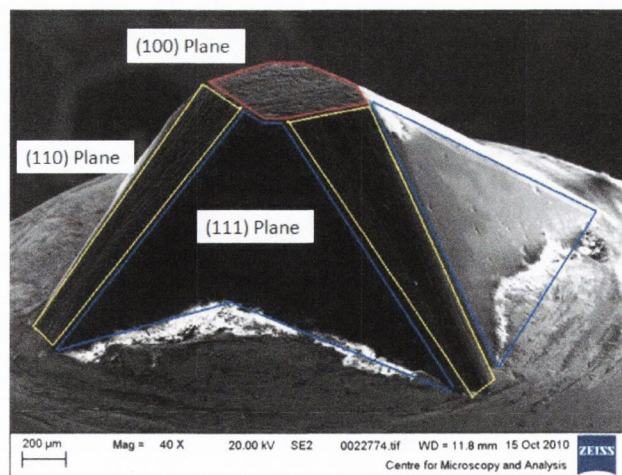


Figure 3.16: Diagram showing the different planes of a natural diamond

The results from the directionality tests performed on the (100) plane of the single crystal natural diamond dresser can be seen below in Figure 3.17a. The D-ratio values differed by a factor of 3 in this study depending on the direction chosen. The hardest direction was 135° which resulted in a D-ratio value of 33 million whereas the lowest value of 11.2 and 15 million were seen around the 90 degree soft direction. By plotting the results of the different directions on a graph of D-ratio value versus direction, it can be seen that a sine wave with four peaks and four valleys could be superimposed on the results which show that peaks correspond to the hard directions at angles of 45° and 135° and that lower values occurring in the 90° direction are found in the valleys or soft directions of the diamond as shown in Figure 3.17b.

The slight difference in experimental values from previously known values may be due to an experimental error in the alignment of the directions as Wilks report, even a small difference in the orientation may produce an appreciable difference in the abrasion resistance [137].

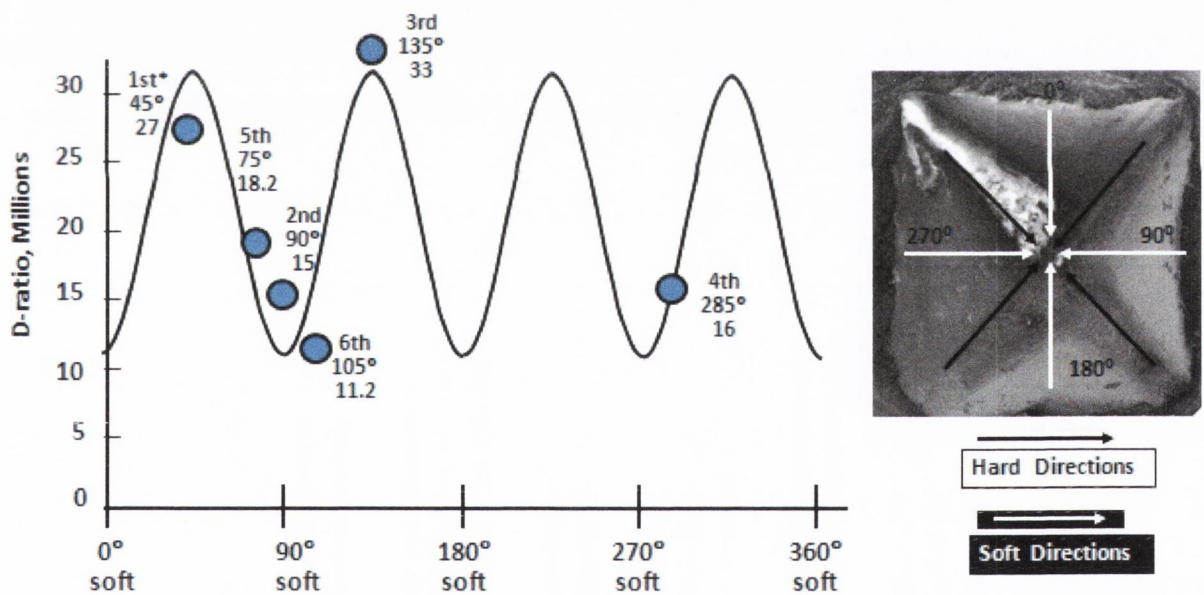


Figure 3.17: a) Graph showing results of D-ratios from directionality tests which correspond to b) the hard and soft directions of natural diamond

The reason for the variation in results between the hard and soft directions can be explained by looking at the spatial arrangement and distribution of the carbon atoms

in the diamond. The carbon atoms in the diamond lattice show different arrangements in different crystal planes leading to anisotropy in the mechanical and physical properties of diamond. Fields estimated the fracture or cleavage of diamonds in the different crystallographic planes. The values of cleavage energies calculated for different sets of crystallographic planes was equal to the number of bonds between particular planes to be fractured multiplied by the energy of the carbon-carbon bond.

CVD diamond

CVD diamond is reported to have high wear resistance due to the controlled environment under which it is manufactured which result in the diamond having less impurities, great hardness, high thermal conductivity and general low adhesion. Due to the growth of CVD diamond, the microstructure varies depending on the direction chosen. CVD diamond is manufactured in plates whereby the diamond grows from a nucleation side to the growth side [116, 138]. After the plate has been produced, the diamond is laser cut which results in a dressing log with a fine crystal size on the nucleation side (180°) and a coarse grain size on the growth side (0°) with a mixed microstructure on the intermediate side (90°) as seen in Figure 3.18b.

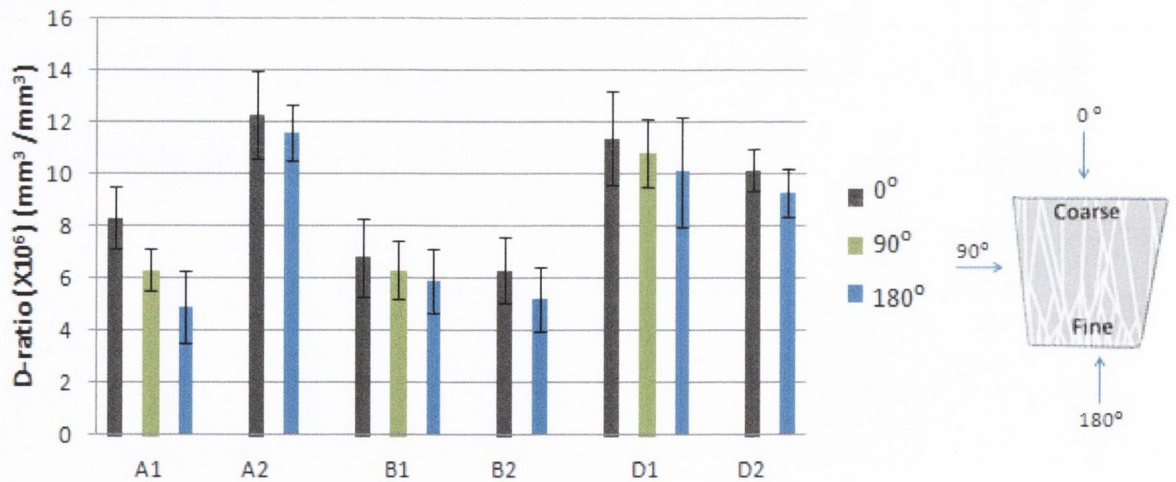


Figure 3.18: a) Tests performed with relation to growth direction and grain size. b) Results from test in each direction

The results from the directionality are shown in Figure 3.18a. As can be seen, a variation exists between the different diamonds due to the grade and manufacturing method used to produce the diamond. Within each diamond there is slight difference between the different directions with the coarse side having a slightly larger D-ratio than the nucleation side and the mixed side having a value in between the two. This variation is quite prominent in diamond A1 where the D-ratio value decreased by 41% from 8.3M in the 0^0 direction to 4.9M in the 180^0 direction as the grinding wheel hits the finer grain side first. However, tests performed on a second sample of Diamond A (A2) show only a slight decrease of 5.6% in the D-ratio value from 12.3 to 11.6 million when dressing in the 0^0 and 180^0 directions respectively. This trend was repeated for both samples tested on diamonds B and D where only a slight difference of the D-ratio value could be seen between the 0^0 and 180^0 direction. Diamond B had the larger decrease in D-ratio value of 13% and 17% for diamonds B1 and B2 respectively. While diamonds D1 and D2 D-ratio values varied by 11 and 8 percent respectively when dressing the wheel with the diamonds in the 0^0 and 180^0 directions.

3.6.3 Discussion of results

Natural diamond

The difference in removal rates between the various planes is due to density of carbon atoms and the density of covalent bonds between the carbon atoms. In order to remove a carbon bond from the surface, the covalent bonds between the carbon atoms must be broken down. The smaller the density of covalent bonds between the Carbon atoms, the easier it is to break down. The density of covalent bonds for the $\{110\}$, $\{100\}$ and $\{111\}$ plane are 1.22, 1.73 and 3 respectively. This implies that the $\{110\}$ plane would be the easiest to remove bonds from and the $\{111\}$ plane would be the hardest. Therefore, orientating the diamond dresser so as the $\{111\}$ plane comes in contact with the grinding wheel first would be the best choice as shown in order to gain the maximum life of the tool. However, the diamonds were positioned so as the $\{100\}$ plane was the plane protruding from the metal matrix. In this case, it is best to align the diamond with the hard directions, i.e. 45^0 , 135^0 , 225^0 and 270^0 in line with the grinding wheel in order to gain the maximum life of the tool.

CVD diamond

Considering, the scatter of results that may be present in wear tests and the range of D-ratios present in the natural diamond directionality tests where a factor of three was seen depending on the direction chosen, it would seem that the synthetic polycrystalline diamonds are isotropic and exhibit uniform properties in all directions. If anisotropy did exist, it would appear that the fine grains gave a slightly lower value than the coarse side. This is in line with studies performed previously whereby it is stated that as the grain size is increased so too is the wear resistance of the material [139]. One possible reason for the increased wear on the fine grain size may be due to micro chipping of the fine grains. The nucleation side would have a greater amount of grain boundaries due to the size of the grains which would result in more areas for the diamond to break down. A 3D METS analysis of CVD diamond A was performed which shows micro-chipping on the fine grain side, this is the narrower side of the diamond as shown by the illustration in the Figure 3.19.

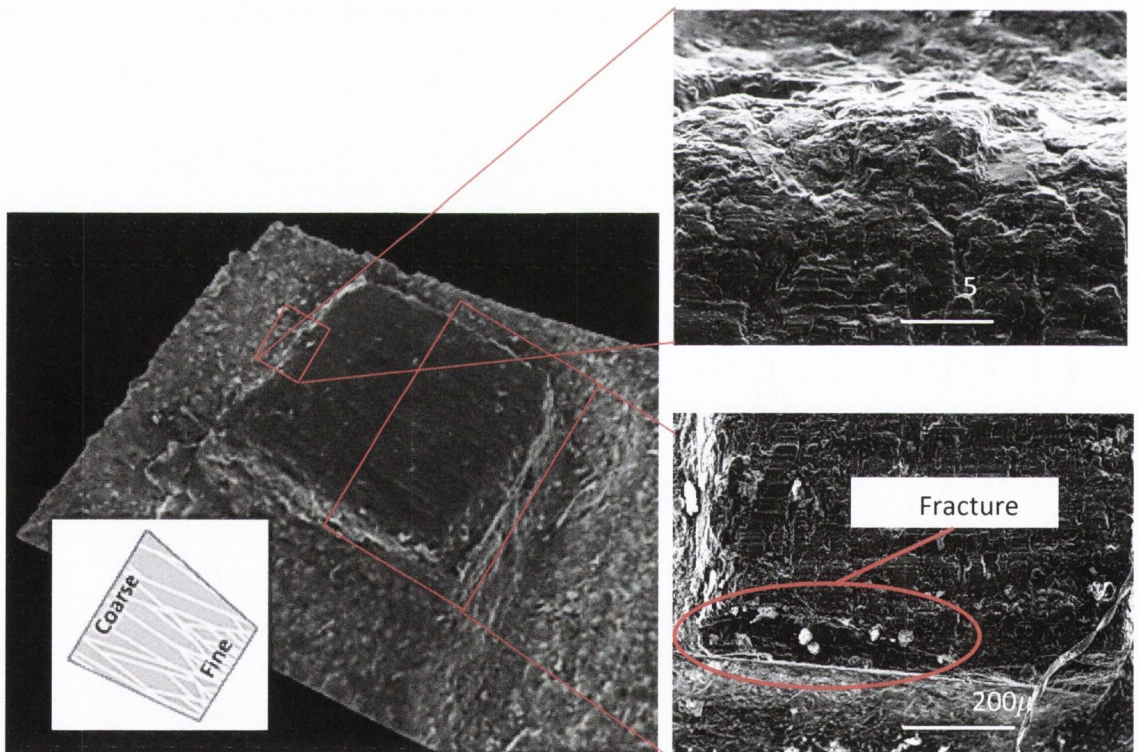


Figure 3.19: Mets Analysis of synthetic Diamond A showing greater fracture on the nucleation side

3.7 Change in geometry of the diamond

The profile of the natural and synthetic diamonds were assessed during the directionality tests using a Leica L2 microscope and detailed analysis was performed using a scanning electron microscope and white light analysis. During the initial stages of the break in period, a wear pattern can be seen as shown in Figure 3.20. Brittle fracture by cleavage is the main wear mechanism which occurs on the top and leading edges but not on the bottom trailing edge. Micro-fracture of the diamond occurs due to the high stresses involved as the grinding wheel comes in contact with the new sharp cutting edges of the diamond dresser.

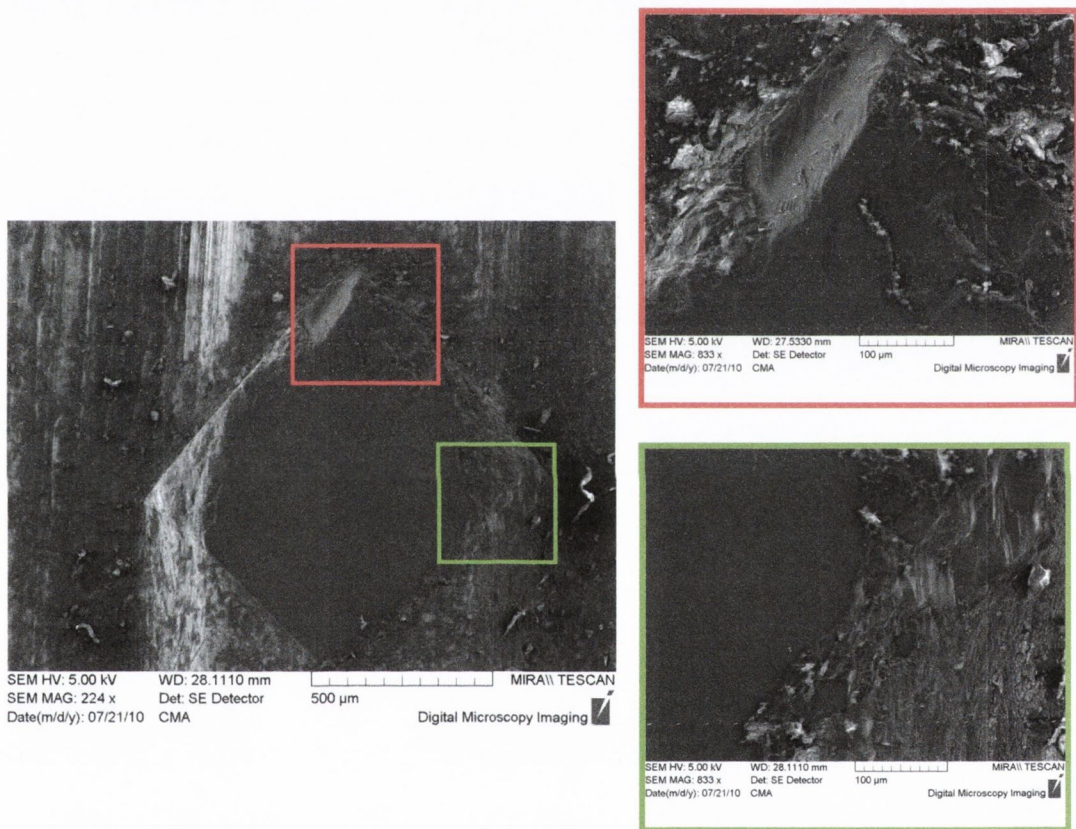


Figure 3.20: SEM photos of a worn diamond after 4 dressing passes

As the dressing passes increase, gradual wear through micro-fracture and abrasion is observed and the wear area is increased. Once the diamond has broken in, the grits on the grinding wheel would have less of an impact on the diamond dresser. It can be observed that the main wear mechanism occurring is more mechanical wear but due to abrasion this time as the grits come in contact with diamond face. This can be seen in

Figure 3.21 whereby abrasive marks from the grits can be seen in the direction of wheel rotation.

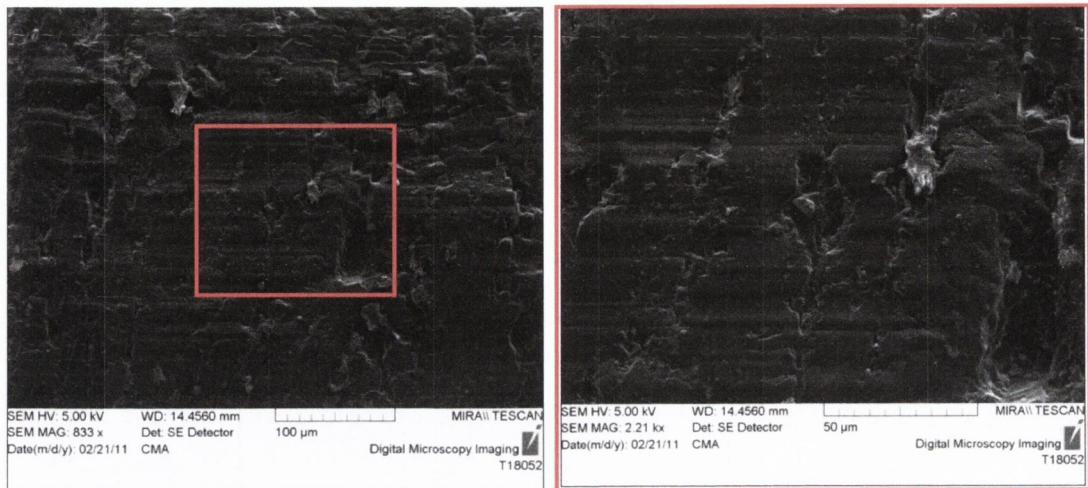


Figure 3.21: SEM photos showing the abrasive wear of the diamond as horizontal scratches on the surface

As the diamond has broken in and the wear flat has progressed, the profile of the diamond stays consistent throughout the course of the tool life and it maintained a consistent dressing effective width. Whereas natural diamond starts off sharp and pointed and as the diamond is used, a wear flat progresses as can be seen in Figure 3.22. Here, the effective width of the diamond develops from 0.1mm to 1.6mm as the diamond wears which would have a direct impact on the dressing conditions. For example, if a lead of 0.2mm/rev was used for a natural diamond at the start and end of the tool life, a difference in overlap ratio of 8 compared to 0.5 can be seen when using a natural diamond with a width of 1.6mm compared to 0.1mm. The wear can be quite rapid during the initial stages of its tool life use as the diamond starts off with a pyramid shape and loses as much as 1 mm of height after dressing only 250 dressing passes.

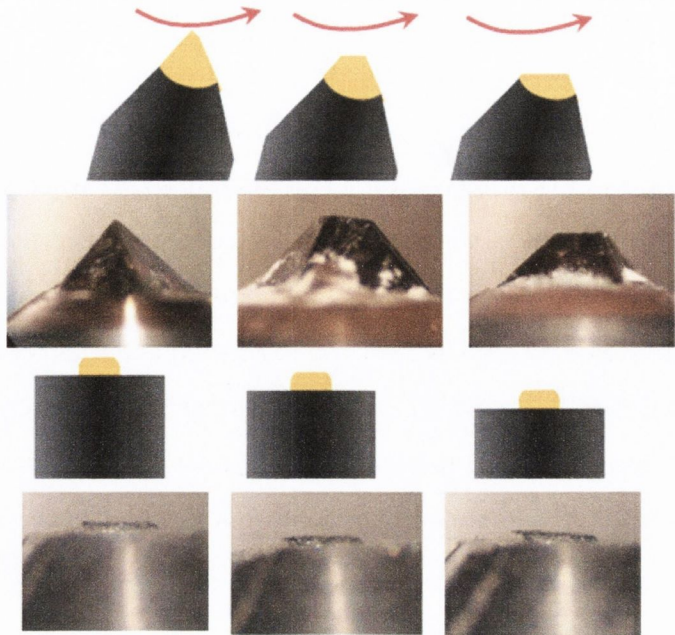
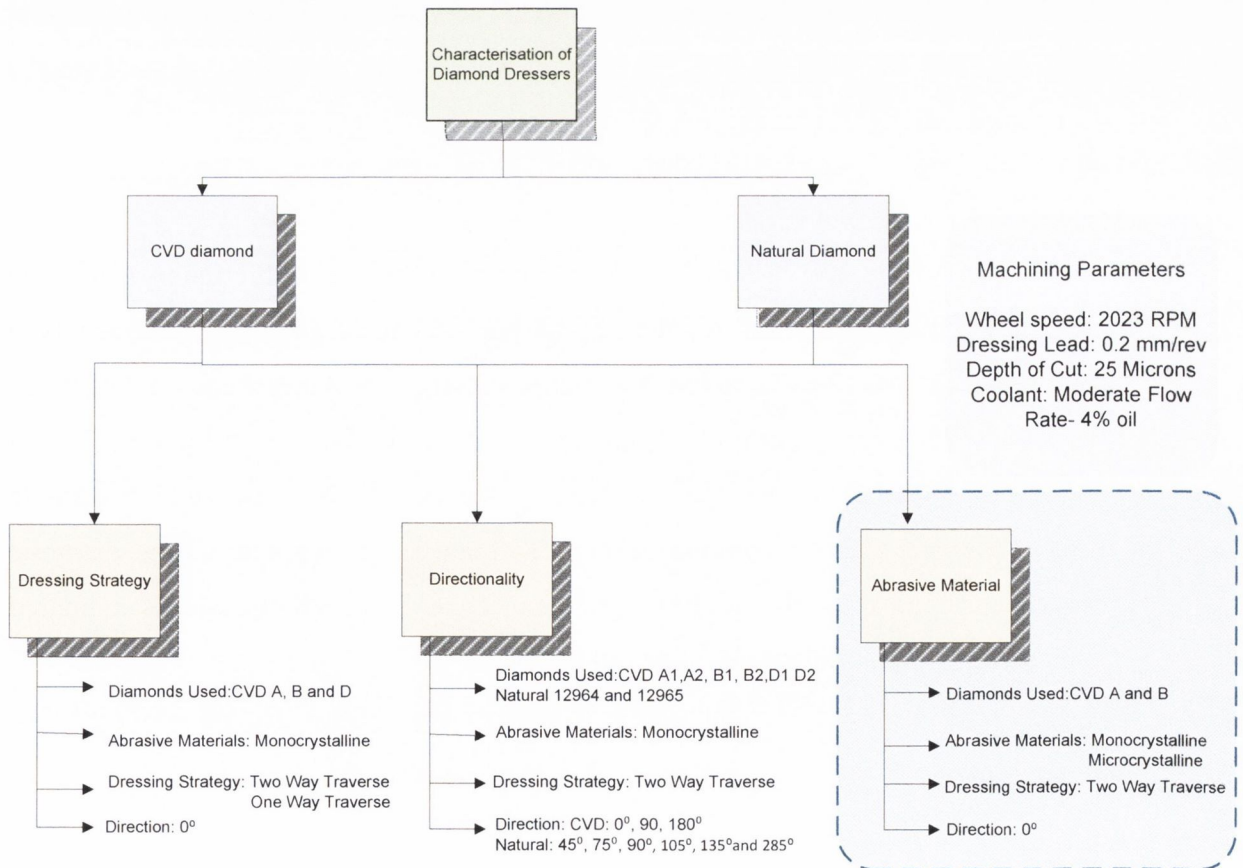


Figure 3.22: Progression of the diamond dressers wear profile

3.8 Abrasive material



3.8.1 Methodology

The wear of the diamond was investigated when dressing a conventional aluminium oxide grinding wheel and a ceramic grit (SG) grinding wheel. The ceramic grits claim to have 3 times the tool life of conventional aluminium oxide wheels in terms of parts produced in between dressing. However, it has been observed that the SG wheels consumed the diamond at a much greater rate compared to Al_2O_3 wheels. Therefore, diamond wear tests were performed on two CVD diamonds A and B with the standard mono-crystalline grit grinding wheel and a ceramic grinding wheel, containing 50% Norton-SG abrasive and 50% aluminium oxide grit held in a vitrified bond to assess the difference in wear rates when dressing both wheels. The wheels were dressed with a depth a cut of 25 microns and a dressing lead of 0.2mm/rev using the two directional tool path as discussed in section 3.4.

The size of the fractured grits produced while dressing aluminium oxide and ceramic grit wheels were examined to study any difference in the wear mechanisms of the grits. This was performed by collecting swarf from the dressing process, filtering the swarf through filter paper to separate the grits from the coolant, at which stage the grits could be cleaned with rubbing alcohol. The samples were then mounted on stubs and viewed in a Tescan MiraXMU Scanning electron Microscope.

3.8.2 Experimental results

The wear of diamonds A and B while dressing conventional aluminium oxide and ceramic grinding wheels are plotted against the volume of grinding wheel removed (Figure 3.22). The D-ratio values for each test were calculated from the linear red region of each graph. The results from the wear tests can be seen in Figure 3.23. An increase in the wear of the diamond dressers was noted when dressing the ceramic wheels compared to conventional wheels. In both cases, the wear of the diamond dresser was approximately four times greater when dressing ceramic wheels compared to conventional aluminium oxide wheels.

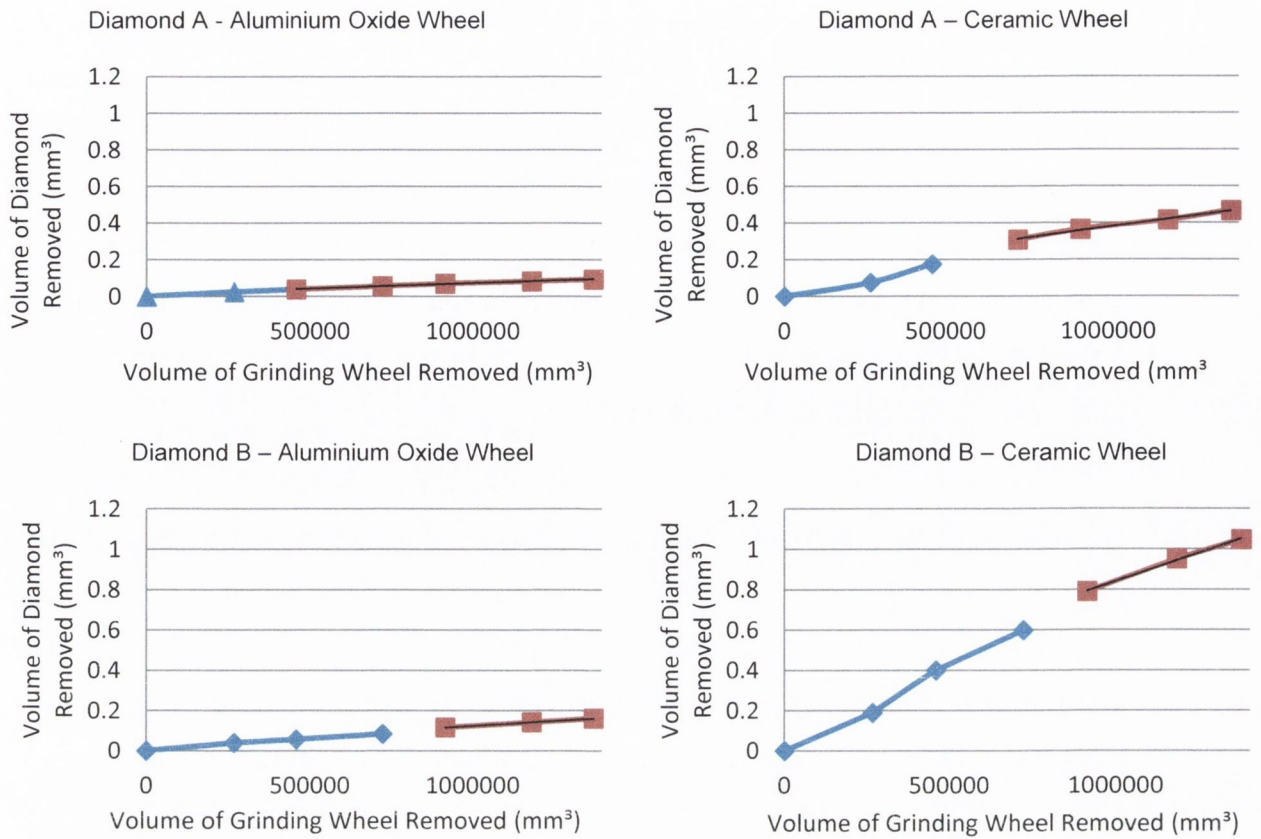


Figure 3.22: Wear graphs of diamonds A and B when dressing conventional and ceramic wheels

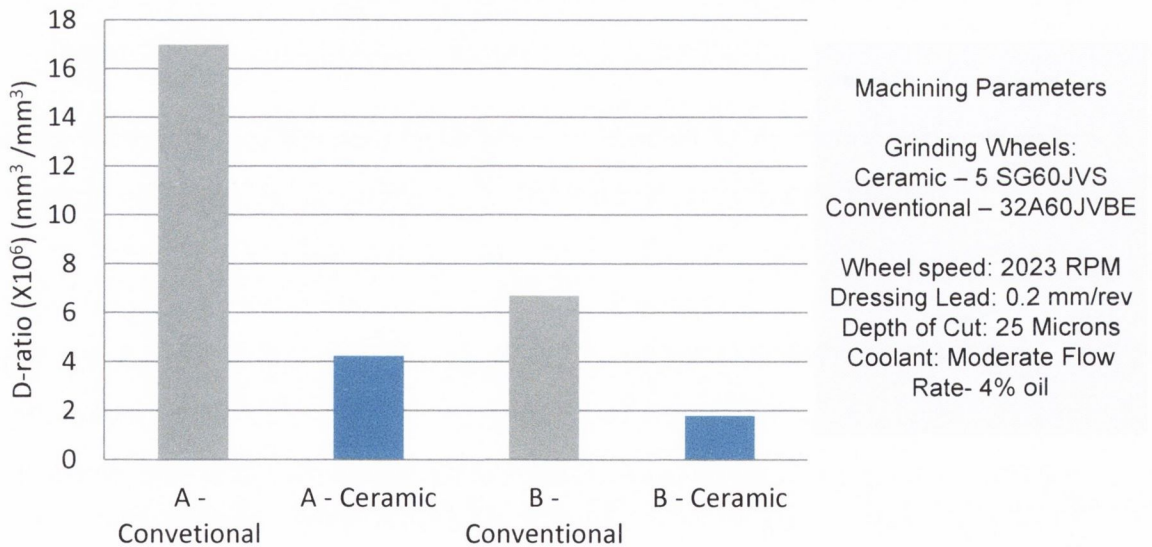


Figure 3.23: Comparison of D-Ratio values for SG and Al₂O₃ Wheels

3.9.3 Discussion of results

The ceramic wheels wore the diamond about 4 times faster than conventional aluminium oxide wheels. The ceramic wheels consisted of mixture of 50% sol gel microcrystalline abrasive and 50% aluminium oxide monocrystalline grit whereas the aluminium oxide wheels consisted of 100% aluminium oxide grit. By equating the percentage of grit and the wear experienced on the diamond for both wheels, it would appear that the sol gel microcrystalline abrasive wears the diamond about 7 times faster than conventional aluminium oxide grit.

This increased wear could be due to the nature of fracture of the SG grits. SG wheels are made up of microcrystalline alumina which is a tougher and more fracture resistant grit whereas aluminium oxide wheels are made up of monocrystalline fused alumina which have larger crystals and are easier to fracture. The increase in toughness of the ceramic grits would result in greater force acting on the diamond dresser as it conditioned the wheel which would cause the diamond dresser to wear faster.

Shih and Akemon compared D-ratio values with similar diamond dresser wear tests that had been performed by Werner and Minke, it was noted that a significant reduction in G-ratio values could be seen in their results. It was reported that the increase in wear was due to the use of SiC abrasives being tougher than the Aluminium oxide wheels which were used in tests performed by Werner and Minke [140].

Study of grit size

In order to study the type of fracture occurring when dressing both wheels, the swarf was collected and looked at under an SEM as shown in Figure 3.24. The grits were categorised into three groups, grit pull-out, grit fracture and grit micro-fracture. Pull out grits were classified as grits with an average diameter of 250 microns in size, the grit fracture group consisted of segments ranging in size from 100-200 microns, while micro-fracture grits were less than 100 microns in size. Table 3.4 shows the results of the percentage of grits, it can be seen that grit fracture is the main wear mechanism occurring when dressing conventional wheels with 57% of the swarf material consisting of grit segments with an average size of between 100 and 200 microns. This is in contrast to swarf collected from the ceramic wheels where 63% of the swarf consisted of grit micro-fracture. The difference in percentage of the grit fracture size is due to the composition of the grits as the ceramic grits are made of a microcrystalline

structure which would resist large grit fracture and fracture into smaller segments instead. This would result in more interaction of the diamond dresser with the wheel as the grit fractured into smaller pieces. In both cases the main wear mechanism occurring is grit fracture as the bond strength J of both wheels resisted grit pull out under the dressing conditions chosen. This supports the argument made that the grits in a ceramic wheel would resist

Wheel Type	Grit pull out	Grit Fracture	Grit Micro-
Conventional	19%	57%	24%
Ceramic	7%	30%	63%

Table 3.4: Percentage of grit types collected when dressing conventional and ceramic wheels.

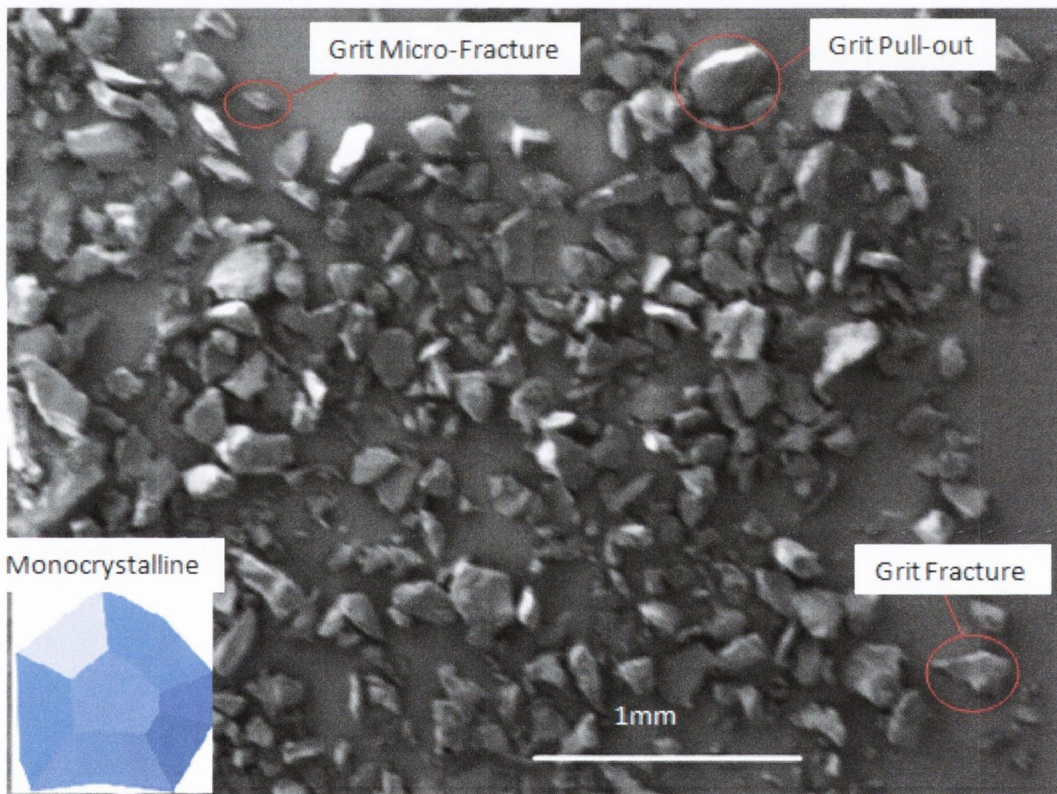


Figure 3.24a: SEM image of grits collected after dressing an Aluminium Oxide wheel

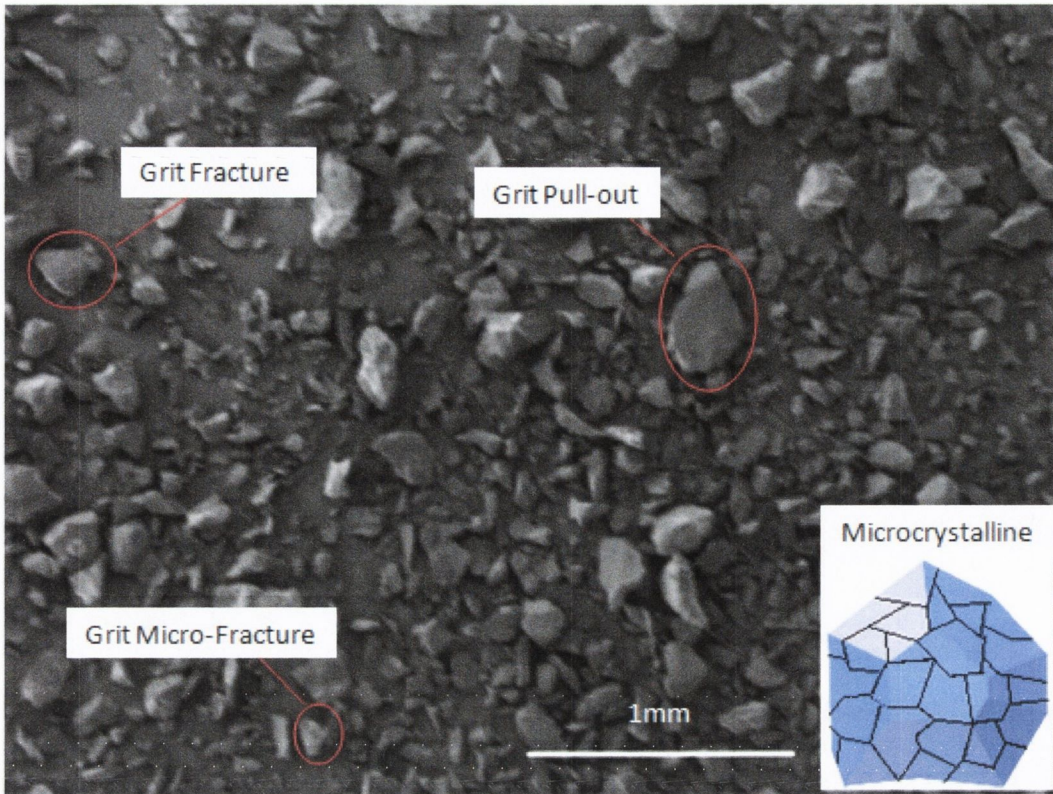


Figure 3.24b: SEM image of grits collected after dressing a ceramic microcrystalline grinding wheel

Chapter 4 Dressing process characterisation methodology

The main parameter contributing to the outcome of the dressing process is the overlap ratio of the diamond which is the number of times a point on a wheel comes in contact with the diamond dresser [141]. This is defined as:

$$U_d = \frac{S_d}{b_d} \quad (4.1)$$

Where S_d is the dressing lead given by

$$S_d = \frac{V_{tr}}{N_s} \quad (4.2)$$

where V_{tr} is the traverse speed of the diamond dresser in mm/minute, N_s is the rotational wheel speed in revolutions per minute and b_d is the width of the diamond.

As shown in chapter 3, significant wear of the diamond occurs throughout the life of the dressing tool. This would cause the value of b_d , the width of the diamond to increase as the wear progresses. This increases the value of the overlap ratio as the larger diamond width results in a greater amount of collisions of the grits with the diamond. This can lead to burning of the workpiece as the consecutive hits of the diamond dresser blunt the wheel resulting in greater specific energies while grinding. In practice, the diamond should be rotated to reveal a fresh cutting edge or else the traverse speed, V_{tr} should be increased to accommodate for the increase in the diamond width, b_d . Investigations were performed using a CVD diamond dresser with an effective width of 0.8mm x 0.8mm. The traverse speed of the CVD diamond was then altered to replicate the wear of natural diamond and the resulting increase in overlap ratio.

By monitoring the dressing process and the diamond wear, corrective action could then be taken to ensure workpiece tolerances are maintained within their limits. This could only occur once the dressing and grinding process had been characterised for a given set of dressing and grinding parameters.

The device used to monitor the dressing process was an Acoustic Emission (AE) sensor. AE sensors have been applied to various aspects in grinding, the most notable is contact and collision detection [20] which has seen widespread use in industry and to a lesser extent wheel imbalance, wheel roundness and part roundness [19, 20]. Other

authors have also looked at using the AE sensor to detect grinding burn [20, 142], grit workpiece contact mechanisms and wheel wear mechanisms [20, 143]. In spite of this and the fact just previously explored that dressing conditions have such an impact on the specific energies and surface finish during grinding, research has not been performed looking at the relationship between the AE signal and the wheel sharpness. Therefore investigations were made into the dressing AE signal and its correlation with the grinding specific energy. Tests were then performed to study the effect of the AE signal with a growth in the diamond dresser wear which is a major problem in the industry contributing to unstable grinding operations and high specific energies.

Figure 4.1 shows the input factors that contribute to wheel topography at the beginning of the grinding process which is influenced by the dressing tool, the dressing kinematics and the grinding wheel. The dressing tool and dressing kinematics have been studied by many authors [6, 27, 34, 46, 49, 144, 145]. One factor that has received little attention is the grit size of the wheel and its effects on the specific energy and workpiece surface roughness.

It is generally believed that there is a trade off between surface finish and the heat generated in grinding. It is the dressing process that contributes significantly to these two outcomes whereby finer dressing conditions (larger overlap ratios) lead to better surface finishes but increase the risk of thermal damage and chatter. In large scale production, it is often seen that coarser grits are used with dull dressing conditions to achieve a fine surface finish resulting in elevated temperatures being experienced which can affect the integrity and lifespan of the workpiece. However it appears that finer grits with a more aggressive dressing process may lead to similar surface finish values with lower heat generation. While there is research performed which shows the relationship between dressing conditions and specific energy values and surface finish [27, 32, 145], the effect of dressing conditions while using different grit sizes on the surface finish and specific energy during grinding has not been established. The work presented below will explore the effect various grit sizes have on the grinding specific energy and surface roughness of the workpiece while being dressed at different overlap ratios.

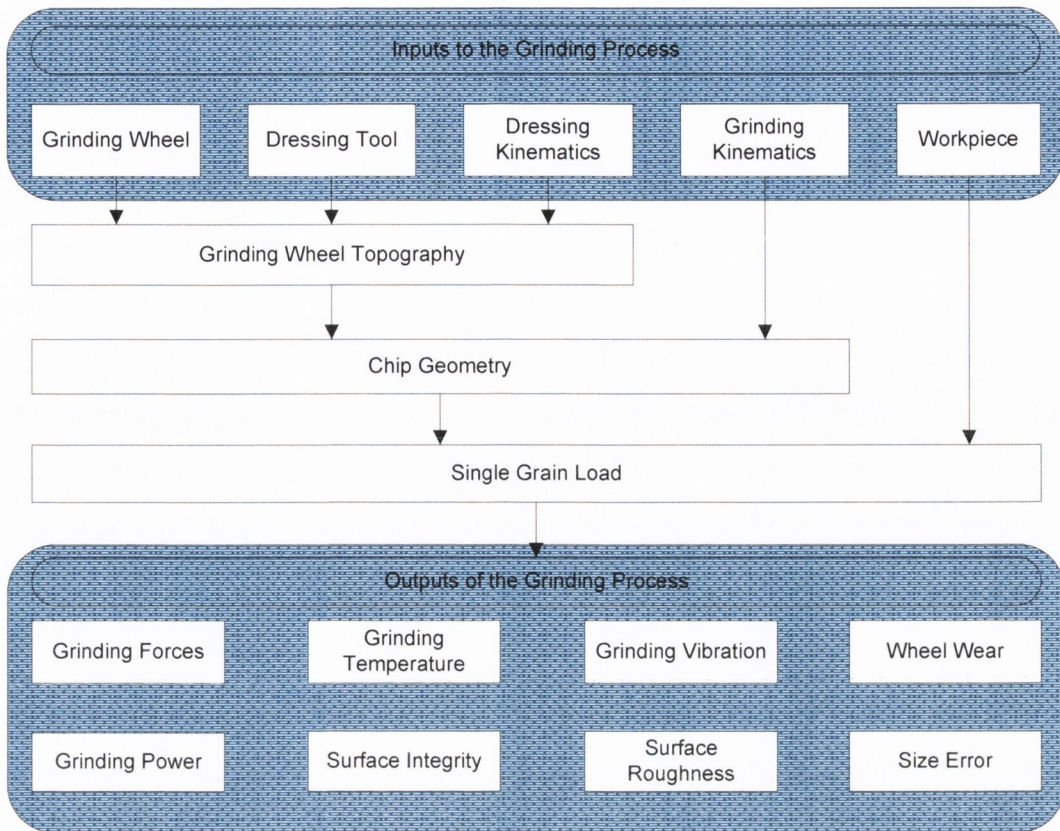


Figure 4.1: Inputs and outputs of the grinding process

The specific energy was studied by recording the grinding forces using a Kistler 3 axis dynamometer. Grinding forces are one of the most important factors affecting the grinding process as they influence the chip formation mechanisms, grain wear and the temperature of the workpiece. High normal forces can lead to self induced vibration which causes chatter and high tangential forces cause an increase in heat generation which can lead to thermal damage of the workpiece. By monitoring the grinding forces in these experiments, the condition of the wheel can be determined, with a sharp wheel resulting in lower forces while high forces are experienced when using a blunt wheel.

The surface finish of the workpiece dressed and ground under the above conditions with various grit sizes and overlap ratios was examined using a stylus profilometer and white light interferometry. Outlying peaks or troughs on the surface will be identified which could have a detrimental effect of the performance of the part when such high tolerances are required.

In contrast to theory, the practice of performing the dressing process with a finishing pass is often used in industry. However, the effect of a finishing pass has not been

examined at a scientific level. This operation involves traversing the diamond dresser across the wheel after a dressing pass has been performed with zero infeed. It is believed that the purpose of the finishing pass is to pick up any outlying grits on the surface of the wheel that the diamond dresser has missed and in turn creates a more uniform surface. The effect a finishing pass has on the grinding performance and surface finish will be studied by monitoring the grinding forces and measuring the surface roughness of the workpiece following grinding using a stylus profilometer. The AE signal was recorded during the dressing process to study the AE intensity of a finishing pass. The specific energy was then examined following dressing to investigate whether a correlation exists between the AE signal intensity and the grinding specific energy.

The methodology for the investigations can be seen in Figure 4.2. This methodology enabled the effect of overlap ratio, grit size and dressing finishing pass on specific energy and surface finish to be examined. Similarly, the insight into the dressing process from the AE signal during dressing was investigated to establish whether a correlation exists between the AE signal and the grinding specific energy and workpiece surface finish.

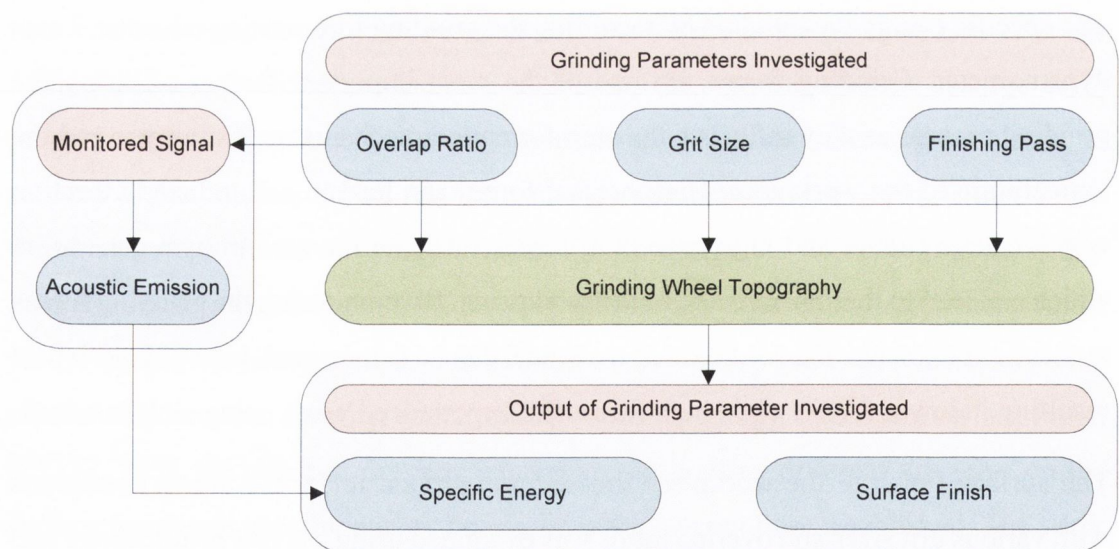


Figure 4.2: Summary of the dressing and grinding investigations performed

4.2 Equipment

The equipment and sensors used during the dressing and grinding investigations and post machining for analysis of the workpiece and tool are identified and briefly described in this section.

4.2.1 Grinding machine

A Jones and Shipman surface grinder located in the Mechanical and Manufacturing Engineering department in Trinity College Dublin was used to perform the dressing and grinding experiments.

The machine consists of a reciprocating table, coolant system, and magnetic chuck. The reciprocating table can be driven manually using a flywheel or it can be driven automatically by using a hydraulic traverse. 4% oil based coolant was provided by means of a pump and the swarf is collected so that it can be removed before the coolant re-circulates again. In order to enable a precise traverse speed of the diamond dresser, the cross-feed which was previously driven manually was converted to be controlled by a motor. A precision servo motor was used for this conversion and code was written using the smart motor interface. This enabled the diamond dresser to traverse back and forth across the wheel at precise traverse speeds so as the desired dressing overlap ratios could be obtained. Fixtures were custom built to connect the servo motor to the drive shaft. A steel clamp coupling was used to connect the spindle of the motor to the plate attached to the drive shaft. Slots were machined in the side of the coupling to allow for any rotational run out that may be present between the spindle and the plate.

The wheel speed was measured prior to and during the grinding tests to ensure that a constant wheel speed was maintained. A handheld tachometer held 10cm from the wheel was used to measure this. The device works by placing a piece of reflective tape on the edge of the grinding wheel. A flashing beam of light is shone at the periphery of the wheel and the wheel speed is recorded from the light that is reflected back to the tachometer. It was found that values for the wheel speed did not differ by more than +/- 4 RPM. The workpiece speed V_w was checked throughout the experiments by measuring the time to travel the 200mm of wheel head and was found to be within 5% of the experimental value of 100mm/min.

The dynamometer was secured to the magnetic chuck during machining. The workpiece specimen (length=100mm, width=60mm, height= 30mm) was held in a clamp that was bolted to the three axis dynamometer. A dressing tool holder was manufactured to hold the diamond dresser to the tool bed. A hole with a tolerance fit of 10mm in diameter was drilled to ensure a tight fit of the diamond dresser, two grub screws were used to secure the dresser in place so that any unwanted vibration during dressing would be eliminated. An M6 bolt was used to mount the acoustic emission sensor to the tool holder which enabled the acoustic emission signal to be recorded throughout dressing (Figure 4.3).

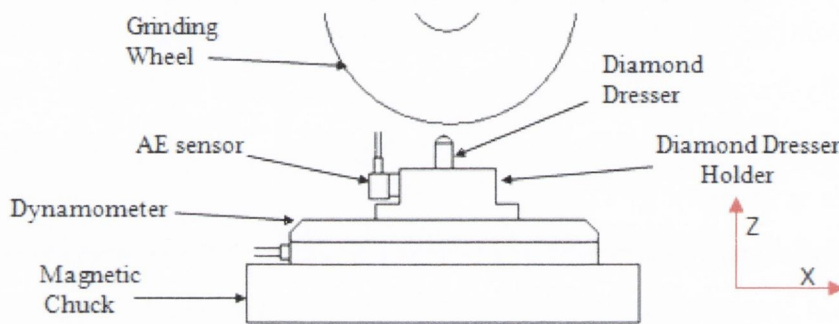
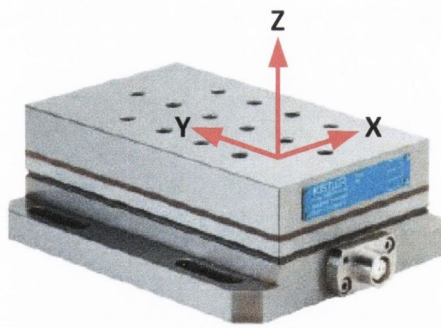


Figure 4.3: Schematic diagram of experimental set up

4.2.2 Dynamometer

A piezoelectric force dynamometer was used to measure the tangential force (X-direction) and normal force (Z-direction) during the grinding process. The sensor measures charge generated by deflection caused by a force during the grinding process. The charge signals are then converted into force components where comparisons of the force experienced during grinding could be compared for various wheel conditions based on the dressing parameters. A Kistler three-component type 9257B workpiece dynamometer as shown in Figure 4.4a was used for these experiments. It has high rigidity and hence a high natural frequency that enables very small dynamic changes to be measured in large forces. The technical data is shown in 4.4 b.



a)

Range	F_x, F_y, F_z	kN	-5 to 5
Sensitivity	S_x, S_y	pC/N	≈ -7.5
	S_z	pC/N	≈ -3.5
Rigidity	R_x, R_y	kN/ μm	>1
	R_z	kN/ μm	>2
Natural frequency	$f_o(x, y, z)$	kHz	≈ 2.3
Capacitance		pF	≈ 220

b)

Figure 4.4 a) Kistler type 9257B workpiece dynamometer with orientation of the three force components. b) Technical data of dynamometer, 9257B

The dynamometer consists of four three-component force sensors with each sensor containing three pairs of quartz plates, one sensitive to force in the Z-direction and the other two sensitive to shear in the X and Y directions. The electric charge generated as a result of changes in force in the crystals is converted to a proportional voltage via Kistler Type 5011B charge amplifiers. Due to the length of the data acquisition time, a build up of the charge was seen which lead to drift of the signal being sent from the charge amplifiers. This was minimised by resetting the charge amplifiers before each test run. It was important to identify any drift and account for it in the raw data when analysing the signal. The sensitivity of the charge amplifiers ($F_x, F_y = -7.5 \text{ pC/N}$, $F_z = -3.7 \text{ pC/N}$) and a time constant (long) were preset and validated during dynamic load calibration experiments on an Instron 8874 axial-torsion fatigue testing system located in the department of Mechanical and Manufacturing Engineering in Trinity College Dublin. The calibration curve and coefficients obtained during the calibration are shown in Figure 4.5.

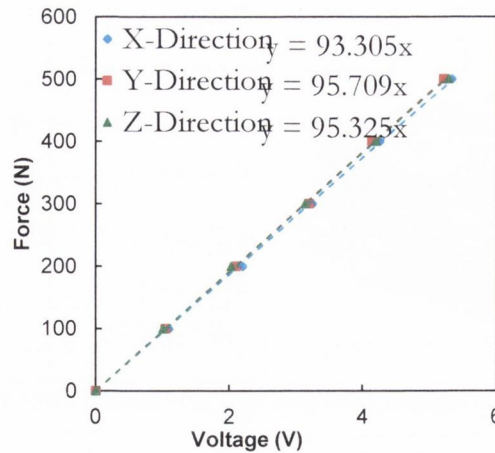


Figure 4.5: Dynamometer Calibration Curve

4.2.3 Acoustic emission sensor

The Acoustic Emission (AE) sensor used for the dressing investigations was a Kistler type 8152B1 piezotron AE sensor as described in section 3.2.1. The AE sensor was mounted on the custom made diamond dresser tool holder with an M6 bolt. General purpose grease was used as a couplant for the interface between the tool holder and AE sensor to remove any air which would interfere in the transmission of the ultrasonic energy. A piece of polymer was placed in between the AE sensor and tool holder to attenuate the signal as can be seen in Figure 4.6a.

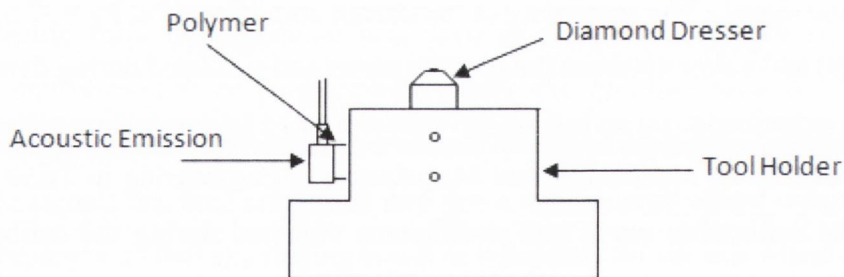


Figure 4.6: Acoustic emission set up

4.2.4 Stylus profilometer

Post machining analysis of the workpiece surface finish was performed using a Mitutoyo Toolmaker's Microscope (Figure 4.7). Measurements of the surface roughness of the workpiece were made in the direction perpendicular to the feed of the grinding wheel. A sampling length of 4mm and cut off length of 0.8mm was used depending on the overlap ratio chosen. The profilometer has a diamond probe stylus

tip of $2\mu\text{m}$, a measuring force of 0.75mN and an angle of 90° . To avoid vibration, the unit and workpiece were placed on a levelled granite bench. Measurements of the workpiece were recorded at three locations along the workpiece surface and a mean average value of the surface roughness was calculated based on the three recordings. R_a and R_z values of the surface roughness were obtained for analyses of the workpiece surface.

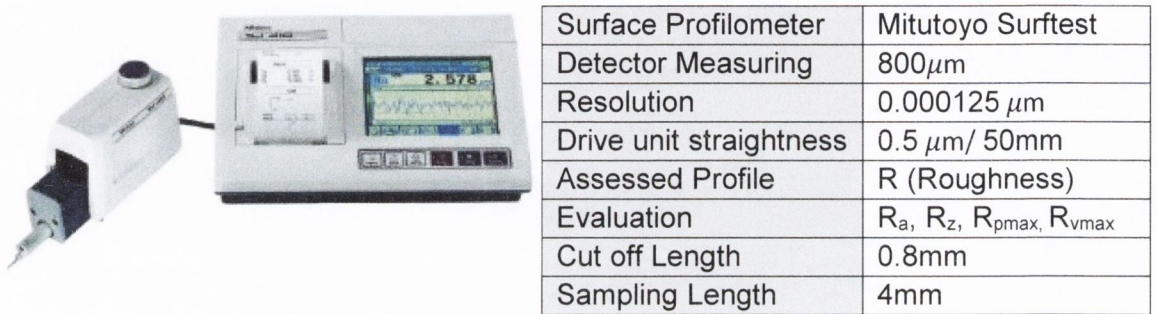


Figure 4.7: Mitutoyo SurfTest SJ-402 Stylus Profilometer

4.3.1 Diamond dressers

Diamond dressing tools were supplied through industrial diamond manufacturer Element Six. The dressing tool used in these investigations was a grade 5 polycrystalline CVD diamond log with a dimension of $0.8\text{mm} \times 0.8\text{mm}$ in cross section and 10mm in length. The diamond is held in a steel mounting and only the top of the diamond is exposed at the depth of the dressing depth of cut. As the diamond wears, the metal matrix around the diamond wears also. The diamond was chosen due to its superior wear and material properties which are shown in Table 4.1.

Properties	A
Density (g/cc)	3.52
Hardness(GPa)	85-100
Fracture Toughness ($\text{MPa}\cdot\text{m}^{1/2}$)	8.5
Young's Modulus (GPa)	1000-1100
Poisson's Ratio	0.07
Tensile Strength (MPa)	560-1100
Compressive Strength (GPa)	9
Thermal Conductivity @ 20°C (W/m.K)	1800-2200
Thermal Conductivity @ 200°C (W/m.K)	1700-2100

Table 4.1: Material properties of the CVD diamond A used in the dressing investigations.

4.3.2 Grinding wheels

Aluminium oxide wheels of various grit sizes were used throughout the experiments to assess the effect of grain size on the grinding performance under varying dressing parameters. The wheels used and properties of each are listed in Table 4.2. The size of the wheels were 200mm X 13mm X 38.5mm where the values represent the outer diameter, wheel thickness and bore size respectively. The wheels were maintained within a diameter of 198mm-203mm in order to keep a consistent wheel speed between the different wheel types. It was very important to balance the grinding wheels prior to testing in order to avoid any run out or eccentricity.

Wheel	32A60JVBE	32A120JVBE	32A220JVBE
Manufacturer	Norton	Norton	Norton
Grit	Aluminium Oxide	Aluminium Oxide	Aluminium Oxide
Grit Size	60	120	220
Grade	J	J	J
Bond	Vitrified	Vitrified	Vitrified

Table 4.2: Grinding wheel properties

4.3.3 Workpiece Material

All the dressing investigations were performed on a block of 304L Stainless steel, 60Rc (C:0.03%; Mn:2%; Si:1%; S:0.03%; P:0.05%; Cr:18%; Ni: 19%; Fe:70%). The surface was first pre ground on both the upper and lower surfaces in order to achieve a surface suitable for testing. The dimensions of the workpieces were 100mm x 60mm x 30mm in size. As the width of the workpiece was 60mm, 4 tests could be performed on each block. The workpieces were held in a vice bolted to the dynamometer and placed in position parallel to the direction of the table traverse so that one pass could cover the length of the workpiece.

4.4 Experimental procedure

The influence of the overlap ratio on the grinding forces and surface finish was studied by varying the overlap ratio from 1-40 while keeping the remaining dressing parameters constant. The dressing investigations were performed on a conventional aluminium oxide grinding wheel (32A60-JVBE) running at 2880RPM. The wheel was 180mm in diameter, 12mm in width and had an inner hole with a diameter of 31.75mm

for mounting of the wheel onto the shaft. The grinding wheel was balanced and trued prior to each experimental run. Approximately 1.5mm of wheel material was removed by truing after wheel mounting. The wheel was first dressed in order to establish the location of the diamond dresser with respect to the wheel and to remove any debris adhering to the wheel from the previous grinding test, two fine dressing passes were then conducted with no in-feed of the diamond dresser to ensure that the grinding wheel was restored to a normal condition prior to each dressing investigation.

Once the diamond dresser was flush with the wheel, 4 dressing passes were performed at a 25 micron depth of cut with overlap ratios ranging from 1 to 40. The Acoustic Emission signal was recorded for the final two dressing passes at a sample rate of 1MHz. Following dressing, the wheel was then used to grind a workpiece with the grinding parameters given in Table 4.3.

Grinding Wheel	32A60-JVBE
Grinding Mode	Surface Grinding
Depth of Cut/pass (μm)	2
Wheel Speed(m/s)	27
Table speed (mm/min)	100
Workpiece	D2 Tool steel

Table 4.3: Grinding Parameters used in the experiments

Normal and tangential forces were recorded during grinding following the dressing process using a Kistler force dynamometer. It has been reported by a number of authors that the grinding wheel exhibits wheel wear while grinding initially after the wheel has been dressed which affect the grinding forces [49].

A grinding depth of cut of 2 microns was used in this study to achieve a surface finish which was representative of the previous dressing test. It was also noticed for higher overlap ratio values, that a grinding depth of cut beyond this value of 2 microns, caused discoloration on the workpiece surface due to thermal damage. 30 passes of the wheel were performed on the workpiece to allow the grinding wheel to stabilize and for the forces to reach a steady state. The workpiece surface was pre ground to ensure that the dressed wheel was grinding a fully flat surface. Normal and tangential forces were recorded for 30 seconds. Each of the signals were sent to a charge amplifier where it was amplified and sent to a PC for storage. Data Analysis was performed in Matlab

were voltages were converted to force. A moving average filter with a window length of 100 points was used to remove the noise from the data.

4.5 Wheel wear measurement

The grinding wheel wear measurement adopted was the ‘razor-blade’ technique [146]. The method involves grinding a workpiece that is narrower than the width of the grinding wheel. A groove is worn into the wheel profile after each investigation; wheel wear was measured by grinding a razor blade to produce a mirror image of the wheel surface. The wear was then measured on a microscope with an x and y coordinate measuring device.

4.6 Feature extraction

4.6.1 Acoustic Emission

Acoustic emission signals are the acoustic pulses transmitted through a material when the strain energies stored in a solid material are released during the deformation and fracture processes, due to external forces. Acoustic emission signals were recorded while dressing at varying overlap ratios and the RMS signal was extracted to quantify the dressing intensity.

Raw Data

The acoustic emission signal while dressing the grinding wheel was recorded for the last two dressing passes of each investigation. Figure 4.8 shows the raw data of the acoustic emission signal after a dressing pass of 20 micron depth of cut and an overlap ratio of 10 was used. It is identified in Figure 4.8 that the acoustic emission signal was not uniform during the dressing pass and there is a rise and fall in the acoustic emission signal as the diamond dresser enters and exits the periphery of the wheel. For this reason, the AE signal value was taken from the centre of the signal.

As the AE signal is quite sensitive and is influenced by background noise, it was necessary to determine the effect of residual noise coming from grinding wheel, the spindle bearings, the coolant and any ambient noise created by machines in the vicinity of the area that could contribute to the overall experimental reading of the acoustic emission signal. Figure 4.8 shows a signal of a dressing pass, including data before

and after entry and exit of the diamond with the wheel when the grinding machine is running. An RMS value of this reading shows that the signal was near negligible with a reading of 0.0023 volts.

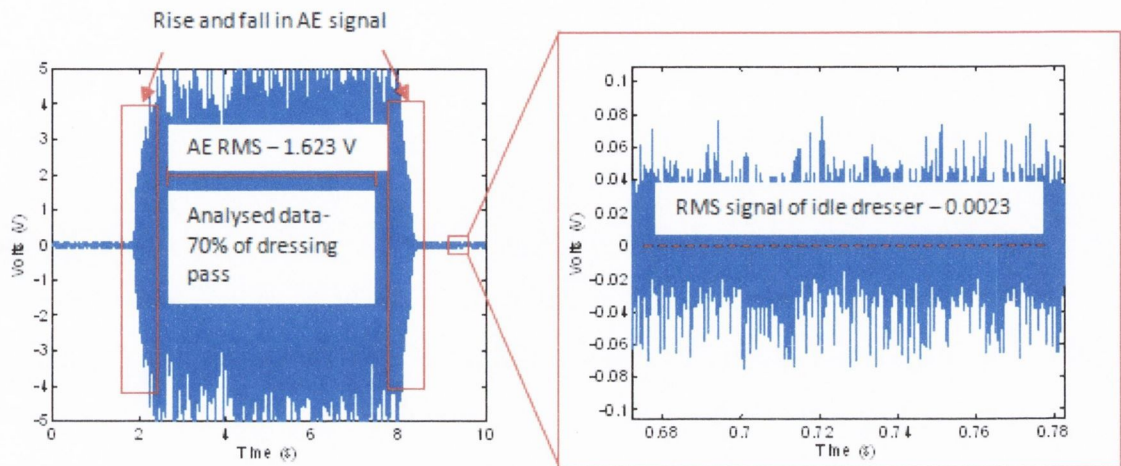


Figure 4.8: Graphs showing the signal of an idle sensor while grinding machine is running

Data processing

The AE_{RMS} value of the signal was taken as a metric for the signal intensity of the dressing pass. This metric has been used by many authors previously due to its simplicity in sampling and processing the data at a much lower sampling rate compared to analysing the data using counts, kurtosis and spectral analysis [147-149]. The acoustic emission data was recorded at a sample rate of 1Mhz and a mean value of the AE_{RMS} was calculated based on Equation 4.1 [150].

$$AE_{rms} = \sqrt{\frac{1}{N} \int_{i=1}^N AE_{rms}^2(i)} \quad (4.1)$$

Where N is the discrete number of AE data points within the time interval chosen.

4.6.3 Grinding forces

One of the most notable differences between grinding and other metal cutting processes is that the position and geometry of each individual grain is probabilistic. Considering that grinding speeds are typically 30-60 m/s, and the positions and state of the grains are constantly changing due to wear and fracture, the grinding process therefore changes as a result which makes it a very complex process. Normal and tangential forces while grinding were measured with a workpiece dynamometer to monitor the condition of the wheel and its cutting efficiency. The workpiece surface

was ground before testing to ensure that a flat even surface existed across the workpiece. The force data was recorded to a PC using Matlab and saved for post processing.

Raw data acquisition

Figure 4.9 shows the raw force data in blue and the RMS data in red. It can be seen that it takes almost three passes for the grinding wheel to fully engage with the full length of the workpiece. This is due to the stiffness of the wheel head and the tendency for it to climb over the workpiece. There is a slight increase in the force data for passes 3, 4, 5 and 6 as the wheel first engages with the wheel. The force data is then seen to steady off and a value is achieved where the depth of cut that was set on the machine was equal to the actual depth of cut. A reading of the force is taken on the third last grinding pass to calculate the average force value for that experiment. The average value of the force was taken from the middle 70% of the data as shown in Figure 4.10 as the force increased and then fell off as it entered and exited the wheel.

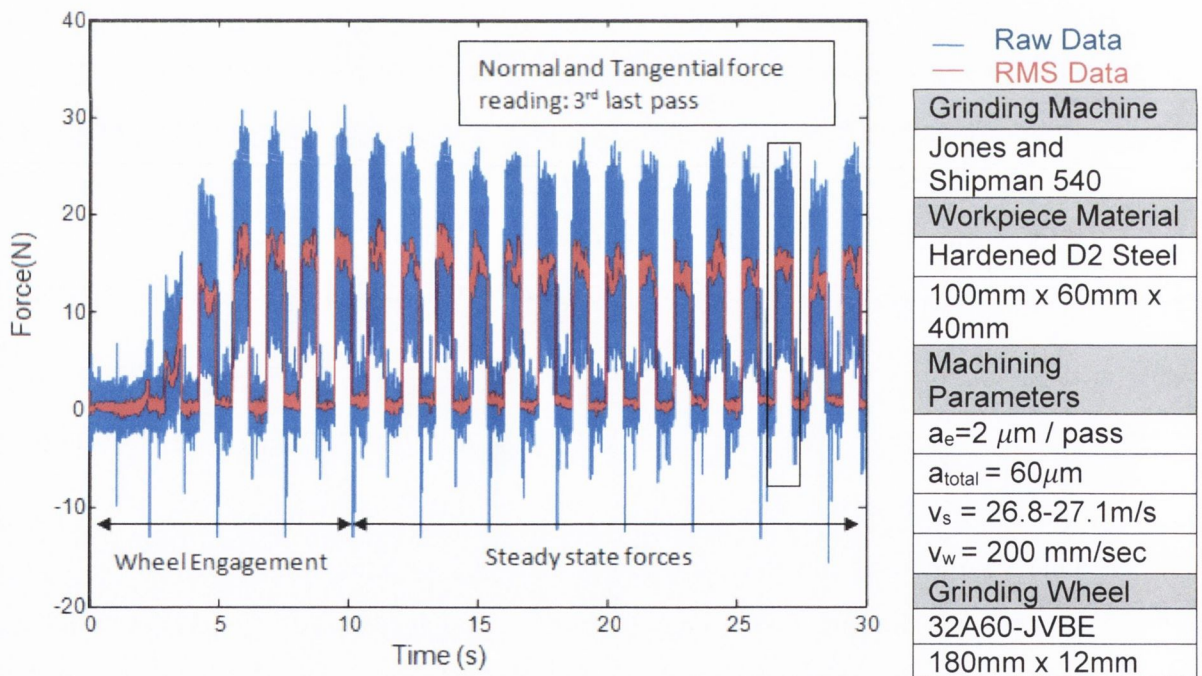


Figure 4.9: Grinding force data showing the rise in forces during wheel engagement and the reading of 3rd last grinding pass during steady state period

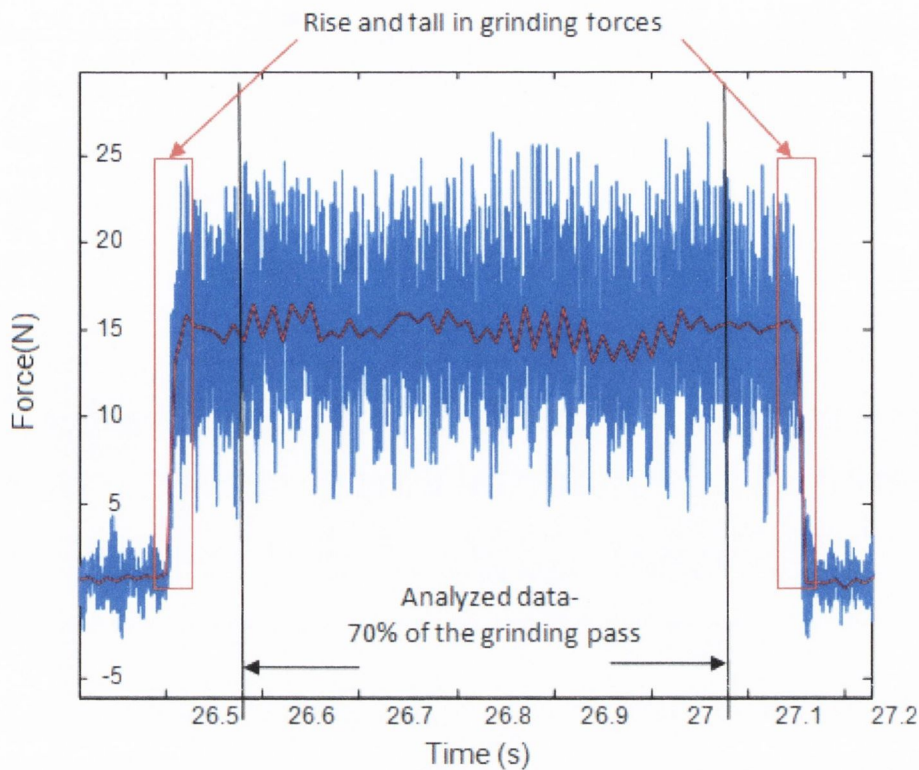


Figure 4.10: Force data of a single grinding pass taken from data set in Figure 4.9 showing the rise and fall of the signal and the region of analysed data.

Up and down grinding

As the reciprocating table traverses back and forth during the surface grinding process, grinding is performed by up-grinding and down grinding. Up-grinding occurs when the tangential velocity of the grinding wheel is opposite to that of the workpiece velocity. Conversely, down grinding occurs when both the direction of the workpiece and the grinding wheel are the same as illustrated in Figure 4.11.

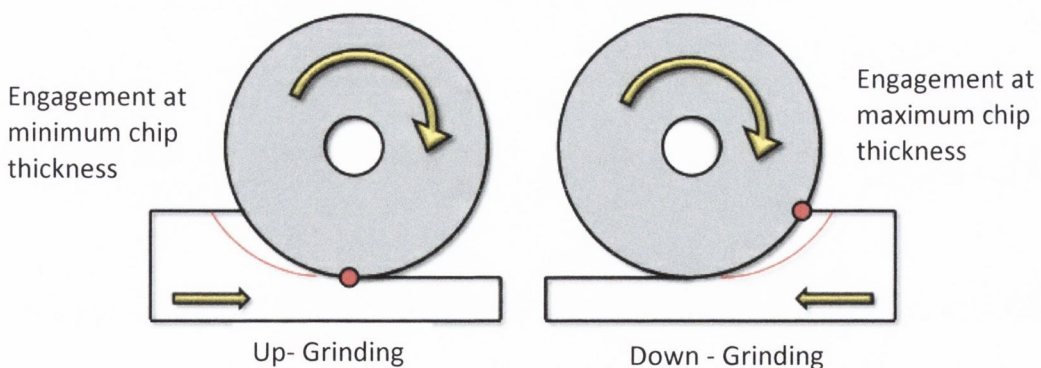


Figure 4.11: Difference between up grinding and down grinding

There are significant differences in the material removal process that are a direct result of choosing either up grinding or down grinding. In the case of up-grinding, abrasive

grains begin their cutting path from an initial chip thickness of zero and finish at the maximum chip thickness position. Down grinding has the opposite effect whereby the abrasive grains enter the cut at the maximum chip thickness and exit at zero chip thickness. It has been reported in the literature that down grinding forces are higher than up grinding due to the length of contact being greater in down grinding [151]. Grinding forces were analysed for both up and down grinding and it was found that no difference in the amplitude of the forces recorded could be seen. The reason for this was due to the shallow depth of cut of 2 microns which created a small arc of length cut compared to previous research where a larger depth of cut of 15 microns was used.

Grinding power and specific energy

Grinding power (P) was calculated using the tangential forces recorded based on the equation:

$$P = F_t \cdot V_w \quad (4.2)$$

The Specific energy (U) which is defined as the energy per unit volume of material removed could then be calculated as the grinding power (in watts)/Material Removal Rate (in mm³/s) as shown in Equation 4.3:

$$U = \frac{F_t \cdot V_s}{V_w \cdot a \cdot b} \quad (4.3)$$

Where the following quantities are included:

F_t – Tangential cutting force (N)

V_s – Grinding wheel speed (mm/s)

b – width of cutting zone (mm)

V_w – Workpiece speed (mm/s)

a – Depth of cut (mm)

4.6.4 Surface finish of workpiece

The surface of each of the workpieces was studied following grinding using a stylus profilometer. Traces of the stylus were made perpendicular to the direction of the cut to produce a map of the peaks and troughs. Three traces of each workpiece were performed to give an average value for each investigation.

Surface parameters

The parameters chosen for analysis were R_a , the arithmetic average variation of all the peaks and valleys from a mean measured over the sample distance as represented by Equation 4.4.

$$R_a = \frac{1}{L} \int_0^L |Z(x)| dx \quad (4.4)$$

Where Z is the height of the surface profile about the mean line and L is the sample length.

Graphically, the average roughness is the area between the roughness profile and its centre line divided by the evaluation length which is divided into five sample lengths with each sample length equal to one cut-off length, L (Figure 4.12)

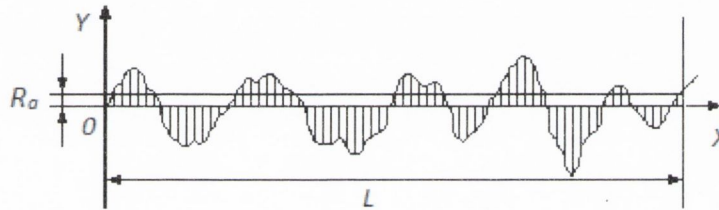


Figure 4.12: Measurement of the average surface roughness R_a

Roughness parameters, R_p , R_v and R_t

The peak roughness R_p , is the height of the highest peak in the roughness profile over the evaluation length. Similarly, R_v is the depth of the deepest valley in the roughness profile over the evaluation length. The total roughness, R_t is the sum of these two, or the vertical distance from the deepest valley to the highest peak as shown in Figure 4.13.

$$R_p = |\max(z(x))|, \quad R_v = |\min(z(x))|, \quad 0 < x < L [\mu\text{m}] \quad (4.5)$$

$$R_t = R_p + R_v \quad [\mu\text{m}] \quad (4.6)$$

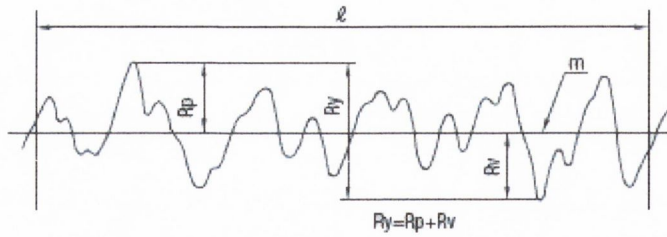


Figure 4.13: Diagram of the surface parameters recorded

Ra is the most commonly recognised standard of surface roughness measurement which measures the arithmetic mean of the absolute departures of a roughness profile from the mean line of measurement. Some authors who have studied the surface finish of a workpiece after grinding have only reported on the outcome of the Ra value [49, 152]. However, this measurement can be quite misleading as one extreme Rp or Rv value will affect the overall Ra value. In order to consider the full surface characterisation, Rt values were also studied to identify any outlying grits on the periphery of the wheel which can cause deep scratches on the workpiece surface.

Chapter 5

Experimental Results Dressing Characterisation Investigations

5.1 Background

Dressing and grinding experiments were performed for a variety of wheel types under a range of dressing overlap ratios. The dressing overlap ratio was chosen as it is the most influential dressing parameter on the grinding process [141]. The dominant effect of the overlap ratio over the dressing depth of cut is highlighted in the graph below (Figure 5.1). It can be seen that a decrease in depth of cut from 30 microns to 10 microns for an overlap ratio of 4 results in a change of just 0.15 microns R_a . Whereas, a change in overlap ratio from 1 to 10 for a dressing depth of cut of 20 microns results in a change of 0.73 microns R_a .

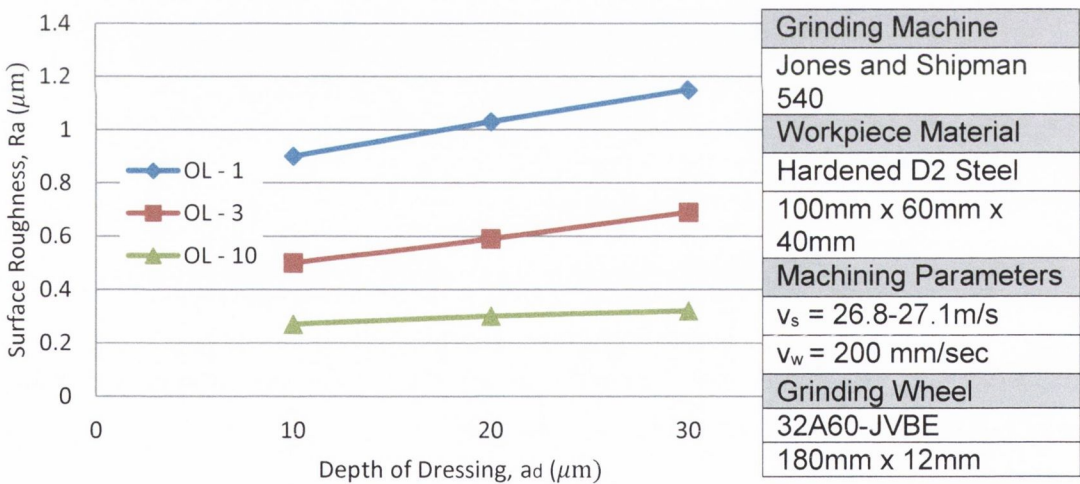


Figure 5.1: Preliminary investigations to show the effect of dressing depth and overlap ratio on surface roughness

Many authors have studied the effect of dressing parameters on the sharpness of the wheel [6, 27, 34, 46, 49, 144, 145]. With aggressive dressing conditions, creating sharp wheels leading to lower grinding forces and rougher surface finishes. While more timid dressing

conditions tend to dull the wheel, resulting in high grinding forces and a smoother workpiece.

It is also generally believed that smaller grit sizes gives an improved surface finish. However, the accompanying specific energies and change in overall ratio when using these fine grit sizes have not yet been established.

The effect of grit size for varying overlap ratios on the specific energy and surface finish of the workpiece was examined. Forces were recorded during grinding and the surface finish of the workpiece was analysed after grinding. Using the information gathered in the experiments and the chip formation model, greater insight can be given on the unknown variables c , the grit density and r , the shape factor of the grit.

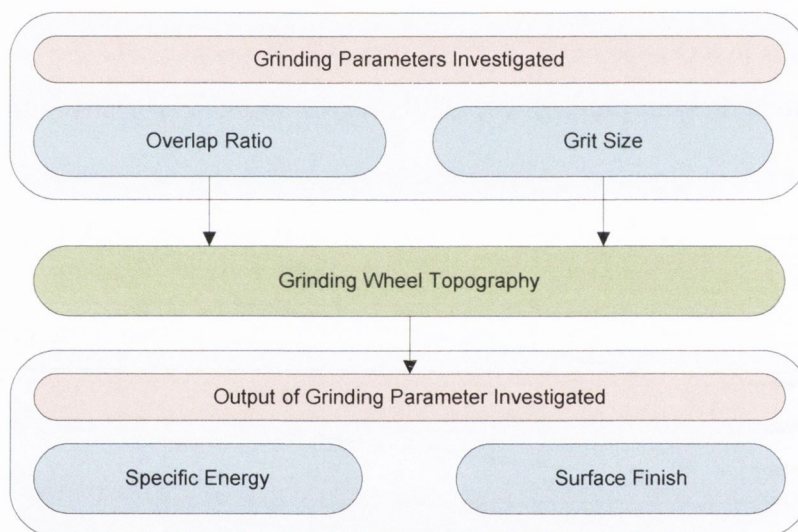


Figure 5.2: Investigations of overlap ratio and grit size on the specific energy and surface finish

5.1.1 Effect of overlap ratio on specific energy

The grinding tangential forces were recorded after each dressing investigation. Using the experimental parameters, wheel speed (V_s) = 27m/s, workpiece velocity (V_w) = 100mm/s, grinding wheel thickness (b) = 12mm and grinding depth of cut (a) = 0.002mm. The specific energy could then be calculated based on Equation 5.1:

$$U = \frac{Ft \cdot Vs}{Vw \cdot a \cdot b} \quad (5.1)$$

Figure 5.3 shows the specific energy values plotted against the overlap ratio for four grinding wheel mesh sizes tested of 60, 120, 150 and 220. A significant increase in the specific energy, U was found with an increase in the overlap ratio. The increase in specific energy can be attributed to the abrasive-workpiece interaction and chip removal mechanism occurring due to the geometry of the grits [153]. As the overlap ratio increases, the contact between the diamond dresser and the grits on the wheel increase leading to a blunt wheel. The total specific energy for grinding can be shown to consist of chip formation, ploughing and sliding components. Due to the dull nature of the grits created at the high overlap ratio, rubbing and ploughing of the grains would be the main material removal mechanisms, which create a much higher specific energy compared to chip formation. An increase in the magnitude of specific energy of $\sim 100 \text{ J/mm}^3$ can be seen when dressing the 60 grit wheel with a high overlap ratio of 40 compared to a low overlap ratio of 1. The increase in specific energy can have quite a significant effect on the process as the large specific energy values are converted to heat and absorbed into the workpiece which can result in thermal damage to the workpiece surface.

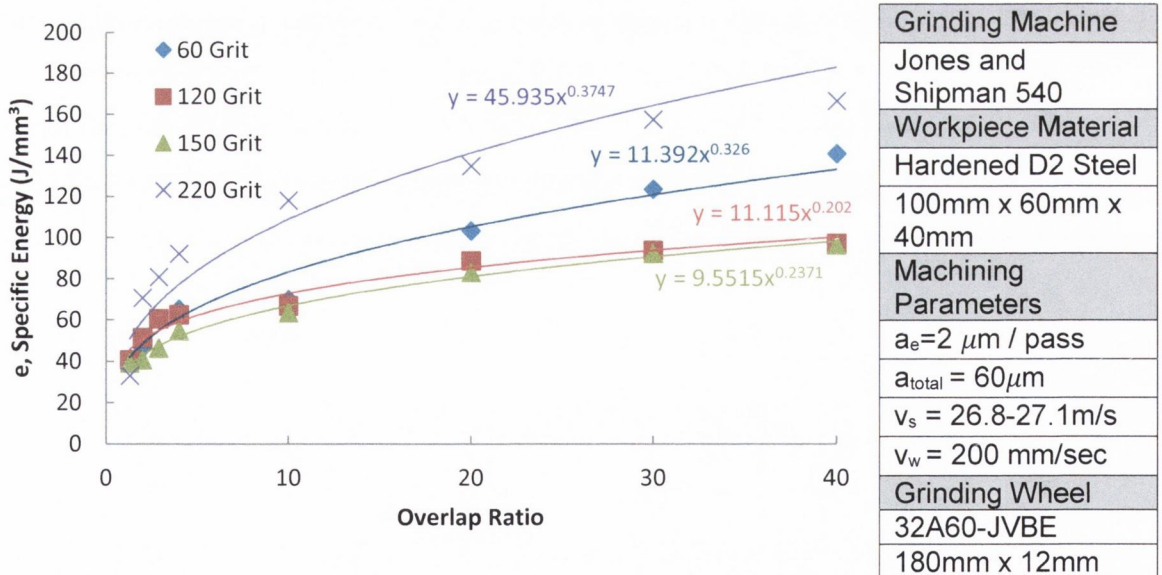


Figure 5.3: Specific Energy Vs Overlap ratio for various grit sizes

This trend was repeated for all grinding wheels with finer mesh sizes (smaller grits) producing smaller specific energy values with the exception of the 220 grit wheel, which will be discussed later. The reason for this is due to two factors that are seen in the maximum chip thickness equation h_m , C and r . C is the number of active cutting points per unit area on the wheel surface and r , the shape factor of the grit which is the ratio of chip width to chip thickness. Wheels that have a larger grit size number have smaller grits and as a result, the number of active cutting points per unit area, C is seen to increase. The average distance from one cutting edge to another reduces which results in a decrease in the individual grit contact forces leading to an overall reduction in the grinding force. The value of r is also seen to change with a larger overlap ratio value, as the increase in contact time between the dresser and grits on the wheel will result in a change of shape of the grit from triangular which Rowe states has a shape factor of 10, to a square dull structure which is given a shape factor value of up to 40 [66].

5.1.2 Effect of overlap ratio on grinding force ratio

The effect of dulling of the grits with an increase in the overlap ratio is also quite evident in the grinding force ratio. This is a ratio of the normal forces over the tangential forces and is a similar term to the coefficient of friction which provides a measurement of the friction occurring in the grinding zone [154]. Figure 5.4 shows the force data for both the normal and tangential forces for a single pass, it can be seen that normal (frictional) forces during grinding are much greater than tangential (cutting) forces. This is due to the highly negative rake angles that are presented in the grinding wheel due to the random nature of the grits.

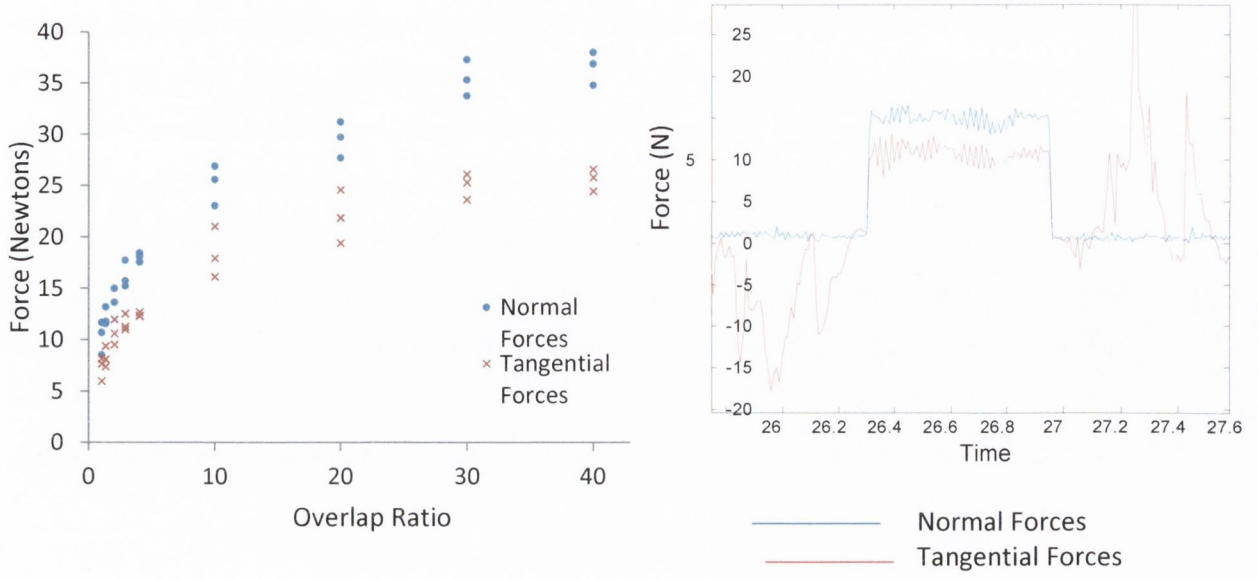


Figure 5.4: Normal and tangential forces for a range of grinding tests performed at different overlap ratios

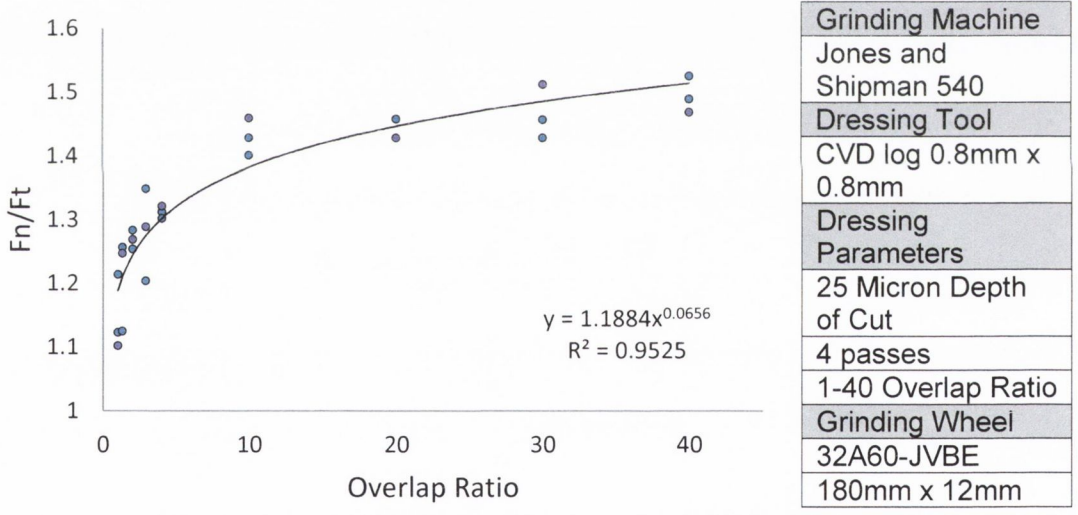


Figure 5.5: Plot showing the variation in grinding force ratio with a change in the overlap ratio

A closer look at the ratio reveals that this value increases with a greater overlap ratio value (Figure 5.5). The rise in the value of F_n/F_t with an increase in the overlap ratio is due to grit penetration depth. With a larger overlap ratio, the grits on the wheel start to dull. This causes rubbing and ploughing of the grains on the workpiece surface as the grains fail to

penetrate the material. It has been reported that rubbing or ploughing of the grits creates larger normal forces as the grit wears. This is due to the rise in contact pressure between the wheel and workpiece as the tip area of the worn grit increases. A power curve was fitted to the data points from the investigations and an equation with an R^2 value of 0.9525 was developed showing a good correlation to the experimental data. A sharp rise in the ratio is observed with an increase in the overlap ratio at smaller values. This is due to the rapid change in shape of the grits. The ratio is then seen to level off and only a gradual rise in the ratio is observed after a dressing overlap ratio of 10, whereby the grits has reached its maximum dullness and the wheel starts to become glazed contributing to the increase in contact pressure.

5.1.3 Effect of overlap ratio on surface finish

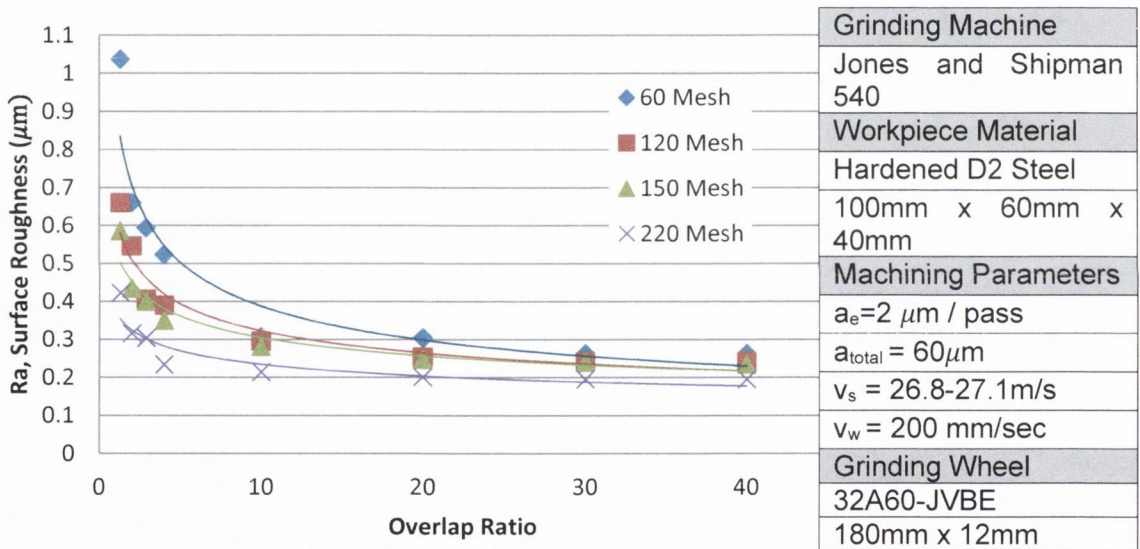


Figure 5.6: Effect of Overlap Ratio on ground surface using various wheel grit sizes

Figure 5.6 shows the effect of varying the overlap ratio on the workpiece surface roughness value Ra and the range of different values that can be achieved with each grit size. It is clear that a wheel dressed with a higher overlap ratio produces a better finish on the workpiece due to the geometry of the grits. It can also be seen with all four curves that the surface finish reaches a steady state value once an overlap ratio of approximately 10 is used, after which point, increased contact of the diamond dresser with the grits does not

improve workpiece surface finish. The limiting surface finish values for each of the mesh sizes are $0.26\mu\text{m}Ra:60M$; $0.24\mu\text{m}Ra:120M$; $0.23\mu\text{m}Ra:150M$; $0.20\mu\text{m}Ra:220M$. A look at the Ra values that are achievable for different machining processes reveals that the experimental Ra values obtained with these high overlap ratios are at the top end of the scale of those in the grinding industry (Table 5.1). Another observation that can be made is that the steady state value of surface finish occurs at lower overlap ratio values as the mesh size becomes smaller.

Ra(μm)	0.025	0.05	0.1	0.2	0.4	0.8	1.6	3.2	6.3	12.5	25	50
N-grade	N1	N2	N3	N4	N5	N6	N7	N8	N9	N10	N11	N12
Triangular Indication												
Finish	Lapping/ Superfinishing			Ground Finishes			Smooth Turned		Medium Turned		Rough Machined	

Table 5.1: Surface roughness values achieved through different machining processes

The high Ra values experienced after the wheel has been dressed with a low overlap ratio of 1 can be explained in the following manner. At an overlap ratio of 1, the diamond dresser traverses across the wheel at 0.8mm/rev . The diamond is said to have an effective width of 0.8mm so in theory, the diamond dresser should come in contact with each grit on the surface of the wheel, as the dresser moves 0.8mm for every revolution. However, SEM images of the CVD diamond dresser reveal that wear on the leading and trailing edges of the diamond result in the diamond dresser having an effective width of 0.7mm . This in effect would result in a saw tooth pattern being machined on the surface of the wheel as the smaller effective width misses some of the grits as it traverses across the wheel. This results in a pattern being developed on the wheel which would transfer over onto the workpiece surface, causing a large Ra value (Figure 5.7).

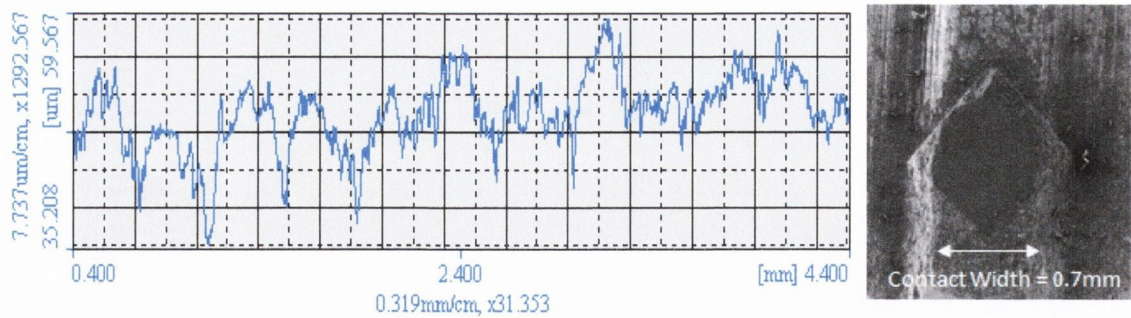


Figure 5.7: Surface profile of a workpiece and a SEM of the worn dresser used with an effective width of 0.7mm

One disadvantage of the Ra value is that it is not a good discriminator for different types of surfaces where deep valleys and high peaks may be present. Ra values are a measure of the average absolute values on the roughness profile of a workpiece, whereas Rt values take into account the maximum profile height on the surface of a workpiece from the top of a peak to the bottom of a valley. Rt values are a good metric to use when single defects on a surface are not permissible. This is true in the case of surfaces which have been ground, as a surface finish with a high peak could have a significant effect on the life of a part.

The Rt values were examined for overlap ratios between 1 and 40. It was found that as the overlap ratio increased, the Rt values reduced significantly. With an overlap ratio of 1, the value for the maximum peak on the surface of the workpiece was found to be approximately 14 microns while values of approximately 3 microns were recorded once an overlap ratio of 10 or more was used to perform the dressing process.

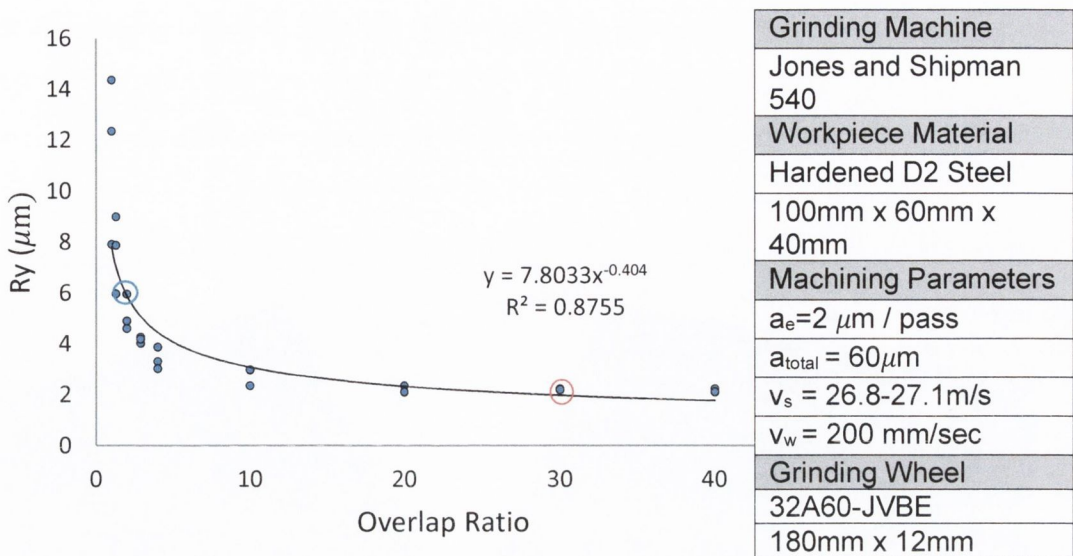


Figure 5.8: Overlap Ratio vs. the maximum peak to valley height on ground hardened D2 Steel

Examination of two surfaces with a Ra value of 0.6 and 0.24 which correspond to the two data points in the above graph marked with a blue and red circle respectively is shown below in Figure 5.8. The respective surfaces were studied using an Alicona infinite focus system, Figure 5.9a shows a surface with an Ra value of $0.6 \mu\text{m}$ created with an overlap ratio of 1, while Figure 5.9b was created with an overlap ratio of 30 and had a surface roughness of $0.24 \mu\text{m}$. It can be seen in Figure 5.9a that even though the majority of the depths are in the blue and green zones which correspond to depths of 0.5 and 1 respectively, certain sections of the surface appear in purple. These scratches are caused by grits on the surface of the wheel which have not been in contact with the diamond dresser and which protrude above the surrounding grains. This highlights the fact that grinding wheels have a very non-uniform structure and in turn creates a non-uniform surface on the workpiece.

Figure 5.9b shows a surface which was created with a dressing overlap ratio of 30. Upon inspection, the surface of the workpiece appears more uniform as a greater section of the sample is seen in green which corresponds to peaks and valleys with a height of 0.5 microns. However, it can be seen that due to the kinematic grinding process and the

topography of the wheel, certain areas of the workpiece have deeper scratches which are shown by the blue lines. Again, this highlights the fact that even when a large overlap ratio is used, the surface still consists of deep valleys and great care should be taken when using an Ra as a representative value of surface roughness of the part.

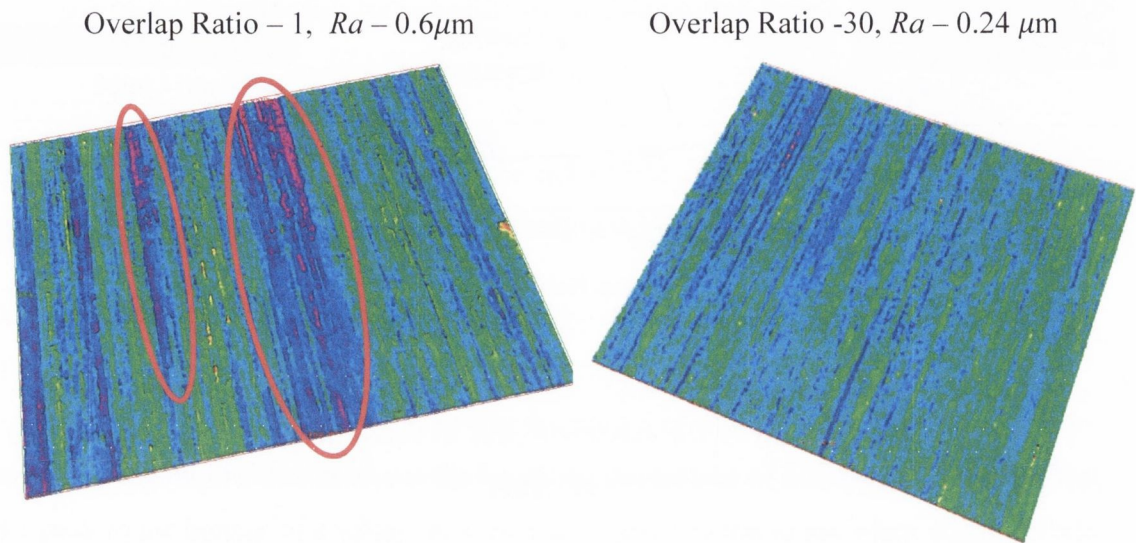


Figure 5.9: Alicona scans of two workpiece surfaces showing the peaks and troughs

Further investigations into the maximum peak to valley depth (Rt) along with the average surface roughness was studied for surface finishes created with grit sizes of 60, 120, 150, and 220 for varying overlap ratios of between 1 and 40 using a mitotoyo surface profilometer. The ratio of Rt/Ra is important, as design criteria for many engineered surfaces is often Rt rather than Ra . For example, in cutting processes, the stress required to cause fracture depends on the material toughness, which is an intrinsic material property dependent on the maximum defect size that can come in the form of the largest grinding scratch. It can be seen that the ratio of Rt/Ra rises as the overlap ratio increases (Figure 5.10). Whereby values above an overlap ratio of 10 converged to around $Rt/Ra=10-11$ for the three smaller grit sizes and $Rt/Ra=14$ for the larger grit. At smaller overlap ratio values, the values are slightly less with Rt/Ra converging to a ratio of approximately 8 for the smaller grits and Rt/Ra equal to about 11 for the larger grit at an overlap ratio of

approximately 1 to 2. The difference is not large and it might be expected to see decrease in the value of Rt/Ra with an increase in the overlap ratio, as grits dulled and ploughed the workpiece. One explanation for the increase in Rt/Ra with an increase in overlap ratio is that occasionally chip formation is occurring with a few single sharp grits. This would create a deep valley and a large peak causing the associated value of Rt/Ra to increase also.

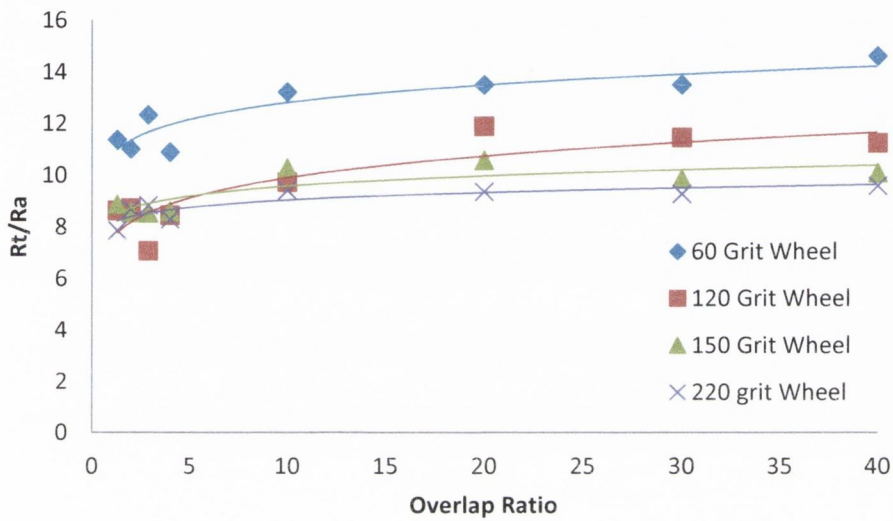


Figure 5.10: Rt/Ra Vs Overlap Ratio for a range of grit sizes

5.1.4 Ra vs. specific energy

The surface finish was plotted against the specific energy to investigate the effect of grit size and overlap ratio on these two process outcomes.

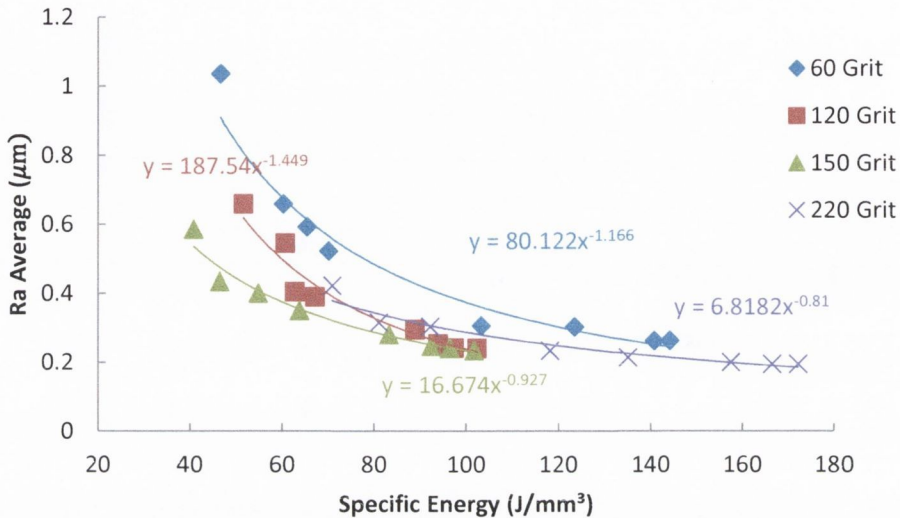


Figure 5.11: Ra values achieved through grinding vs Specific energy for different grit sized wheels.

It can be seen in Figure 5.11 that surface finishes which were created with low specific energies result in a large Ra value. While grinding processes with a high specific energy produce surfaces with a lower Ra value. This is due to a significant portion of the energy being consumed by rubbing and ploughing of the grits due to the nature of the wheel created during the dressing process. Dressing processes with high overlap ratios result in grinding wheels having a lower effective surface roughness and a larger number of grits per unit area with little grain protrusion. This results in rubbing and ploughing actions of these grits leading to a better surface finish, however it comes at the expense of high specific energies. High specific energies during grinding are known to generate excessive workpiece temperatures which can lead to thermal damage. This is especially true when using an aluminium oxide wheel as the thermal conductivity is so small, meaning relatively little heat is conducted by the grits and approximately 80% of the generated heat is conducted into the workpiece [155]. For this reason, it is important that grinding specific

energies are maintained as low as possible for a given grinding process where certain material removal rates or surfaces finishes have to be met.

It is also noted that for a given surface finish, finer mesh sizes and a smaller grit yield lower specific energies. The better than expected low *Ra* value that was achieved with a 60 mesh wheel was created with a large overlap ratio whereby the dresser dulled the grits. In return, the dull grits plough the workpiece surface creating larger specific energies. Whereas with a finer grit size, the accompanying low surface roughness value of 0.2 μm *Ra* was achieved with smaller sharp grits. These grits create the workpiece surface with less rubbing and ploughing and greater chip formation.

For the 220-mesh wheel, the trend starts to reverse and an increase in the specific energy is seen. The reason for this requires an investigation into the undeformed chip thickness. As stated by Malkin the “size effect” is affected with how deep the grits penetrate into the workpiece. As the grits penetrate deeper into the material, they are more likely to form a chip rather than plough or rub the material. Consequently, the chip formation material removal mechanism produces smaller specific energy. In contrast, grits that only slightly penetrate the material are more likely to rub and plough the material, resulting in higher specific energies.

If an approximation of the cutting point density for each wheel is given with the simple formula as shown by Badger and Krajnik [156] based on the measurements of Shaw, calculations of the undeformed chip thickness can be made as shown in Table 5.2.

Grit Size	Undeformed chip thickness (μm)
60	0.791
120	0.559
150	0.5
220	0.413

Table 5.2: Undeformed chip thickness values

It can be seen that finer grits produce a smaller undeformed chip thickness due to the larger number of grits. Considering the size effect alone, it could be assumed that a smaller grit penetration depth would produce a larger specific energy. However, the size effect

assumes a given set of grinding conditions for a given wheel. In these investigations, the grit size was different and, more importantly, the sharpness of the grits also varied with grit and overlap ratio.

In addition, each grinding wheel will have a characteristic curve of specific energy vs. undeformed chip thickness, with small chip thickness giving high specific energies and larger chip thicknesses producing smaller specific energies with a value that asymptotically approaches the chip formation energy [17]. The curve is quite different for each grinding wheel as Hillier discusses the grit spacing and grit protrusion is determined by various parameters including, wheel diameter, grinding velocity, table speed, wheel depth of cut, grit size, sharpness and cutting point density [157]. The investigations were run under one set of grinding conditions which would correspond to a different point on each of the curves.

Considering this, it appears that there are two dominant factors that strongly influence the final specific energy, grit sharpness which is altered by the dressing overlap ratio and the “size effect” which is achieved with different cutting point densities. It appears here that the size effect starts to dominate for the finest grit in the region of 0.5 microns chip thickness. At this stage, the main chip removal mechanism grits is rubbing and ploughing. This is evidenced in Figure 5.3, where the specific energy in the 220 grit approaches its near-steady state higher value of at a lower overlap ratio, whereas the 60 grit wheel doesn't reach a steady state specific energy until an overlap ratio of 20 to 30 is used.

Therefore it could be said that the trend shown above whereby smaller grits produce smaller specific energies for a given surface finish compared to larger dull grits, apply for the grinding conditions here in the 60-150 mesh range. The size effect then starts to dominate at finer grits of 220 mesh where chip thickness value of 0.5 microns is not a sufficient depth to form a grit and rubbing and ploughing start to dominate.

Wheel wear

The wear experienced for all four mesh sizes was investigated by measuring the G-ratio value as shown in Figure 5.12. It is clear that smaller grit sizes tend to give smaller G-ratio values. This is due to there being less supporting bond material to hold the grits in place

and also smaller grit have a larger cutting density point density resulting in less force acting on individual grits, leading to reduced wear and larger G-ratios.

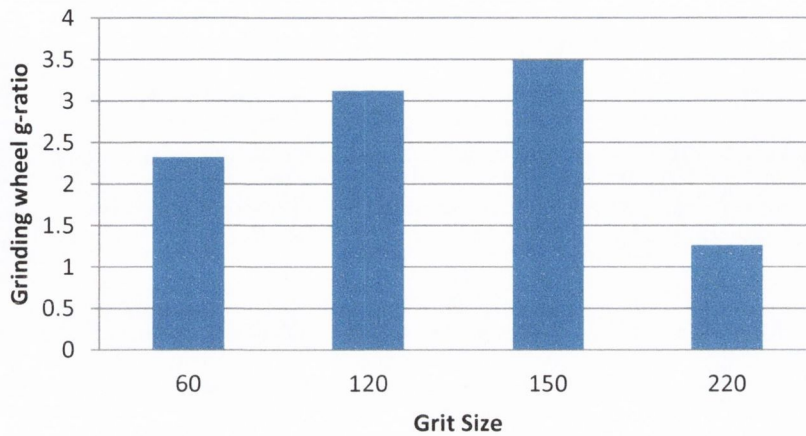


Figure 5.12: Graph of the wear of each grinding wheel measured as a G-ratio value

Table 5.3 shows the G-ratio value and chip thickness after a dressing overlap ratio of 3 was used for each grit size. It can be seen that a larger chip thickness values results in greater wear of the grinding wheel as the greater grit penetration depth results in grit fracture and increased wear. However, again there is notable change in the G-ratio value for the 220 grit whereby the wheel experiences the greatest wear. The reason for this appears to be due to the grit penetration depth being too small for the grit size. According to Badger [158], too small a chip thickness will result in excessive rubbing, larger specific energies and excessive wear upon collapse. This criteria is met in these investigations for the 220 mesh grit which explains the excessive rubbing and increased grinding wheel wear.

Grit Size	G-ratio	Undeformed chip thickness (μm)
60	2.325	0.791
120	3.125	0.559
150	3.488	0.5
220	1.26	0.413

Table 5.3: Table of G-ratio value and the corresponding undeformed chip thickness value for each grit size

The difference in specific energy values experienced between the different grit sizes was explained using t' , the undeformed chip thickness model whereby an increase in the chip thickness value due to a change in the C and r values results in a decrease in the specific energy during grinding [13, 159]. The product of C and r is considered a single factor, that is affected by dressing conditions, grit cutting edge radius and also by t' itself, and it is assumed to be a constant, on average, under given grinding conditions. However, due to the range of specific energy values experienced during these tests, it is clear that the values of C and r change considerably.

Estimates of these values are quite often used to calculate values of the chip thickness which lead to calculated engineering values not coinciding with experimentally measured values. Wearing of the grits through grinding or previous dressing operations is a factor which quite often leads to inaccuracies of the values of C and r . Using the vast amount of specific energy values obtained experimentally with various grit sizes and overlap ratios, values of r can be obtained through the relationship $U' \propto 1/t'$ for the different grit sizes and overlap ratios.

$$U' \propto \frac{1}{t'} = \frac{1}{\left[\frac{1}{C \cdot r} \left(\frac{V_w}{V_s} \right) \left(\frac{a}{d_e} \right)^{\frac{1}{2}} \right]^{\frac{1}{2}}} \quad (5.2)$$

Solving the equation for $C \cdot r$, gives the following equation:

$$C \cdot r = U'^2 \frac{V_w}{V_s} \cdot \frac{a}{d_e}^{\frac{1}{2}} \quad (5.3)$$

Values of C for each wheel can be calculated using the following equation for the cutting point density as stated by Badger [156]:

$$C = \frac{2}{\frac{15.2}{\text{Mesh Number}}} \quad (5.4)$$

Which yields values of the grit density for each wheel as follows (Table 5.4):

Grit Size	60	120	150	220
Grit Density Grits/mm ²	7.89	15.79	19.74	28.98

Table 5.4: Grit density values for different grit size wheels

Using the grit Density values and the value of the $C.r$ product, a value for r , the shape factor could be approximated for each of the wheels under the different dressing conditions.

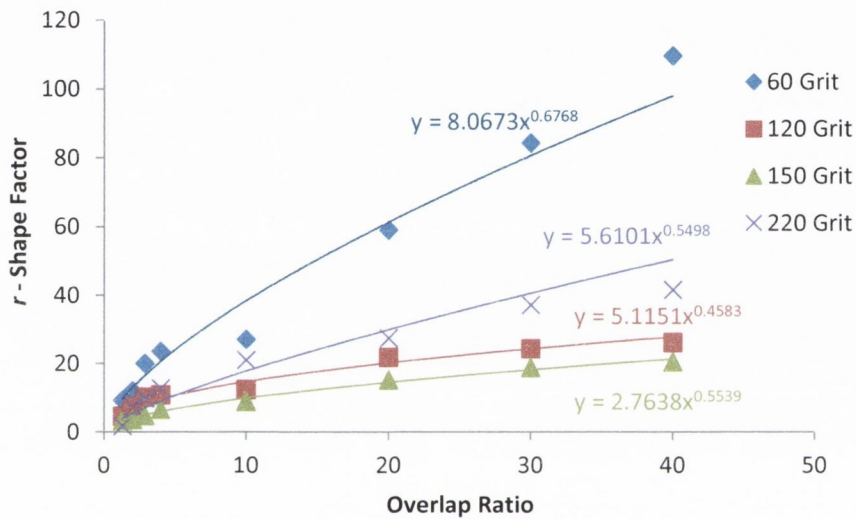


Figure 5.13: Change of the shape factor, r with relation to the overlap ratio for different grit size wheels

A trend is seen for each wheel whereby there is an increase in the value of r with overlap ratio. This is due to a greater chip width for a given thickness caused by dull grits created with a large dressing overlap ratio. The increase is greatest in the 60-mesh wheel because larger grits typically have larger cutting edge radii [66], meaning that for a given penetration depth into the grit, the penetration width will be larger as the cutting edge radius increases. For the 60 mesh wheel, the shape factor value increases from 10 to 110 as the grits are sharp for lower overlap ratios and generate large wear flats for higher overlap ratios as illustrated in Figure 5.13. As the average grit diameter reduce for the 120, 150 and 220 grit wheels to a value of $63\mu\text{m}$ compared to an average grit diameter of $254\mu\text{m}$

for a 60 grit wheel (Table 5.5), the change in shape of the grits is less dramatic and as a result the shape factor values are much smaller. This trend was also seen by Kannappan and Malkin [160], where a smaller cutting point density in larger grits was offset by a larger value of r , owing to the larger cutting edge radius with larger grits. The range of grit size in the authors investigations was mesh to 120 mesh.

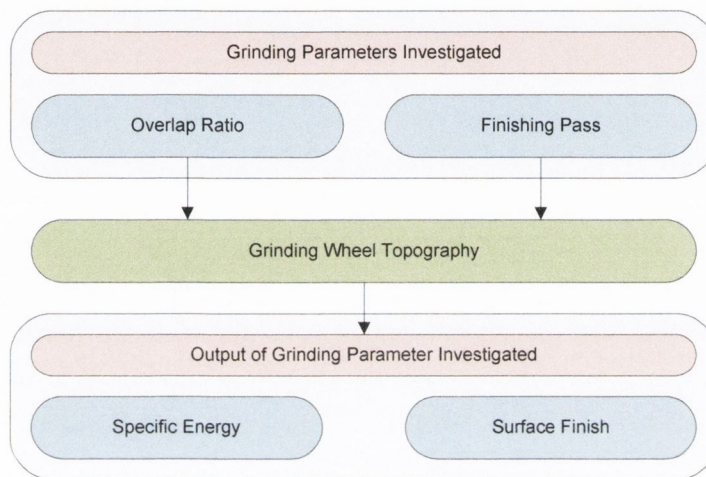
This explains why the specific energy for a given Ra in the 220 mesh wheel started to increase again, from one point of view, smaller grits give a larger value of C and consequently, a smaller value of t' , and in turn a larger specific energy. It can also be argued that smaller grits give a smaller value of r and consequently, a larger value of t' and in turn, a smaller specific energy. The transition where C starts to dominate over r appears to begin, for the grinding conditions used here, at grit diameters in the range of 63 to 89 μm .

Grit Size	60	120	150	220
Grit Diameter Average (μm)	254	102	89	63

Table 5.5: Average diameter of grit sizes 60, 120, 150 and 220 for an Aluminium Oxide Grinding Wheel

5.2 Effect of finishing pass

Previous studies have looked at the effect of the overlap ratio on the specific energies and surface finish of the grinding performance. Many operators perform a finishing pass similar to the operation found in grinding whereby the diamond dresser is passed across the wheel after a dressing pass is performed with zero in-feed. The acoustic emission response during dressing for the dressing pass and a dressing finishing pass was examined. Grinding forces and surface finish roughness were then investigated and compared to with conventional dressing experiments.



5.2.1 Effect of finishing pass on AE signal

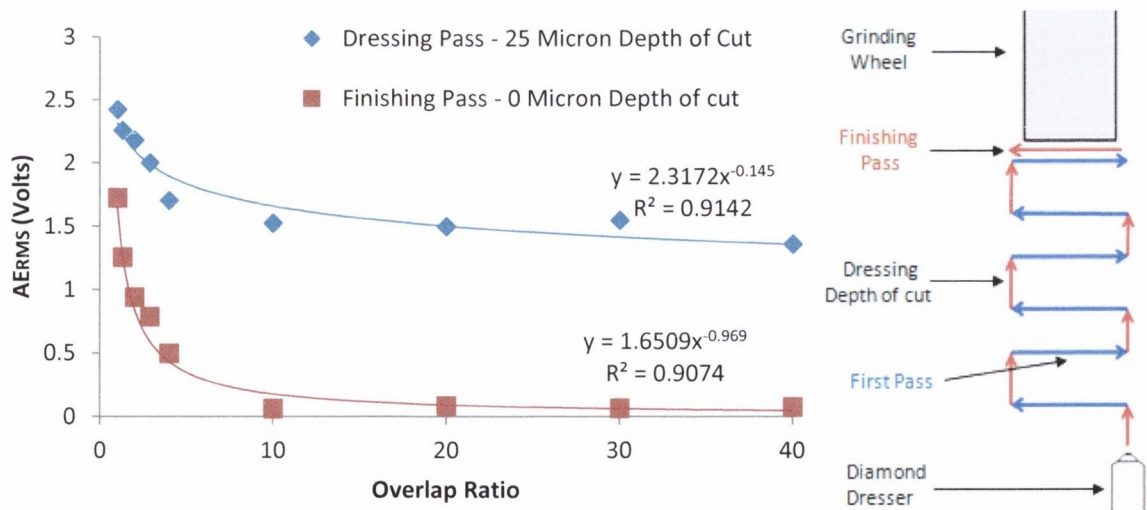


Figure 5.14: Plot of the overlap ratio vs. acoustic emission signal recorded for dressing and finishing passes

Figure 5.14 shows the effect of overlap ratio on the AE_{RMS} signal for a dressing pass of 25 micron depth of cut and a proceeding finishing pass whereby the diamond dresser passes the wheel with zero depth of cut. The results of these investigations show that for low overlap ratios, the AE_{RMS} value for the dressing pass is high with a value of 2.5 volts, while the subsequent finishing pass with zero depth of cut following this dressing pass, also has a high value of 1.7 volts. The AE_{RMS} signal is seen to decrease with an increase in the overlap ratio for both the dressing pass and finishing pass of the diamond dresser up till an overlap ratio value of 10, after which point, the AE_{RMS} remains steady. The high AE values experienced with low overlap ratios can be explained by the increase in contacts of the dresser with the wheel per second which results in greater fracture and stress release of the grits contributing to a greater AE signal. A subsequent high AE_{RMS} value of 1.7 volts is then seen for a finishing pass with an overlap ratio of 1. The reason for this result is that with a low overlap ratio of 1, the diamond dresser does not interact with each grit during the dressing pass as it traverses across the wheel at 38.4 mm/s. When the finishing pass is performed, the diamond dresser comes in contact with the remaining grits on the periphery of the wheel which have not been picked up by the previous 25 micron depth of cut dressing pass.

With higher overlap ratios of 10 and above, the diamond dresser traverses across the wheel at a much slower rate of 3.84 mm/s. This results in less contacts occurring per second leading to lower levels of stress energy released which explains the reduction in the AE signal. With an overlap ratio of 10, the diamond dresser theoretically should come in contact with each grit on the wheel 10 times. When a finishing pass is performed, the AE_{RMS} signal is seen to be almost zero as there is no stress impulses caused by the interaction of the diamond dresser with the grits on the wheel. The AE_{RMS} values are then seen to steady off for the dressing pass and finishing passes whereby signal values for finishing passes are almost zero indicating minimal contact of the diamond dresser and the grinding wheel. This would imply that the preceding dressing pass with large overlap ratio has left the wheel in its bluntest condition and greater dressing contact at that depth would not result in a change in the wheel condition.

5.2.2 Effect of finishing pass on specific energy

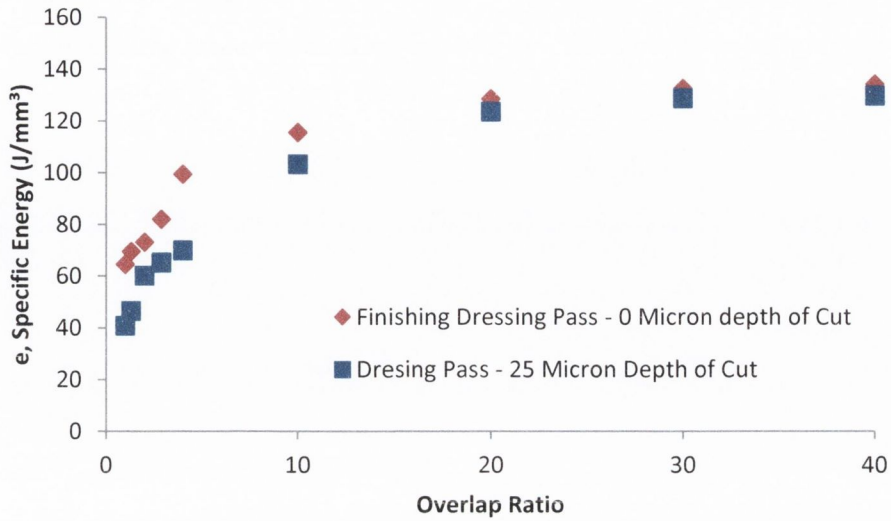


Figure 5.15: Normal and tangential grinding forces after the wheel has been dressed with and without a finishing pass

The normal and tangential forces were recorded during grinding after the wheel has been dressed using conventional dressing with a 25 micron depth of cut for both passes and also for a dressing process with a finishing pass whereby the last pass of the diamond dresser had a dressing depth of cut of 0 Microns. Using the tangential forces recorded and the equation for specific energy, the results could then be plotted against the overlap ratio to study the effect a dressing finishing pass has on the specific energy during grinding (Figure 5.15).

Again, it can be seen that wheels dressed with a low overlap ratio result in a grinding process with lower specific energies. The specific energies are seen to rise with an increase in the overlap ratio as the wheel dulls. The specific energy then levels off after an overlap ratio of 20 is used and a maximum specific energy value of approximately 130 J/mm³ is reached for this grinding process. A comparison of the grinding specific energies reveals that for low overlap ratios, a dressing process with a finishing pass results in specific energy values that are approximately 50% greater than those performed with conventional dressing. A look at the specific energy values for both conventional dressing and a dressing

process ending in a finishing pass reveals that the values are almost exactly identical. This implies that the wheel has reached its maximum dullness and performing a dressing process with a greater overlap ratio or one with a finishing pass will not result in higher specific energies being achieved.

Figure 5.16 shows a plot of the length of time the diamond dresser spends in contact with the periphery of a wheel for a certain depth of cut is plotted against the succeeding grinding specific energy. For example, a dressing process with an overlap ratio of 10 is in contact with the grinding wheel for 3.125 seconds whereas when an overlap ratio of 10 is performed ending with a finishing pass, the diamond is in contact with the wheel for 6.25 seconds at that given depth.

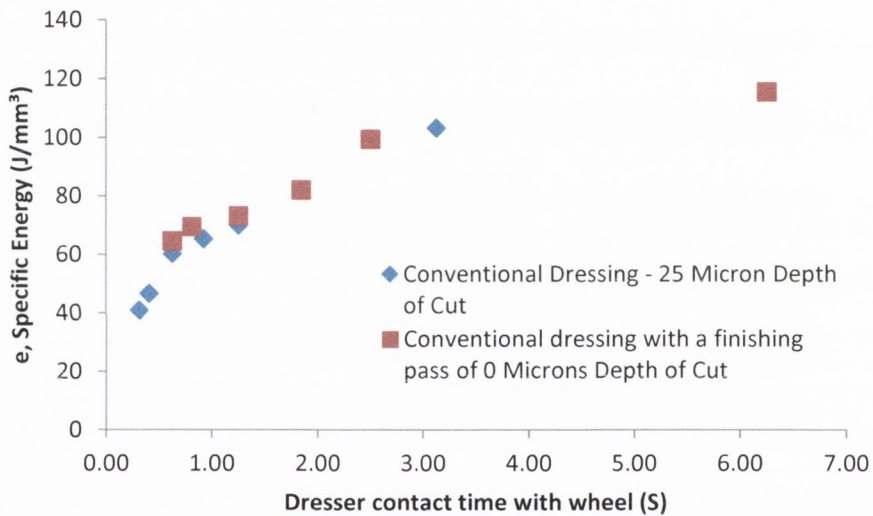


Figure 5.16: Plot of the dresser contact time with wheel against the specific energy

It is noted that a dressing process with an overlap ratio of 2 and a finishing pass which would have a total contact time of 1.25 seconds with the wheel produces specific energy values of approximately 70J/mm³. The same specific energy values are experienced when conventional dressing is performed with an overlap ratio of 4. The length of time the dresser spent in contact with the wheel is also 1.25 seconds indicating that the dressing process is determined by the length of time the dresser is in contact with the wheel or the amount of times the dresser comes in contact with each grit on the wheel.

5.2.3 Effect of finishing pass on surface finish

Similar to the results experienced for specific energy while grinding with both dressing processes, it can be seen that a dressing process with a finishing pass gives lower Ra values than conventional dressing. Again, this is due to the increase in contact time of the diamond dresser with the wheel as the diamond traverses back across the wheel with 0 in-feed of the diamond dresser. This results in the grits having greater contact time with the diamond dresser which would dull them leading to smoother surface finish when grinding. Once an overlap ratio of 10 is used, it can be seen that the surface roughness values, Ra remains constant at a value of approximately $0.27\mu\text{m}$ (Figure 5.17).

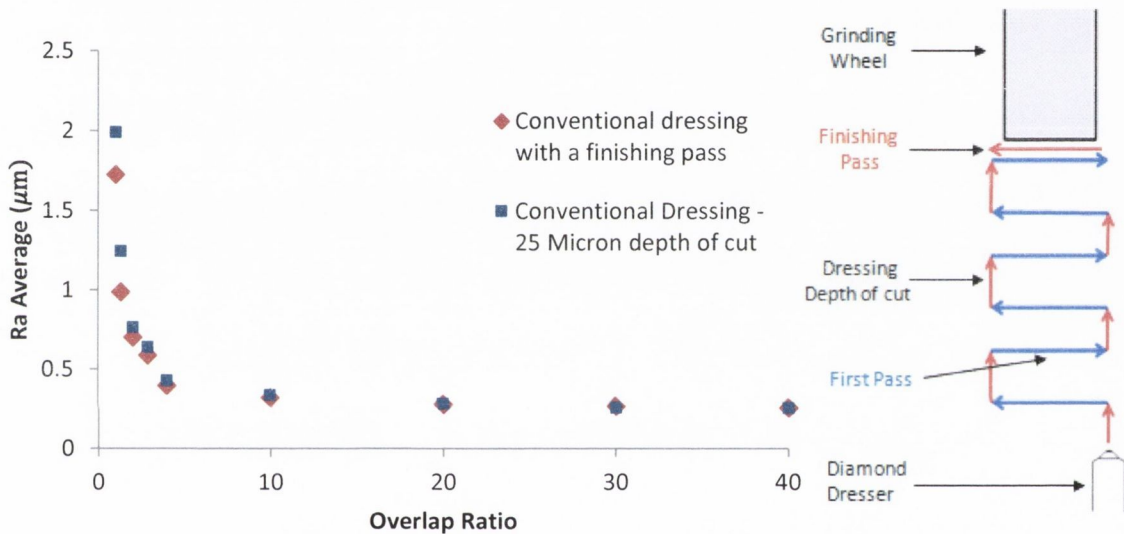


Figure 5.17: Average surface roughness after conventional dressing and dressing with finishing pass

5.3 Acoustic emission signal and specific energies during grinding

The AE signal was monitored while dressing the wheel with a range of overlap ratios to replicate the effect of diamond wear. Grinding tests were then carried out and the forces were recorded to calculate the grinding specific energy. Investigations were performed to study the dressing AE signals feasibility into predicting grinding specific energies. Following this, tests will then be performed to study the effect of the AE signal with diamond wear and whether this information can be used to prompt the user to take corrective action when a limit is exceeded.

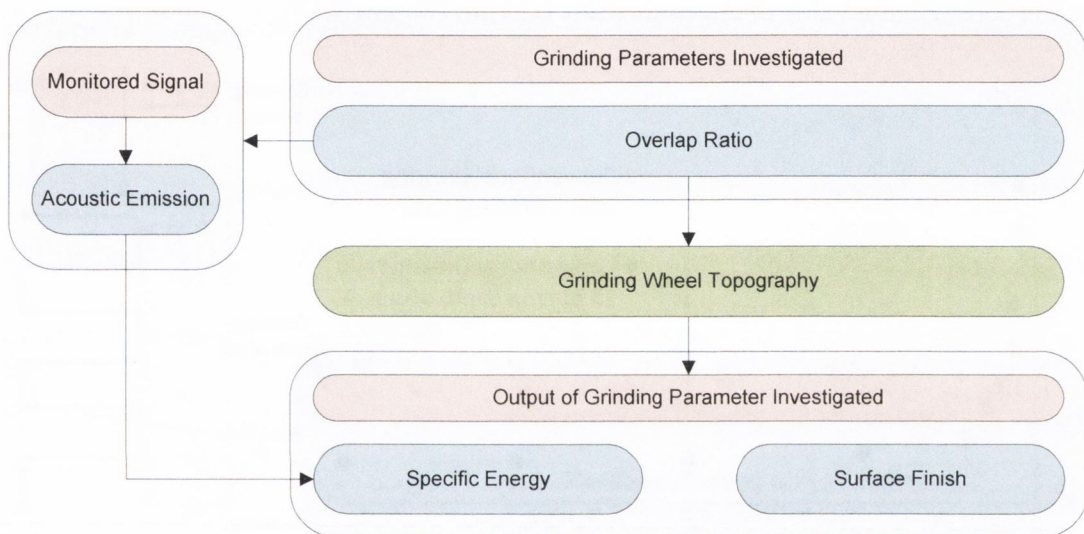


Figure 5.18: Investigations into the effect of the overlap ratio on the acoustic emission signal and its effect on the specific energy and the surface finish

5.3.1 Effect of overlap ratio on acoustic emission

The acoustic emission signal was measured for various dressing conditions. The results for increasing the depth of cut are shown in Figure 5.19 for four different conditions, a) a new diamond (0.1mm width) dressing a fused aluminium oxide wheel, b) a worn diamond (0.7mm width) dressing a fused aluminium oxide wheel, c) a new diamond (0.1mm width) dressing a ceramic grit 3SG aluminium oxide wheel, d) a worn diamond (0.7mm width) dressing a ceramic grit 3SG aluminium oxide wheel.

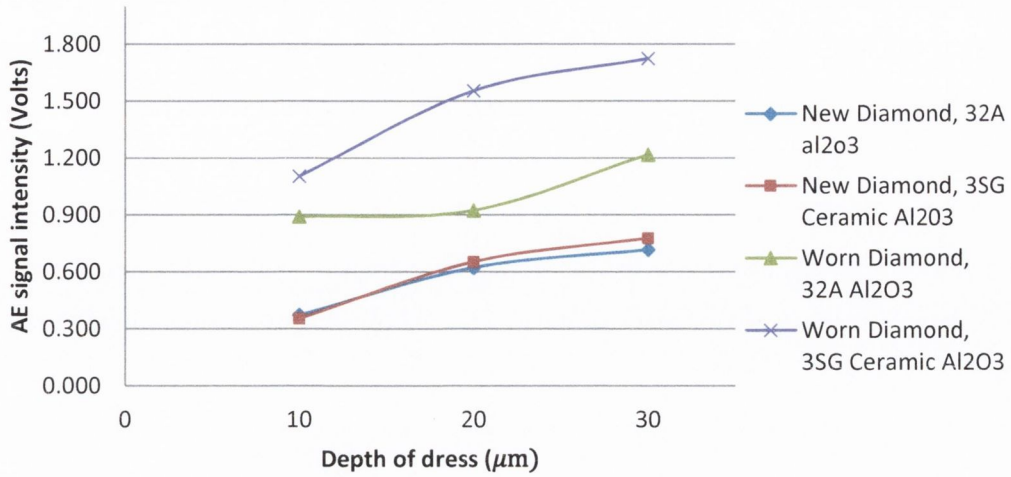


Figure 5.19: Change in acoustic emission signal with dressing depth

It can be seen that an increase in the diamond dresser depth of cut leads to a greater increase in the acoustic emission signal. This is due to the larger energy release of the material as the diamond dresser fractures a greater amount of grits. This increase in AE was observed by a number of other authors. In all cases the increase in energy did not increase proportionally with depth of cut and a size effect was observed with larger grit removal rates. Furthermore, it is not clear whether the acoustic emission signal observed gives proportional values for plastic deformation, grit fracture and bond fracture.

For this reason, the acoustic emission intensity was evaluated vs the dressing power which is calculated based on the equation below:

$$P_d = F_T \cdot v_s \quad (5.5)$$

Where F_T is the tangential dressing force and v_s is the wheel speed. The specific dressing energy, e_d is the energy required to remove 1mm^3 of abrasive material which is given by the equation:

$$e_d = \frac{P_d}{Q_d} \quad (5.6)$$

where P_d is the dressing power and Q_d is the grit removal rate.

Malkin has shown that a correlation exists between the dressing specific energy and the grinding energy whereby an increase in the dressing specific energy resulted in a consequent increase in the specific energy during grinding [45]. Therefore, if it is possible to establish a relationship between dressing specific energy using the dressing power and the acoustic emission signal, it should be possible to correlate the AE signal strength with the grinding specific energy. As grinding specific energy is a valuable parameter to predict the onset of grinding, this information can be used to prevent thermal damage occurring to the workpiece.

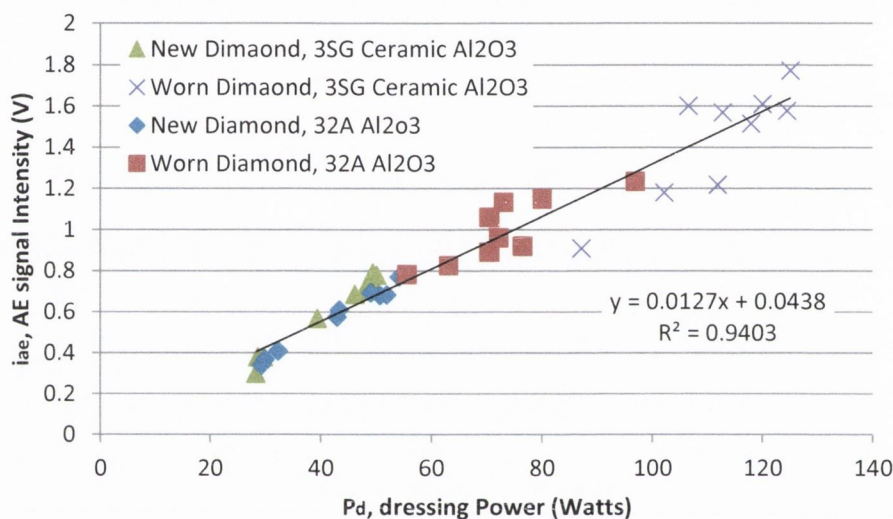


Figure 5.20: Acoustic emission signal Vs power during dressing

A plot of the dressing power vs the acoustic emission signal intensity is shown in Figure 5.20. Despite the difference in dressing depths, diamond shape and abrasive type, it can be seen that a direct correlation exists between the two signals. A linear regression line of best fit plotted through these data points gives an R-squared value of 0.8608 along with a close to zero intercept value which shows a good correlation of the two signals. Using the equation of the line, the AE signal intensity can be calculated based on the Equation 5.7.

$$i_{ae} = PF_{ae} \cdot P_d \tag{5.7}$$

Where PF_{ae} is the acoustic emission power factor for a given set up which in this case is 13.5 millivolts/Watt.

As the dressing power, P_d is proportional to the AE intensity according to the equation $i_{ae} = PF_{ae} \cdot P_d$, we can substitute the acoustic emission intensity value, i_{ae} into the specific dressing energy equation $e_d = P_d/Q_d$, to define the specific AE dressing energy as:

$$e_{ae} = \frac{i_{ae}}{Q_d} \quad (5.8)$$

which is the AE signal strength per mm^3/s grit removal rate. The specific AE dressing energy (e_{ae}) was calculated for three different diamond widths and plotted against their corresponding overlap ratio. (Figure 5.21)

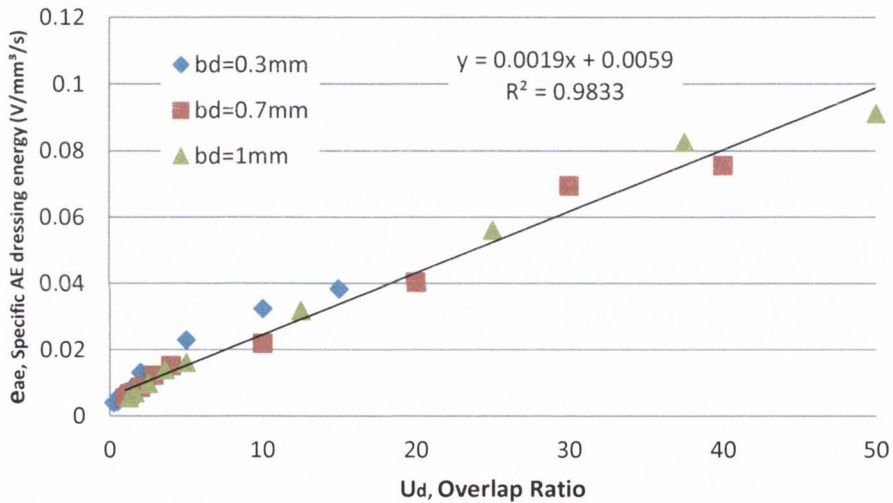


Figure 5.21: Specific AE dressing energy Vs Overlap Ratio

A regression line can be plotted through these points and a relationship between the specific AE energy and the overlap ratio, independent of the diamond width can be obtained through the equation:

$$e_{ae} = 0.0019 \cdot U_d + 0.0059 \quad (5.9)$$

This relationship can be solved for the overlap ratio, U_d in order to predict the overlap ratio for a recorded specific AE dressing energy.

$$U_d = \frac{e_{ae}}{.0019} - 3.1 \quad (5.10)$$

5.3.2 Application of AE to grinding specific energy

Based on the above results, it can be seen that the acoustic emission signal is directly correlated to the dressing energy and since the dressing energy is proportional to the grinding specific energy, the acoustic emission signal could then be used to predict grinding power. Figure 5.22 shows a plot of the acoustic emission experienced during dressing and the subsequent specific energy values while grinding.

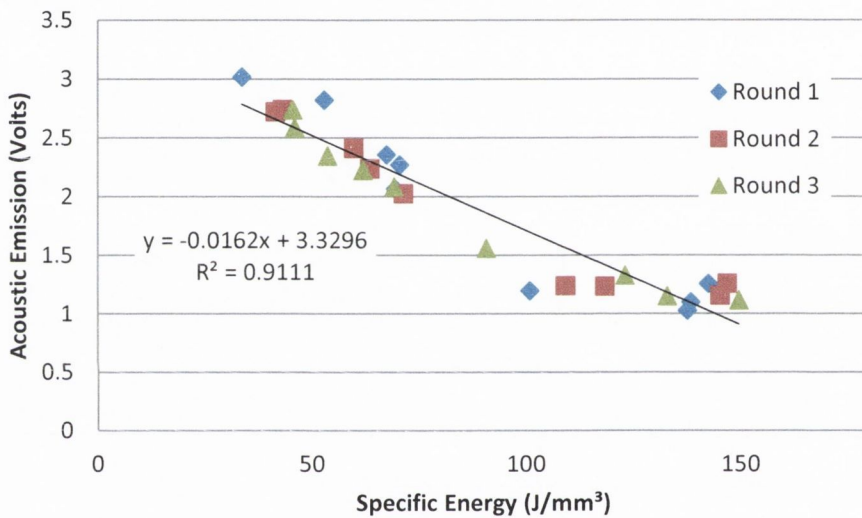


Figure 5.22: Plot of the specific normal forces recorded during grinding against the acoustic emission signal recorded during dressing

It is clear that a strong relationship exists between the AE signal and the grinding forces as a regression line plotted through the data points reveals an R^2 value of 0.911. This is true for the particular surface grinding process presented above and the AE information collected during dressing. This information can be used to predict the power during grinding. For example, a dressing process that emitted an AE signal of almost 3 volts would result in low specific normal forces of 0.7N/mm during grinding as the aggressive dress would create a sharp wheel. Whereas a dressing process with a low acoustic emission

signal would indicate rubbing of the grits which lead to a blunt wheel creating larger specific normal forces during grinding. The limit to this analysis is that the acoustic emission signals recorded and grinding forces experienced are only true of the dressing and grinding parameters described above. An experimental study of the AE signal during dressing and preceding forces during grinding would need to be performed for different grinding operations. Following this, the specific grinding energy values can be predicted based on the acoustic emission signal recorded during dressing.

5.3.3 Acoustic emission and diamond wear

The dressing of Aluminium oxide and CBN wheels with stationary diamond dressing tools suffers severe wear of the diamond dresser over time. The wear appears as an increase in the effective width (b_d) of the diamond dresser over time. As the value of b_d increases, the overlap ratio becomes greater as a result according to the equation:

$$U_d = \frac{S_d}{b_d} \tag{5.11}$$

The effect that an increase in effective width can have on the overlap ratio is presented in Figure 5.23.

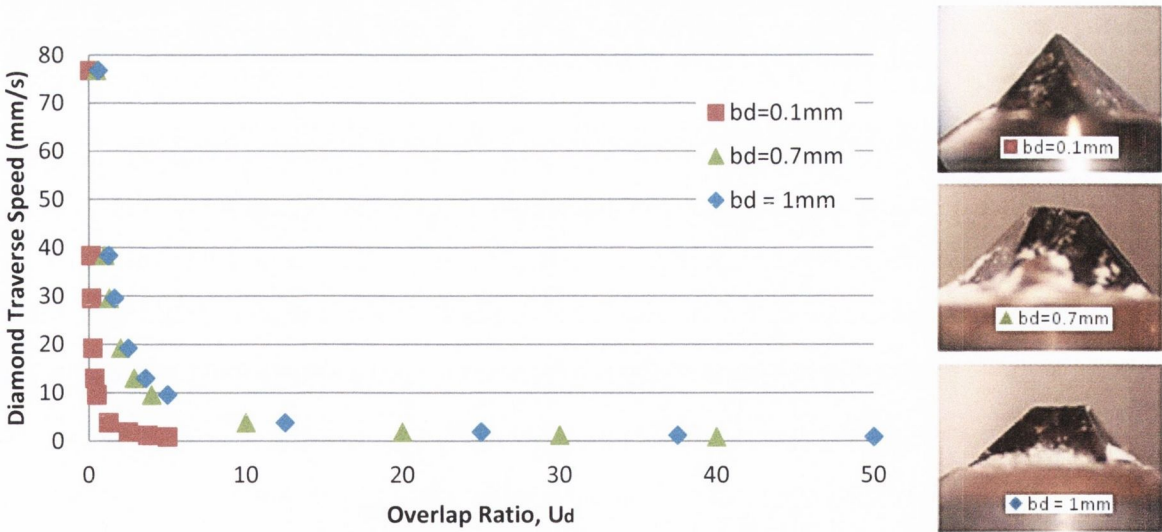


Figure 5.23: Change in the effect of overlap ratio with diamond width when traverse speed has been held constant

Here, it can be seen that when the diamond traverse speed is held constant but the wear of the diamond increases, a significant change in the overlap ratio occurs. This is quite often the case in industry whereby the machining parameters are not changed and overlap ratio increases as a result of wear. This increase in overlap ratio can lead to greater heat generation and risk of grinding burn. To overcome this problem, operators often place the diamond at 10° to 15° angle. The diamond is then rotated once a wear flat has developed, and either a new cutting edge of the diamond is presented to the wheel or it could come in line with a pre-existing wear spot which would grow and in turn increase the overlap ratio. The rotation of the diamond is at the discretion of the operator who often has no way to determine exactly when to rotate. Even, if the diamond is rotated on a regular basis, multiple wear spots on the diamond will develop overtime as shown in Figure 5.24.

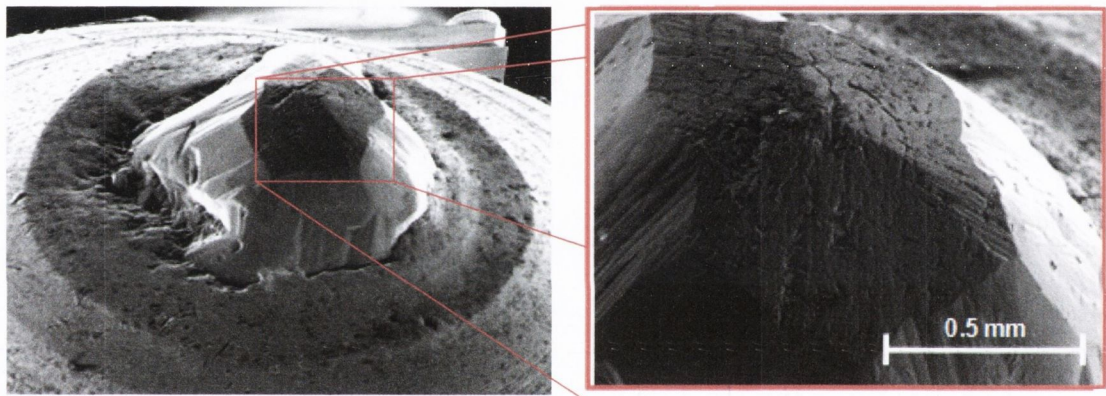


Figure 5.24: Diamond wear spot on a rotated diamond

Dressing tests were performed with diamonds of 3 different widths for a range of diamond traverse speeds (Figure 5.25). It is noted that a rise in the acoustic emission signal can be seen with an increase in the traverse speed of the diamond. The same trend is repeated for each diamond but an increase in the AE signal is noted as the diamond width gets bigger. It can be seen that the acoustic emission signal during dressing rises with an increase in the grit removal rate or speed of the diamond dresser. This is due to the material removal mechanism occurring at these high speeds. For example, when a low overlap ratio is used, the diamond dresser traverses across the wheel at a high speed which causes fracture of the grits and in turn a large acoustic emission signal is recorded. Whereas when a high

overlap ratio is used, the diamond dresser, ends up rubbing the grits, less stress energy or displacement of the material occurs and a lower acoustic emission signals are recorded. This trend is repeated for each of the diamond widths with the acoustic emission rising at the same rate for all three diamond dressers. It is noted that a wider diamond produces a greater acoustic emission signal indicating that the increase in contact time with wider diamonds contributes significantly to the AE response. This is most likely due to plastic deformation of the grits or elastic rubbing as suggested by Malkin [17].

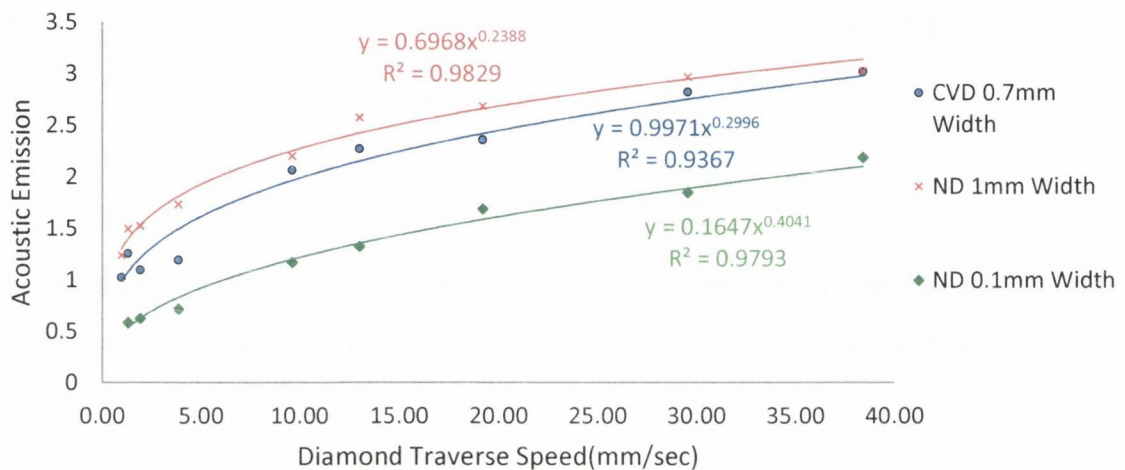


Figure 5.25: Acoustic emission signal vs diamond traverse speed for different diamond widths

Further tests were performed where the acoustic emission was tested throughout the tool life of the diamond dresser as the diamond wear spot developed. The dressing conditions were held constant with a dressing lead of 0.2mm/rev and a depth of cut of 25 microns. 5000 dressing passes were performed on a diamond and measurements of the diamond width and acoustic emission were made for every 250 passes for the first 1000 passes and then every 1000 passes following that, up to 5000 passes. Each acoustic emission value is a mean of three tests performed. It can be seen that as the diamond wear increases, the AE signal increases accordingly indicating that a direct relationship exists between the AE signal and the wear spot of the diamond.